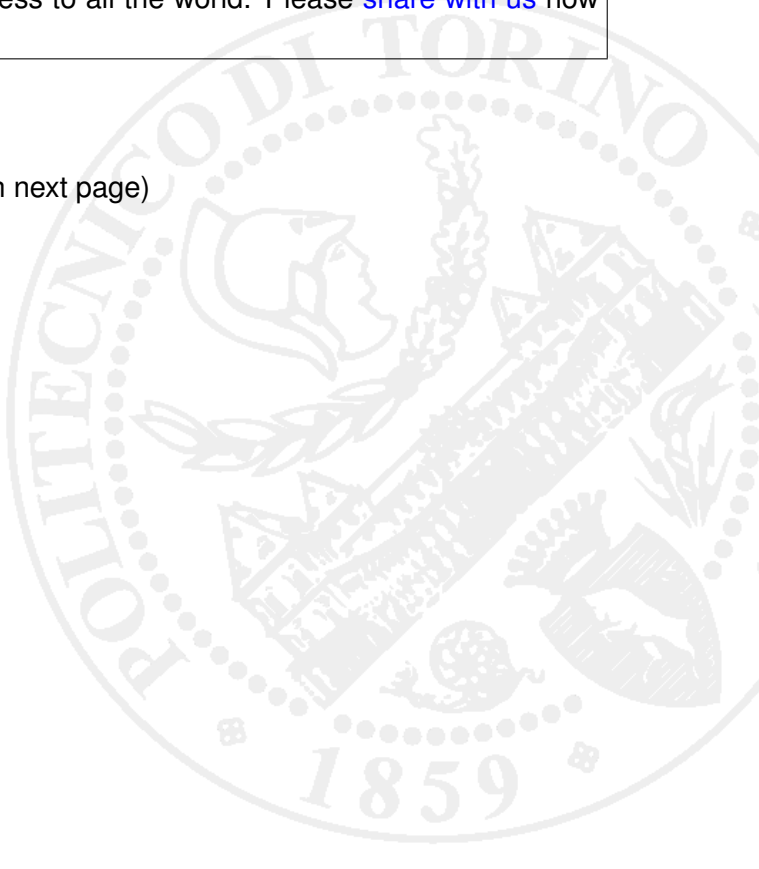

POLITECNICO DI TORINO

Dottorato di Ricerca in
Metrologia: Scienza e Tecnica delle Misure

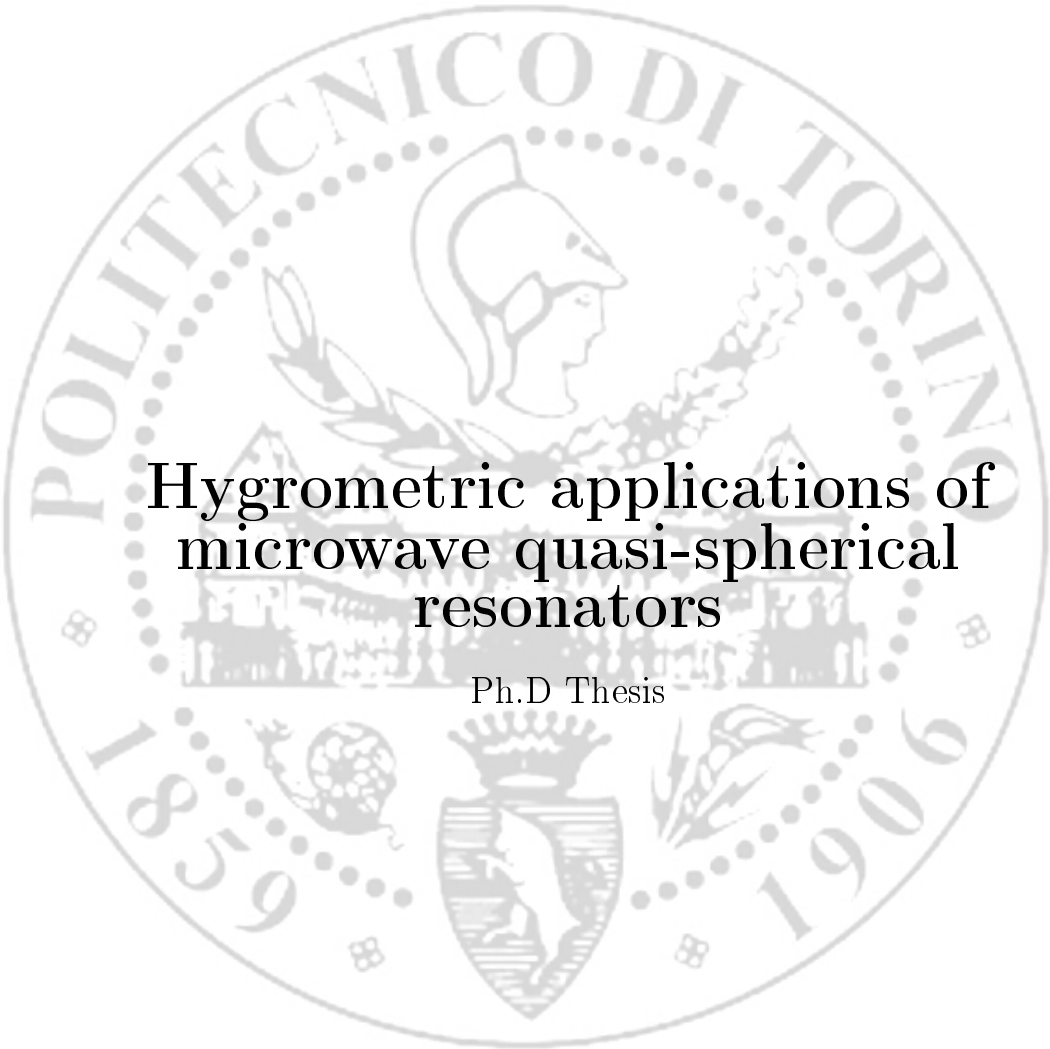

Hygrometric applications of microwave quasi-spherical resonators

Ph.D Thesis

Rugiada Cuccaro

POLITECNICO DI TORINO

Dottorato di Ricerca in
Metrologia: Scienza e Tecnica delle Misure
Ciclo XXIV

Hygrometric applications of microwave quasi-spherical resonators

Ph.D Thesis

Examinee:
Rugiada Cuccaro
Student N: 160192

Supervisors:
Dott. Roberto M. Gavioso
Prof.ssa Maria P. Bussa

Academic Year: 2011/2012

To myself,
Dario and my parents.

A me stessa,
Dario ed i miei genitori.

Contents

Introduction

The amount of water which is present in material substance may represent a critical aspect for life and product quality. Particularly, the abundance of water vapour in air and other gases influences a wide range of physical, chemical and biological processes with a significant effect on safety, cost and health. For these reasons humidity measurements play an important role in industrial, laboratory and process control applications.

Unfortunately humidity is difficult to measure, both because of its wide dynamic range and because measurements have often to be made in presence of a large range of gases and contaminants.

Due to the importance of these measurements, in 2006 a *Roadmap*[1] for Humidity and Moisture Measurement was drafted [1] as a part of the EUROMET iMERA (Implementing Metrology in the European Research Area [2]) activity, whose declared intention is to increase the impact of national investment in European metrology research and development. The roadmap (Fig. 1) identified the main social and economic triggers that should guide the humidity and moisture measurements and the development of novel humidity standards, suggesting a coherent plan to their realisation over the next 15 years. The two identified key triggers were *global warming* and *manufacturing processes*. From the social and economical point of view, they mean: the improvement of climate models through the measurement of atmospheric water vapour; the reduction of carbon emissions, for example with humidity measurements to optimize combustion and heat treatment processes in industries or to improve the energy-efficiency of buildings; the improvement of manufacturing process control in industries where organic or reactive materials are produced or stored.

At the level of national standards and laboratories, the targets mentioned above mean: to improve humidity standards for high temperatures and pressures in non-air gases; to measure and control moisture processes in materials; to improve relative humidity standards (direct measurement traceability of relative humidity instead of dew point and temperature); new water vapour

[1]Business plan for identifying pathways for development in a field.

Figure 1: Roadmap for Humidity and Moisture Measurement [1]: vertical axis shows increasing specialisation of technology towards targets; horizontal axis shows approximate timescale.

formulations and measurements of the saturation water vapour pressure at a given temperature, and of the enhancement factor, aiming at an improved representation of the non-ideality of a real humid gaseous mixture.

Therefore, this analysis indicates the necessity of an improvement both in the field of humidity, for which standards and traceability methods already exist, and in the capability to determine the moisture content of material substance, for which traceability is more problematic.

In spite of the significant previous effort in the development and improvement of humidity sensors and instrumentation, at present the majority of these still require considerable care and maintenance and none is capable to cover the full dynamic range required by water vapour measurements. Moreover, due to the typical design features of standard humidity generators, the calibration of hygrometers are carried out at atmospheric pressure using nitrogen or air as the carrier gas, while such conditions often significantly differ from those encountered in real applications.

Figure 2 reviews a few basic features, such as the humidity and temperature working range, and the operating principle of some common types of hygrometers. Some of these instruments allow a direct measurement of relative humidity, while others derive its value indirectly from measurements of temperature and dew point which is determined by revealing the onset of condensation.

The challenging context of needs, targets and goals, which are relevant for the future development of hygrometry illustrated above, provides the initial motivation to the research work which is described and discussed in this thesis. Here, we suggest that a microwave resonator may be used for an accurate determination of the humidity in a variety of gases over an extended temperature and pressure range. Also, the peculiar features of the proposed method make it an extremely versatile technique, allowing to measure the amount of water vapour which is present in binary humid gaseous mixtures well away from saturation, or alternatively, to directly determine the dew point temperature by a sensitive detection of condensation. This twofold capability, which is possibly unique among hygrometric instrumentation, may exceed some limits of the present devices and is likely to offer a solution to several metrological requirements.

Microwave cavity resonators in metrology date back to 1945, when they were developed and used by Essen and co-workers for the measurement of the speed of light c in vacuum [3]. The value of c obtained by that time, with a relative overall accuracy of 3 parts in 10^{-6} (ppm), differs from that currently adopted ($c = 299792458$ m·s^{-1}) [4] by only 0.1 ppm. In spite of the metrological quality of this determination and its successive refinements, the

Sensor type	Absolute or relative humidity	Typical range (extended range in brackets)		Typical units in which readings are displayed	Contamination tolerance[2] (bracketed ratings after cleaning)	Sampling, configuration	Guideline best humidity uncertainty in use[3] (±)
		Humidity	Temperature[1]				
Mechanical	R	20 %rh to 80 %rh	Near room temperature	%rh	* * *	Whole immersion	5-15 %rh
Wet- and dry-bulb aspirated (Psychrometer)	R	5 %rh to 100 %rh	0 °C to 100 °C (also useable above and below this range)	%rh (often hand-calculated from temperature readings)	* (* *)	Whole immersion (or sample gas flow)	2-5 %rh
Resistive	R	5 %rh to 95 %rh (and up to 99 %rh)	-30 °C to +60 °C (-50 °C to 200 °C)	%rh	* *	Probe (or whole immersion)	2-3 %rh
Capacitive	R	5 %rh to 100 %rh (and down to near 0 %rh)	-30 °C to +60 °C (-40 °C to 200 °C)	%rh	* *	Probe (or whole immersion)	2-3 %rh
Impedance dew-point types	A	Dew points of -85 °C (or below) to +60 °C	Most temperatures up to +60 °C, avoiding saturation	Dew point, vapour pressure	* *	Probe	2-5 °C
Condensation	A	Dew points below -85 °C to +100 °C	-85 °C to +100 °C (main body of instrument at room temperature)	Dew point	* (* *)	Sample gas flow (or probe)	0.2-1.0 °C
Lithium chloride	A	Dew points of -45 °C to +60 °C, gas always over 11 %rh and not saturated	-20 °C to +60 °C (some use -40 °C to +100 °C)	Dew point	*	Probe	2-4 °C
Electrolytic (phosphorous pentoxide)	A	Below 1 ppm_v to 1000 ppm_v	Near room temperature	ppm_v or vapour pressure	*	Sample gas flow	3-10 percent of reading
Spectroscopic	A	Extremely wide range, depending on type	Very wide range (main body of instrument at room temperature)	ppm_v (and others)	* * *	Gas sample (line-of-sight sampling at high humidity)	3-10 percent of reading in high range, much more at low end.
Colour change	R	20 %rh to 80 %rh	Near room temperature	%rh	* *	Paper test card (or pump with glass vial)	10-20 %rh

Figure 2: Summary of some basic features of the main types of humidity measurements [5].

microwave technique for the measurement of the speed of light was later superseded by more accurate optical methods. Resonant cavities newly aroused interest in the metrological community by the end of the '70s when Moldover and co-workers [6] first suggested to use the purely radial modes of a spherical acoustic resonator to increase the accuracy of speed of sound u measurements in dilute gases. In 1986, after spending a decade of careful experimental and theoretical research work to develop this idea, the determination of the molar gas constant R with a relative uncertainty below 2 ppm was achieved using a spherical acoustic resonator [7].

In the same year, it was proposed by Mehl and Moldover [8] that a combined acoustic/microwave resonator might determine the ratio between the speed of sound and the speed of light, leading to a determination of the thermodynamic temperature with unprecedented accuracy. Recently, the geometrical perturbation model needed for the microwave determination of the volume of a quasi-spherical resonator (QSR) was achieved [9, 10] leading to a 100-fold in the accuracy of such type of measurement. Nowadays, acoustic and/or microwave QSRs are widely used to pursue metrological applications which include acoustic thermometry [11, 12], the determination of the Boltzmann constant, the measurement of dielectric properties of gases [13 - 15] and the development of a pressure standard [16].

In this work, triggered by the initial suggestion and the preliminary results obtained at the National Institute for Standards and Technology (NIST) by Huang and co-workers [17], we have explored the possible application of a microwave resonant cavity to realise a reference standard hygrometer.

Particularly, we have measured the microwave resonance frequencies of a small volume (69 cm^3) triaxial elipsoidal cavity to determine the water vapor mole fraction x_w of H_2O/N_2 and H_2O/air mixtures. The mixtures were prepared using the INRiM standard humidity generator for frost-point temperatures T_{fp} in the range between 241 K and 270 K and a commercial two-pressure humidity generator operated at dew-point temperature T_{dp} between 272 K and 291 K.

Following these tests, we demonstrated the performance of the QSR operated as a condensation hygrometer. For this demonstration, a suitable experiment was prepared in cooperation with the National Physical Laboratory (NPL), which allowed to compare the performance of the QSR with that of a calibrated chilled-mirror hygrometer.

Finally, with the aim of reducing the uncertainty currently associated to the literature values of the constants in the Debye equation, we have measured the dielectric constant of pure water vapour in the temperature range from 320 K to 470 K at pressures up to 1.7 MPa.

As a whole, the results obtained in these experiments demonstrated the validity and satisfactory performance of the microwave technique for hygrometry. Particularly, for all the measurements in humid binary mixtures, the reference and measured water mole fractions x_w were found to agree within their combined expanded uncertainty. The quality of the agreement is indeed remarkable, considering that x_w in these mixtures spans the range between 3 parts in 10^4 and 2.1 parts in 10^2, corresponding to relative permittivities which differ from unity by less than 700 ppm. Also, the microwave QSR demonstrated its capability to perform direct measurements of the dew-point temperature T_{dp}, although in this case a difference of (0.08 ± 0.02) °C in the dew-point temperature as measured by the resonator and the reference chilled mirror hygrometer was observed. This difference, which is larger than the combined uncertainty of T_{dp} measured by the hygrometer and the resonator, is likely to be due to the imperfect thermal uniformity of the resonator, caused by the limited performance achieved in thermostatting the apparatus in the course of these preliminary tests. Finally, the results achieved in the determination of the polarizability of water vapour over an extended temperature and pressure range, demonstrated that the technique is indeed suitable for tolerating the extreme industrial conditions required by several hygrometric applications without undergoing to significant degradation of its performance.

Summarizing the organization of the contents of this thesis: in Chapter 1 the basic theory dealing with the solution of the Maxwell equations in a spherical cavity is briefly revised together with a description of the main perturbative effects affecting the cavity eigenfunctions in a practical case. These include the major perturbation induced by quasi-spherical geometry. Within the same chapter, the basic relations which link the measured microwave resonance frequencies to the electric properties of a humid binary mixture are reviewed and the working equations which allow to determine the water mole fraction x_w and the dew-point temperature T_{dp} are illustrated; in Chapter 2 a basic description of the salient design features of the QSR used in this work is given, together with a description and a few illustrative examples of the procedure and methods used for the acquisition of the relevant microwave data. Also, the initial calibration of the microwave resonator from the results of vacuum and helium measurements is given, leading to a quantitative assessment of the thermal expansion and the elastic compression of the cavity dimensions as a function of temperature and pressure; in Chapter 3 the results of microwave measurements in pure water vapour are presented together with their analysis which leads to an estimate of the Debye constants,

the dielectric virial equation and the dipole moment of water; in Chapter 4 the experiments conducted at INRiM, where the resonator performance is tested in humid mixtures prepared using a standard humidity generator and a commercial two-pressure generator, are discussed; in Chapter 5 the experiments carried out at NPL to test the performance of the resonator as a condensation hygrometer by comparison with a reference chilled-mirror hygrometer are discussed; finally, in the Conclusions, the perspectives and future possible developments of the microwave hygrometer are discussed.

Chapter 1

Basic principles of microwave hygrometry

1.1 Basic theory of a microwave resonant cavity

We consider the electromagnetic stationary field bounded within a spherical cavity of radius a, whose internal surface is a perfect electrical conductor.

A general method for the determination of the resonant frequencies consists of solving Maxwell's field equations to obtain the field intensities which satisfy given boundary conditions.

Recalling the Maxwell's equations for a space where there are no charges or currents:

$$\nabla \times \vec{E} = -\frac{\partial \vec{B}}{\partial t} \tag{1.1}$$

$$\nabla \cdot \vec{E} = 0 \tag{1.2}$$

$$\nabla \times \vec{B} = \mu_0 \varepsilon_0 \frac{\partial \vec{E}}{\partial t} \tag{1.3}$$

$$\nabla \cdot \vec{B} = 0 \tag{1.4}$$

where $\vec{E}$ is the intensity of the electric field, $\vec{B}$ the magnetic field, ε_0 the dielectric permittivity in vacuum and μ_0 the magnetic susceptibility in vacuum.

Applying the curl operator $\nabla\times$ to Eq. (1.1) and Eq. (1.3) and making use of the vector-analysis identity for a generic vector quantity $\vec{F}$:

$$\nabla \times \nabla \times \vec{F} = \nabla(\nabla \cdot \vec{F}) - \nabla^2 \vec{F} \tag{1.5}$$

we obtain:

$$\nabla^2 \vec{E} - \frac{1}{c_0^2} \frac{\partial^2 \vec{E}}{\partial t^2} = 0 \tag{1.6}$$

and

$$\nabla^2 \vec{B} - \frac{1}{{c_0}^2} \frac{\partial^2 \vec{B}}{\partial t^2} = 0. \tag{1.7}$$

Eqs. (1.6) and (1.7) are the wave equations of the electric and magnetic field and can be summarized in a general equation:

$$\nabla^2 f - \frac{1}{{c_0}^2} \frac{\partial^2 f}{\partial t^2} = 0 \tag{1.8}$$

where f is a scalar quantity and alternatively represents each component of $\vec{E}$ and $\vec{B}$ and c_0 is the speed of light in vacuum.

In any material substance the speed of propagation of light c, the dielectric permittivity of the material ε and its magnetic susceptibility μ are linked by the relation:

$$c = \sqrt{\mu\varepsilon}. \tag{1.9}$$

To solve Eq. (1.8), we use a separable function such as:

$$U(\vec{r}, t) = \Phi(\vec{r})T(t) \tag{1.10}$$

where $\Phi(\vec{r})$ expresses the spatial dependence and $T(t)$ the time dependence.

Replacing Eq. (1.10) in Eq. (1.8), we obtain:

$$\nabla^2 U(\vec{r}, t) - \frac{1}{c_0^2} \frac{\partial^2 U(\vec{r}, t)}{\partial t^2} = 0. \tag{1.11}$$

Solving Eq. (1.11) with the method of the separation of variables, we obtain the following relations:

$$\nabla^2[\Phi(\vec{r})T(t)] - \frac{1}{c_0^2} \frac{\partial^2 \Phi(\vec{r})T(t)}{\partial t^2} = 0 \tag{1.12}$$

$$T(t)\nabla^2\Phi(\vec{r}) - \frac{1}{c_0^2}\Phi(\vec{r})\frac{\mathrm{d}^2 T(t)}{\mathrm{d}t^2} = 0 \tag{1.13}$$

$$\frac{\nabla^2\Phi(\vec{r})}{\Phi(\vec{r})} - \frac{1}{c_0^2}\frac{\frac{\mathrm{d}^2T(t)}{\mathrm{d}t^2}}{T(t)} = 0. \tag{1.14}$$

To satisfy Eq. (1.14), its two constitutioning terms of the equation need to be equal. This is possible if both terms are separately equal to the same constant. By indicating with $-k^2$ the separation constant, we obtain:

$$\frac{\nabla^2\Phi(\vec{r})}{\Phi(\vec{r})} = -k^2 \tag{1.15}$$

$$\frac{1}{c_0^2}\frac{\frac{\mathrm{d}^2T(t)}{\mathrm{d}t^2}}{T(t)} = -k^2 \tag{1.16}$$

and Eq.(1.16) becomes:

$$\frac{\mathrm{d}^2T(t)}{\mathrm{d}t^2} = -k^2c_0^2T(t). \tag{1.17}$$

By imposing that:

$$\omega^2 = k^2c_0^2 \tag{1.18}$$

solutions of Eq.(1.17) are:

$$T(t) = Ae^{i\omega t} \tag{1.19}$$

and the function $U(\vec{r},t)$ becomes:

$$U(\vec{r},t) = \Phi(\vec{r})Ae^{i\omega t} \tag{1.20}$$

where A is a proportional constant that defines the amplitude of the field.

We can now consider the spatial component of the wave equation. Eq.(1.15) can be re-written as:

$$\nabla^2\Phi(\vec{r}) + k^2\Phi(\vec{r}) = 0, \tag{1.21}$$

which is called Helmholtz equation.

1.2 Steady EM field in a spherical resonator

Appropriate solutions of the Helmholtz equation may be sought using again the separation of variables method. For a spherical cavity the adoption of a spherical coordinate system (r,ϑ,φ) is suitable. Thus, solutions of Eq. (1.21) can be expressed as: $\Phi(r,\vartheta,\varphi) = R(r)P(\vartheta)Q(\varphi)$.

Suitable eigenfunctions of the Helmholtz equation have the form [18]:

$$\Phi(r,\vartheta,\varphi) = [(kr)j_l(kr)]P_l^m(\cos\vartheta)[B\cos(m\varphi) + C\sin(m\varphi)] \tag{1.22}$$

where $j_l(kr)$ is the spherical Bessel function and $P_l^m(\cos\vartheta)$ is the associated Legendre polynomial. For brevity, we can combine solutions of the two angular functions and define the spherical harmonics:

$$Y_{lm}(\vartheta,\varphi) = P_l^m(\cos\vartheta)[B\cos(m\varphi) + C\sin(m\varphi)]. \tag{1.23}$$

Eq. (1.22) becomes:

$$\Phi(r,\vartheta,\varphi) = (kr)j_l(kr)Y_{lm}(\vartheta,\varphi). \tag{1.24}$$

The Helmholtz equation for the electromagnetic field in spherical geometry admits two classes of solutions: transverse magnetic (TM or electric) modes and transverse electric (TE or magnetic) modes. In a spherical system the TM modes have null $\vec{B}$ component along r direction ($B_r = 0$), while the TE modes have null $\vec{E}$ component along r direction ($E_r = 0$). The intensities of the components of $\vec{E}$ and $\vec{B}$ can be expressed in terms of the scalar wave function (Eq. 1.24). Their expression becomes:

$$\left.\begin{aligned}
E_r &= 0 \\
E_\vartheta &= -\tfrac{i\omega\mu}{r\sin\vartheta}[(kr)j_l(kr)]\tfrac{\partial Y_{lm}}{\partial\varphi} \\
E_\varphi &= \tfrac{i\omega\mu}{r}[(kr)j_l(kr)]\tfrac{\partial Y_{lm}}{\partial\vartheta} \\
H_r &= \tfrac{k^2}{r^2}l(l+1)[(kr)j_l(kr)]Y_{lm} \\
H_\vartheta &= \tfrac{k}{r}\tfrac{\partial}{\partial(kr)}[(kr)j_l(kr)]\tfrac{\partial Y_{lm}}{\partial\vartheta} \\
H_\varphi &= \tfrac{k}{r\sin\vartheta}\tfrac{\partial}{\partial(kr)}[(kr)j_l(kr)]\tfrac{\partial Y_{lm}}{\partial\varphi}
\end{aligned}\right\} \tag{1.25}$$

for TE modes and

$$\left.\begin{aligned} E_r &= \tfrac{k^2}{r^2} l(l+1)[(kr)j_l(kr)]Y_{lm} \\ E_\vartheta &= \tfrac{k}{r}\tfrac{\partial}{\partial(kr)}[(kr)j_l(kr)]\tfrac{\partial Y_{lm}}{\partial \vartheta} \\ E_\varphi &= \tfrac{k}{r\sin\vartheta}\tfrac{\partial}{\partial(kr)}[(kr)j_l(kr)]\tfrac{\partial Y_{lm}}{\partial \varphi} \\ H_r &= 0 \\ H_\vartheta &= \tfrac{i\omega\varepsilon}{r\sin\vartheta}[(kr)j_l(kr)]\tfrac{\partial Y_{lm}}{\partial \varphi} \\ H_\varphi &= -\tfrac{i\omega\varepsilon}{r}[(kr)j_l(kr)]\tfrac{\partial Y_{lm}}{\partial \vartheta} \end{aligned}\right\} \tag{1.26}$$

for TM modes, with $\vec{B} = \mu_0\mu_r \cdot \vec{H}$ for an isotropic and homogenous material.

To remove the arbitrariness of the eigenvalue k, specific boundary conditions need to be imposed.

For the case of interest here, we assume that the internal surface of the cavity is perfectly electrical conductive, with the implication that $\vec{E}$ must be normal and $\vec{B}$ tangential to the internal surface of the resonator. In fact this corresponds to assuming total reflection of the electromagnetic field from its interaction with the cavity surface.

Thus, to satisfy the boundary conditions, it is necessary that $E_\vartheta = E_\varphi = 0$ at the surface where $r = a$. This requires that:

$$j_l(ka) = 0 \qquad \text{from TE modes} \tag{1.27}$$

$$\frac{\partial}{\partial(kr)}[(kr)j_l(kr)]\Big|_{r=a} = 0 \qquad \text{from TM modes} \tag{1.28}$$

Finally, the permitted values of the propagation constant k, an infinite discrete set corresponding to the successive roots of Eqs. (1.27) and (1.28), determine the values of the resonant frequencies. In fact, recalling that $k = \omega/c$ and that $\omega = 2\pi f$, the unperturbed electromagnetic resonance frequencies can be written as:

$$f_{ln} = \frac{\xi_{ln} c}{2\pi a} \tag{1.29}$$

where $\xi = ka$ are the eigenvalues of the Helmholtz equation (Eq. (1.21)).

The index l refers to the order of the spherical Bessel function, while n is an integer denoting the rank of the roots of Eq. (1.27) and (1.28) for a given value of l. Instead m is the periodicity in the φ direction.

The field vanishes if $l = 0$, hence this does not correspond to an allowed mode. The lowest resonant frequency for either the TE or TM modes occurs when $l = n = 1$. The corresponding roots of Eqs. (1.27) and (1.28) are $\xi_{1,1} = 4.49$ for the TE mode and $\xi_{1,1} = 2.74$ for the TM mode.

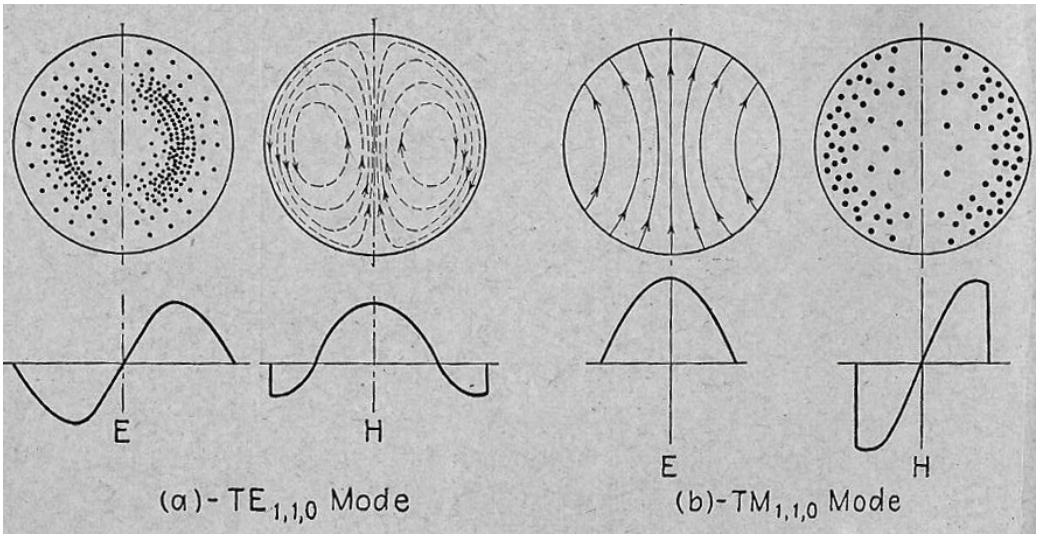

Figure 1.1: Electric and magnetic field distributions of the $TE_{1,1,0}$ and $TM_{1,1,0}$ modes in the meridian plane of a spherical resonator [19]. The electric and magnetic intensities for either mode are in time quadrature. For the TE mode, the current flows in a direction perpendicular to H_φ. For the TM mode, the magnetic lines are parallel to the equator and hence the current flows along the meridian lines from pole to pole.

Since the resonant frequency f_{ln} is independent of the integer m (see Eq. (1.29)), there are degeneracies (same resonant frequencies) among the modes. More precisely electromagnetic modes are $(2l + 1)$-fold degenerate. For example, the three lowest-order $(l = 1, n = 1)$ TE modes have the same mode patterns except that they are rotated 90° in space from each other. The situation for TM modes is analogous.

1.3 Perturbation model for a quasi-spherical resonator (QSR)

Such degeneracy limits the precision and accuracy achievable in the experimental determination of the resonance frequencies of a spherical resonator. In fact, the current limits of machining technology, inevitably lead to shape defects which slightly separate the single components of the multiplet eigenfunction complicating their accurate determination.

To obviate this problem, the realisation and practical use of quasi-spherical resonators (QSRs) became a commonly adopted strategy. The shape of QSRs differs on purpose slightly from a perfect spherical geometry. In this way advantages of perfect spherical resonators are retained, while the geometrical symmetry is broken and the degeneracy of the electromagnetic resonance frequencies is partially or completly lifted. For example in a QSR all the components of the $l = 1$ microwave resonances are resolved and this is the reason why, for simplicity, it is common practice to consider only the triply-degenerate $l = 1$ modes.

The precision achievable in interpolating degenerate microwave modes is favoured by achieving sufficient separation of the single components. Volume-preserving shape deformations of a perfect spherical cavity let to split degenerate modes while limit their effect on non-degenerate modes and on the mean frequency of any multiplet to simple frequency perturbations.

The splitting of the components of the TM and TE modes depends on two parameters (ϵ_1 and ϵ_2), that characterise how the quasi-spherical cavity departs from a perfectly spherical one.

The eingenvalues of a QSR usually differ from the corresponding eigenvalues ξ_{ln} of a reference spherical resonator with the same volume by an amount of order ϵ with $\epsilon \ll 1$ and the mean eigenvalue of any multiplet differs from ξ_{ln} by an amount of order ϵ^2.

So, at first order in ϵ_1 and ϵ_2, the mean eigenvalue of any multiplet coincides with that of a reference perfectly spherical cavity having the same volume.

For a triaxial ellipsoidal resonator with axes a, $a(1+\epsilon_1)$ and $a(1+\epsilon_2)$, its internal shape is defined by the equation:

$$\frac{x^2}{a^2(1+\epsilon_2)^2} + \frac{y^2}{a^2} + \frac{z^2}{a^2(1+\epsilon_1)^2} = 1 \tag{1.30}$$

with $0 < (\epsilon_1, \epsilon_2) \ll 1$. The presence of three axes of different lenght results in unequal frequency perturbations to the single components of the modes

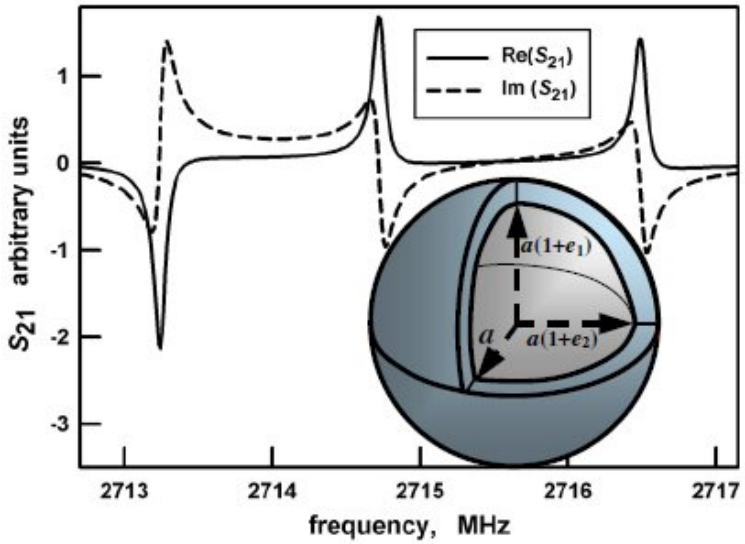

Figure 1.2: Triaxial ellipsoidal resonator and resolution of the three components of a microwave resonance with $l = 1$ [14].

[11]:

$$\frac{f_\zeta - f_0}{f_0} = \frac{2}{15}\Big[-\frac{1}{2} - \frac{3}{(\xi_{1n})^2 - 2}\Big] \begin{cases} (-2\epsilon_1 + \epsilon_2) & \zeta = z, \\ (\epsilon_1 + \epsilon_2) & \zeta = y, \\ (\epsilon_1 - 2\epsilon_2) & \zeta = x, \end{cases} \tag{1.31}$$

where f_0 is the unperturbed resonance frequency (see Eq. (1.29)), ξ_{1n} are the Bessel function zeros (see Eqs. (1.27) and (1.28)) of a perfect spherical cavity having the same volume of the quasi-spherical resonator:

$$a_{\text{eq}} = a\Big[(1+\epsilon_1)(1+\epsilon_2)\Big]^{1/3} \tag{1.32}$$

and ζ represents the rotational symmetry axis of the mode components.

Eq. (1.31) is valid for the TM1n modes, while for the TE1n modes the equation is the same except for the prefactor in square brackets, which is replaced by $-1/2$. This equation, correct at first order in ϵ_1 and ϵ_2, indicates that the mean frequency $\langle f_{ln} \rangle$ of a TM1n or TE1n triplet is not affected by the shape deformation and it coincides with the unperturbed frequency f_0:

$$\langle f_{1n} \rangle = \frac{1}{3}(f_x + f_y + f_z) = f_0 = \frac{\xi_{1n} c}{2\pi a_{\text{eq}}}. \tag{1.33}$$

If a better accuracy is wanted, frequency perturbation at second order in ϵ_1 and ϵ_2 has to be calculated [10]. For a triaxial ellipsoid it is expressed as:

$$\frac{f_\zeta^2 - f_0^2}{f_0^2} = A_{1,\zeta}\epsilon_1 + A_{2,\zeta}\epsilon_2 + B_{11,\zeta}\epsilon_1^2 + B_{12,\zeta}\epsilon_1\epsilon_2 + B_{22,\zeta}\epsilon_2^2 + O(\epsilon^3) \quad (1.34)$$

where $O(\epsilon^3)$ means any combination of terms $\epsilon_1^p\epsilon_2^q$ with $p+q=3$ and ζ is x, y or z. When the mean frequency of an electromagnetic triplets is considered, linear terms sum to zero as observed above referring to Eq. (1.31) and the mean frequency perturbation at second order in ϵ_1 and ϵ_2 becomes:

$$\left\langle \frac{f_\zeta^2 - f_0^2}{f_0^2} \right\rangle_{1n} = \frac{2(33\xi_{1n}^8 - 245\xi_{1n}^6 + 714\xi_{1n}^4 - 1152\xi_{1n}^2 + 160)}{1125(\xi_{1n}^2 - 2)^3}(\epsilon_1^2 - \epsilon_1\epsilon_2 + \epsilon_2^2) + O(\epsilon^3) \quad (1.35)$$

for TM1n modes, and:

$$\left\langle \frac{f_\zeta^2 - f_0^2}{f_0^2} \right\rangle_{1n} = \left[\frac{22\xi_{1n}^2}{375} - \frac{2}{225}\right](\epsilon_1^2 - \epsilon_1\epsilon_2 + \epsilon_2^2) + O(\epsilon^3) \quad (1.36)$$

for TE1n modes.

Values of ϵ_1 and ϵ_2 can be determined from microwave measurements solving Eqs. (1.35) and (1.36) or Eq. (1.31), if perturbation at first order is considered, and compared with values independently determined analysing the resonator shape obtained with coordinate measuring machine (CMM) measurements. In this way, ϵ_1 and ϵ_2 has not to be known independently. Once their values are obtained, corrections to the eigenvalues ξ_{1n} necessary to cancel the perturbative effect due to shape deformations can be calculated.

These corrections are indispensable when the highest accuracy is desirable, such as in experiments for the determination of the Boltzmann constant, but in this work context their effect is completly negligible, as it will be discussed further. In fact, aside from the shape perturbation, the cavity eigenfrequencies are subject to additional perturbations due, for example, to the finite electrical conductivity of the cavity material or the coupling waveguides.

1.4 Perturbative phenomena

1.4.1 Skin effect

Resonators are usually machined from metals, whose electrical conductivity is high but finite. As a consequence, an energy loss mechanism takes place. In fact, because the boundary surface is an imperfect conductor, the electromagnetic fields at the inner surface penetrate into the metal for a short lenght, causing a shift in the eigenfrequencies and a broadening of the resonances through resistive losses. This phenomenon is called "skin effect".

The energy loss is proportional to the penetration of the field within the wall of the resonator. The electrical penetration or skin-depth δ equals:

$$\delta = \frac{1}{\sqrt{\pi \mu_\mathrm{r} \mu_0 \sigma_\mathrm{cond} f}} \tag{1.37}$$

where σ_cond is the electrical conductivity and μ_r the relative magnetic permeability of the cavity surface.

Thus, in the real case, eigenfrequencies are described by a complex expression as $F = f + ig$, where f is the resonance frequency as in Eq. (1.29), while g is the half-width, which represents the enlargement of the ideal resonance. The perturbation on f due to the skin effect can be summarized for TE modes by the formula:

$$\left(\frac{\Delta f_\mathrm{skin} + ig}{f}\right)_{ln}^{\mathrm{TE}} = \frac{\delta}{2a}(-1+i) \tag{1.38}$$

and for TM modes by the formula:

$$\left(\frac{\Delta f_\mathrm{skin} + ig}{f}\right)_{ln}^{\mathrm{TE}} = \frac{\delta}{2a}(-1+i)\frac{(\xi_{ln}^{\mathrm{TM}})^2}{(\xi_{ln}^{\mathrm{TM}})^2 - l(l+1)}. \tag{1.39}$$

To obtain the right values of the resonance frequencies of the cavity, the conductivity perturbation Δf_skin must be added to the measured frequency values f_exp as follows:

$$f = f_\mathrm{exp} + \Delta f_\mathrm{skin}. \tag{1.40}$$

Moreover, observing Eqs. (1.38) and (1.39), the relation $\Delta f_\mathrm{skin} = -g$ becomes evident, which suggests that the conductivity correction can either be calculated with literature μ_r and σ_cond values appropriate to the cavity

material, or obtained experimentally by measuring the half-widths of the modes.

1.4.2 Waveguide perturbations

An other phenomenon to take in account is the perturbing effect of ducts and waveguides in the cavity boundary. The waveguides used to couple electromagnetic energy into and out of the QSR, in fact, perturb the resonator eigenfrequencies even if by a small amount. This effect has been investigated by Underwood et al. [20] both theoretically and experimentally. The model worked out supposes that waveguide used consists of a cylindrical hole in the wall of the cavity into which a partially stripped straight length of semi-rigid coaxial cable is placed and that antennae are flush with the interior surface of the cavity. Due to this type of waveguide, the mean eigenfrequency perturbation to a TM1n triplet is:

$$\left\langle \frac{\Delta f}{f} \right\rangle_{\mathrm{TM}1n} \approx -\frac{r^3}{4\pi a_{\mathrm{eq}}^3} \cdot \frac{0.905(\xi_{1n}^{\mathrm{TM}})^2 - 0.728}{(\xi_{1n}^{\mathrm{TM}})^2 - 2} \tag{1.41}$$

while to a TE1n triplet is:

$$\left\langle \frac{\Delta f}{f} \right\rangle_{\mathrm{TE}1n} \approx -\frac{r^3}{4\pi a_{\mathrm{eq}}^3} \cdot 0.905 \tag{1.42}$$

where r is the radius of the hole in the resonator wall.

The mean perturbation is independent of the hole position on the QSR surface, and also independent of the eigenvalue ξ_{1n}, in the case of the TE1n modes. The perturbation to the TM1n modes rapidly approaches that of the TE1n modes with increasing ξ.

1.5 Resonator in hygrometry

Instrumentation and sensors for hygrometric applications based on the measurement of gaseous mixture relative permittivity or refractive index have been proposed before [21,22], although only recently advances concerning an accurate and independent measurement of the dielectric properties of substances commonly used in hygrometry, such as the dielectric permittivity [23,24] or the zero-density limit of the molar polarizability of argon, nitrogen and oxygen, became available.

Also microwave techniques for the measurement of the humidity of gaseous media have been proposed before. For example, Hasegawa and Stokesberry wrote about a microwave hygrometer used to measure humidity of atmospheric air [21].

Moreover, QSRs capability in the determination of the permittivity of pure gases has been widely demonstrated [15], also comparing their performance to that of cross capacitors [23]. Respect to them, resonant cavities demonstrated to have several advantages as, for example, to permit the measurement of frequency ratios better than 0.01 ppm, where a capacitance ratio can be measured only to about 1 ppm with commercially available bridges.

Due to the above mentioned reasons we decided to follow an idea of Huang and Moldover [17] and to put to the test the potential of a quasi-spherical microwave resonator when used as an hygrometer. Huang and Moldover used in their experiments a re-entrant cavity resonator, while we use a QSR. We believe in the high accuracy reachable with this kind of instrument thanks to a well established experimental practice and theoretical models and we bet on its accuracy both when used for the measurement of the water vapour mole fraction in humid gases, and when used as a condensation hygrometer for the measurement of the dew-point temperature.

1.5.1 Molar polarizability and dielectric permittivity

Several electrical properties of molecules depend on the competing influences of nuclei with different charges or the competition between the control exercised by a nucleus and the influence of an externally applied field. This competition results in an electric dipole moment in the first case or in properties such as refractive index in the second one.

Polar molecules, as in the case of water, have a permanent electric dipole moment, which is temporarily modified when an electric field is applied. If the sample is an isotropic fluid, the polarization, which is the dielectric dipole moment density, is zero in absence of an applied field, because molecules adopt random orientations, while it is different from zero in presence of a field, because dipoles become partially aligned. [25].

Molar polarizability $\wp(\rho, T)$ relates in a quantitative way the relative permittivity $\varepsilon_{\mathrm{r}}(p, T)$ or dielectric constant, of a medium with the molar density ρ of the sample and the electric properties of the molecules.

For a nonpolar fluid this relation is expressed by the Clausius-Mossotti equation:

$$\wp = \frac{\varepsilon_{\mathrm{r}} - 1}{\varepsilon_{\mathrm{r}} + 2} \frac{1}{\rho} \tag{1.43}$$

where ρ is the molar density. For small, non-polar molecules, the molar polarizability is nearly independent of temperature. For polar molecules, the temperature dependence of the molar polarizability becomes significant and the following expansion holds, called the virial expansion:

$$\wp(\rho, T) = \left(\frac{\varepsilon_\mathrm{r} - 1}{\varepsilon_\mathrm{r} + 2}\right)\frac{1}{\rho} = A_\varepsilon[1 + b_\varepsilon(T)\rho + c_\varepsilon(T)\rho^2 + ...] \tag{1.44}$$

where A_ε is the molar polarizability in the limit of zero pressure and b_ε and c_ε are the second and third dielectric virial coefficients respectively.

At low densities, $\wp$ is approximated by the Debye equation:

$$\wp = \frac{4\pi N_\mathrm{A}}{3}\left[\alpha + \frac{\mu^2}{3k_\mathrm{B}T}\right] \tag{1.45}$$

where α is the molecular polarizability and μ the dipole moment [26], N_A is the Avogadro's constant and k_B the Boltzmann constant.

1.5.2 Refractive index microwave hygrometry

Using a simple mixing rule, the molar polarizability $\wp_\mathrm{mix}$ of a mixture can be written as [27]:

$$\wp_\mathrm{mix} = \sum_i x_i \wp_i \tag{1.46}$$

where $\wp_i$ is the molar polarizability of pure component i and x_i is the corresponding mole fraction. The validity of this simplifying assumption, for a mixture whose components differ greatly in volatility, has been recently discussed [28]. For the mixtures (H_2O/N_2 and H_2O/air) of interest in this work and the application considered, $\wp_i$ can be assumed to be independent of density, with the exception of the water vapor, whose polarizability $\wp_\mathrm{w}$ is temperature dependent and indicated in a contracted form of Eq. (1.45) as:

$$\wp_\mathrm{w} = A_\mathrm{w} + \frac{B_\mathrm{w}}{T} \tag{1.47}$$

with the value of the Debye constants A_w and B_w given by a few dated experimental results [21]. Considered these assumptions, the Clausius-Mossotti equation for a mixture can be re-written and conveniently approximated as

$$\varepsilon_\mathrm{mix} = \frac{2\rho_\mathrm{mix}\wp_\mathrm{mix} + 1}{1 - \rho_\mathrm{mix}\wp_\mathrm{mix}} \tag{1.48}$$

where the molar density of the mixture ρ_{mix} is approximated from the truncated density virial equation as:

$$\rho_{\mathrm{mix}} = \frac{\rho_0}{1 + B_{\mathrm{mix}}\rho_0} \tag{1.49}$$

with

$$\rho_0 = \frac{p}{RT} \tag{1.50}$$

where R is the molar gas constant.

The virial expansion of the pressure as a function of the density ρ and temperature T is in fact:

$$p = \rho RT(1 + B(T)\rho + C(T)\rho^2 + ...) \tag{1.51}$$

where $B(T)$ and $C(T)$ are the second and the third density virial coefficients.

It is convenient to treat both the systems considered, humid nitrogen and humid air, as binary humid mixtures of water vapor (w) and a dry component (d). Also the composition of air is intended as CO_2-free, having the standard molar fractions of nitrogen, oxygen and argon usually assumed in thermodynamic formulation [29].

For binary mixtures, the second density virial coefficient B_{mix} is calculated from the mixing rule [30]:

$$B_{\mathrm{mix}} = x_{\mathrm{w}}^2 B_{\mathrm{w}} + 2x_{\mathrm{w}}x_{\mathrm{d}}B_{\mathrm{wd}} + x_{\mathrm{d}}^2 B_{\mathrm{d}}. \tag{1.52}$$

In Eq. (1.52) $x_{\mathrm{d}} = 1 - x_{\mathrm{w}}$, B_{w} is the second virial coefficient relating to interactions between two water molecules, B_{wd} is the second cross virial coefficient pertaining to interactions between one dry air/nitrogen and one water molecule, B_{d} is the second virial coefficient relating to interactions between two dry air/nitrogen molecules.

Thus, if an istrument is capable of an accurate measurement of the dielectric constant of a binary humid mixture, Eq. (1.48) may be solved to determine the water vapour mole fraction. In pursuing such a metrological application with a QSR, the value of the electrical and thermodynamic properties of dry air, nitrogen and water are needed as input quantities, while $\varepsilon_{\mathrm{mix}}$ can be experimentally obtained, assuming that the mixture constituents are non-magnetic, using the following relation:

$$\varepsilon_{\mathrm{mix}} = \left(\frac{f_0}{f}\right)^2 = n_{\mathrm{mix}}^2 \tag{1.53}$$

where f_0 and f are the resonance frequencies of the cavity alternatively in vacuum or filled with the mixture at the same temperature at a total pressure p.

This relation is obtained considering that, from Eq. (1.29), we can write:

$$\frac{f_0}{f} = \frac{\frac{\xi c_0}{2\pi a}}{\frac{\xi c}{2\pi a}} \simeq \frac{c_0}{c} = n_{\mathrm{mix}} \tag{1.54}$$

where c_0 is the speed of light in vacuum and c is the speed of light in the mixture, and that the refraction index and the relative permittivity are linked by the following relation:

$$n_{\mathrm{mix}} = \sqrt{\varepsilon_{\mathrm{mix}} \mu_{\mathrm{mix}}} \tag{1.55}$$

where the relative magnetic susceptibility of the mixture μ_{mix} may be approximated by unity.

Solving Eq. (1.48),the water vapour mole fraction x_{w} may be obtained.

The value of x_{w} is the only physically motivated solution of the equation $a_2 x_{\mathrm{w}}^2 + a_1 x_{\mathrm{w}} + a_0 = 0$, with

$$\begin{aligned} a_2 &= m(B_{\mathrm{w}} - 2B_{\mathrm{wd}} + B_{\mathrm{d}}), && (1.56)\\ a_1 &= 2m(B_{\mathrm{wd}} - B_{\mathrm{d}}) - \wp_{\mathrm{w}} + \wp_{\mathrm{d}}, && (1.57)\\ a_0 &= m(B_{\mathrm{d}} + \rho_0^{-1}) - \wp_{\mathrm{d}}, && (1.58) \end{aligned}$$

where $m = (\varepsilon_{\mathrm{mix}} - 1)/(\varepsilon_{\mathrm{mix}} + 2)$. In this study, second virial coefficients B_{d} of dry air and nitrogen as a function of temperature were calculated from the corresponding wide-range Helmholtz free-energy formulations [29,31]; the second virial cooefficient of water B_{w} can be retrieved from a similar formulation [32]; the cross-second virial coefficient B_{wd} of the air-water and nitrogen-water systems were calculated by Harvey and Huang [33]. Finally, the molar polarizabilities $\wp_{\mathrm{d}}$ of nitrogen and the other constituents of dry standard air are available from recent accurate measurements with cross-capacitors [23].

1.5.3 Microwave condensation hygrometry: theoretical basis

While the refractive index and the speed of light of both pure gases and mixtures are function of density, composition and frequency, the cavity internal dimension varies as a function of the temperature and pressure due to thermal expansion and elastic compression of the shell. However, even by keeping into account this variability, the ratio of two normal modes of the resonator, for example a TM1n and a TE1n mode, is invariant and simply equal to the ratio of the corresponding eigenvalues:

$$\frac{\langle f_{1n}^{\mathrm{TM}} \rangle}{\langle f_{1n}^{\mathrm{TE}} \rangle} = \frac{(ka)_{1n}^{\mathrm{TM}}}{(ka)_{1n}^{\mathrm{TE}}}. \tag{1.59}$$

Instead, when water condenses on the resonator surface, the effect on the mode frequencies is different depending on the mode simmetry and the ratio of two normal modes of the cavity is no longer constant. This difference may be exploited to reveal the onset of this phenomenon.

The principal of a dew-point hygrometer is the formation of condensed water on a surface. The frequency shift Δf_{d} due to a small volume ΔV of dielectric material in a cavity can be approximated using perturbation theory:

$$\frac{\Delta f_{\mathrm{d}}}{f} \simeq -\frac{\int_{\Delta V} \Delta\varepsilon \vec{E}_{\mathrm{int}} \cdot \vec{E}_0^* \mathrm{d}V}{2\int_{V_0} \varepsilon_0 |E_0|^2 \mathrm{d}V} \tag{1.60}$$

where $\vec{E}_{\mathrm{int}}$ is the electric field within ΔV, $\vec{E}_0$ is the unperturbed cavity field, V_0 is the volume of the cavity and $\Delta\varepsilon = \varepsilon_0(\varepsilon_{\mathrm{r}} - 1)$ is the difference in permittivity between the gas in the cavity (ε_0) and the dielectric material (ε_{r}). If the droplet is modeled as a small slab [20], using a quasi-static approximation, the fields in the slab are $\vec{E}_{\mathrm{int}} = \vec{E}_{\mathrm{n,b}}/\varepsilon_{\mathrm{r}}$, where $\vec{E}_{\mathrm{n,b}}$ is the normal electric field at the boundary of the resonator [34]. So Eq. (1.60) becomes:

$$\frac{\Delta f_{\mathrm{d}}}{f} \simeq -\Delta V \Big(\frac{\varepsilon_{\mathrm{r}} - 1}{\varepsilon_{\mathrm{r}}}\Big) \frac{|E_{\mathrm{n,b}}|^2}{2\int_{V_0} |E_0|^2 \mathrm{d}V}. \tag{1.61}$$

Formulae for the ratio of boundary-to volume fields of the TM1n and TE1n modes are given, for example, in Underwood et al. [35]. For the

TE1n modes $\vec{E}_{\mathrm{n,b}} = 0$ and so $\langle \Delta f_{\mathrm{d}} \rangle_{\mathrm{TE}} = 0$, meaning that the TE1$n$ mode frequencies are not affected by the droplet.

For the TM1n modes, the perturbations to the three components that comprise the triplet are:

$$\frac{\Delta f_{\mathrm{d}}}{f} \simeq -\Delta V \Big(\frac{\varepsilon_{\mathrm{r}} - 1}{\varepsilon_{\mathrm{r}}} \Big) \frac{3}{2\pi a^3 [((ka)_{1n}^{\mathrm{TM}})^2 - 2]} \begin{cases} \sin^2 \vartheta \sin^2 \varphi, \\ \cos^2 \vartheta, \\ \sin^2 \vartheta \cos^2 \varphi. \end{cases} \tag{1.62}$$

The magnitude of the frequency perturbation Δf_{d} depends on the position of the droplet on the resonator surface. Moreover if the layer of condensate water is uniform on the resonator surface, Eq. (1.62) foresees equal perturbations for two of the three components of the mode.

However, the mean perturbation $\langle \Delta f_{\mathrm{d}} \rangle$ is independent of position:

$$\frac{\langle \Delta f_{\mathrm{d}} \rangle}{f} \simeq -\Delta V \Big(\frac{\varepsilon_{\mathrm{r}} - 1}{\varepsilon_{\mathrm{r}}} \Big) \frac{1}{2\pi a^3 [((ka)_{1n}^{\mathrm{TM}})^2 - 2]}. \tag{1.63}$$

This equation gives the frequency shift due to a single droplet. Since the fields external to ΔV are unaltered, the effect of many droplets will be cumulative, that means $\langle \Delta f_{\mathrm{d}} \rangle \propto V$, where $V = \sum_{i=0}^{\infty} \Delta V_i$.

Measurement of the droplet perturbation $\langle \Delta f_{\mathrm{d}} \rangle$ is difficult, as it is usually much smaller than the variations in mode frequency associated with temperature, pressure and gas composition. This difficulty is overcome by using the result that f_i / f_j is constant (see Eq.(1. 59)) and that $\langle \Delta f_{\mathrm{d}} \rangle_{\mathrm{TE}} = 0$ to express $\langle \Delta f_{\mathrm{d}} \rangle$ in terms of the ratio $\langle f_{1n}^{\mathrm{TM}} \rangle / \langle f_{1n}^{\mathrm{TE}} \rangle$:

$$\frac{\langle f_{1n}^{\mathrm{TM}} \rangle}{\langle f_{1n}^{\mathrm{TE}} \rangle} \approx \frac{\langle f_{1n}^{\mathrm{TM}} \rangle}{\langle f_{1n}^{\mathrm{TE}} \rangle}\Big|_{V=0} + \frac{\langle \Delta f_{\mathrm{d}} \rangle}{\langle f_{1n}^{\mathrm{TE}} \rangle} \tag{1.64}$$

where the subscript $V = 0$ denotes the frequency ratio in "dry" conditions. Combining this with Eq. (1.63), we have an expression for the total volume of water in the resonator:

$$\Delta V \approx \Big(\frac{\langle f_{1n}^{\mathrm{TM}} \rangle}{\langle f_{1n}^{\mathrm{TE}} \rangle}\Big|_{V=0} \frac{\langle f_{1n}^{\mathrm{TE}} \rangle}{\langle f_{1n}^{\mathrm{TM}} \rangle} - 1 \Big) 2\pi a^3 \Big[\Big((ka)_{1n}^{\mathrm{TM}} \Big)^2 - 2 \Big] \frac{\varepsilon_{\mathrm{r}}}{\varepsilon_{\mathrm{r}} - 1}. \tag{1.65}$$

The last equation forms the basis of our microwave condensation hygrometry technique and serves to highlight some of the potential advantages of this method, which will be discussed in Chapter 5.

Chapter 2

Measurement method and preliminary characterisation of the apparatus

2.1 Basic design features of the QSR used in this work

The resonator used in this work is a maraging steel (VascoMax C-300) triaxial ellipsoidal cavity with an internal volume of about 69 cm^3. Maraging steel was chosen because of its high degree of hardness, strength and toughness. The cavity was originally designed and realised at NIST using conventional workshop techniques (the required tolerance was rather low, in the order of 0.01 mm) and was loaned to INRiM by courtesy of the Process Measurements Division.

The three inner semi-axes of the resonator are nominally equal to a, $a(1+\epsilon_1)$ and $a(1+\epsilon_2)$. The value of the cavity radius a is $a = 25.4$ mm, while ϵ_1 and ϵ_2, the two geometrical parameters which determine the deviations of the cavity shape from sphericity, are $\epsilon_1 = 0.001$ and $\epsilon_2 = 0.003$. The unequal axes of the cavity let to split the triply degenerate microwave resonance frequencies of a sphere into three non-overlapping peaks, allowing to achieve a more accurate determination of the corresponding frequencies. Figure 2.1 shows the original drawings prepared for machining the resonator at NIST.

The cavity surface was electro-plated with a 10 μm thick layer of gold to enhance the resonance quality factors and increase its chemical inertness, making it suitable for measurements with humid mixtures or even pure water vapour over a wide pressure and temperature range. A total of four holes with a diameter of 2.3 mm were machined through the shell; two of these holes

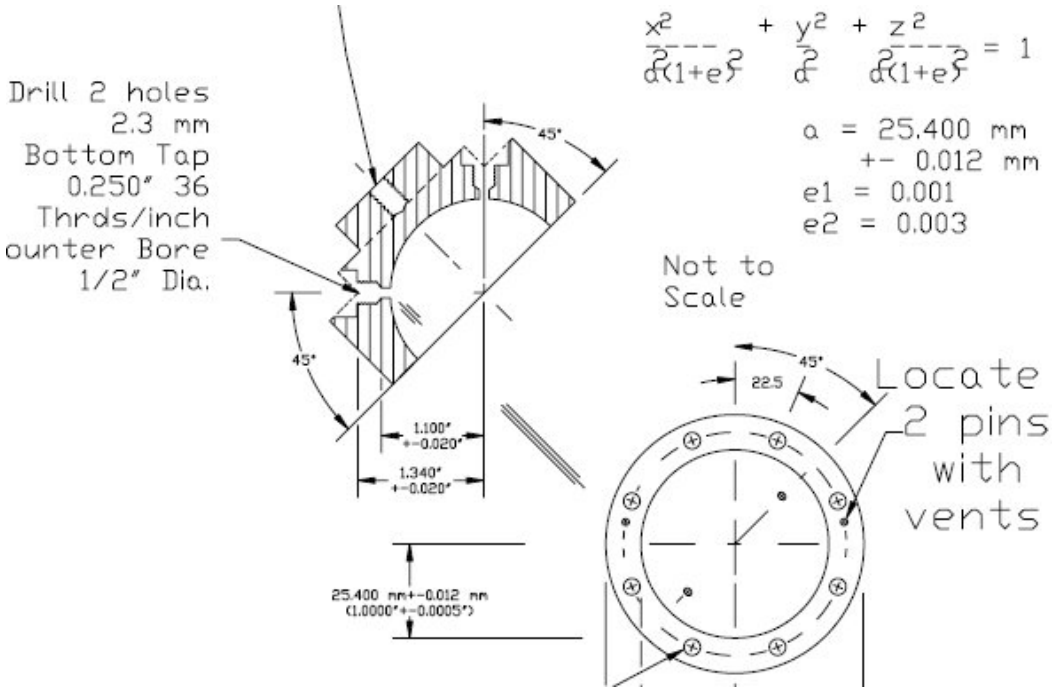

Figure 2.1: Schematic plot of the dimension and mechanical features of the triaxial ellipsoidal resonator used in this work.

were used to mount electromagnetic loop probes which allow the excitation and detection of both classes of TM and TE modes. Two additional holes were left open and served as gas inlet-outlet.

Figure 2.2 shows the interior of the two hemispheres of the cavity, while Figure 2.3 shows the assembled resonator with the two antennas inserted in the north hemisphere.

Figure 2.2: Image of the interior cavity surface of the resonator.

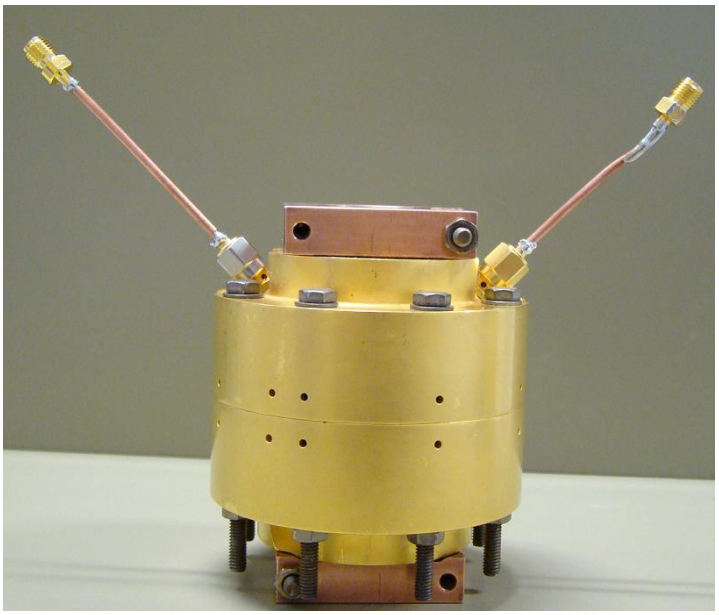

Figure 2.3: Assembled resonator with two antennas.

2.2 Measurement and analysis of microwave resonances

Once the resonator was assembled and the two hemispheres were tightly bolted together, loop antennas were inserted inside the cavity. Antennas were connected to the ports of a network analyser by using flexible microwave cables. In order to achieve sufficient excitation and detection of the microwave resonances, the central conductor of the cables was extended by passing it through the front hole of the ducts in the antenna housings, using a short section of insulated copper wire. The wire was coiled in multiple turns to form the loop antenna and positioned as close as possible to the front surface of the housing.

Coupling to the normal component of the electric field within the QSR, probes perturb resonant frequencies and their widths. In fact the presence of antennas causes a shape perturbation due to the changes in the cavity boundary near the entrances and a variation in the resonance widths due to the transfer of power from the QSR to the associated electronics. To limit any such effect, the coupling of the probes was minimised. This means that, once the angular orientation of the loop probes was adjusted so that, for each mode monitored, the three components were excited with approximately equal magnitude, antennas were withdrawn slowly from the resonator while monitoring the halfwidths of the components of one of the mode measured, until half-widths stopped decreasing.

To determine the frequencies and half-widhts of each triplet, the network analyser was set to sweep through 201 discreet frequencies, spanning approximately 6 MHz centred around the average triplet frequency. In this way the resonace curves for each mode under study were recorded and fitted using the sum of three lorentzian functions plus a quadratic complex background, as reported in Eq. (2.1):

$$u + iv = \sum_{m=-1}^{1} \left[\frac{if A_{ln}^{m}}{\left(F_{ln}^{m}\right)^{2} - f^{2}} \right] + B + C\left(F_{ln}^{m} - f\right) \tag{2.1}$$

where A, B, C are complex constants and F_{ln}^{m} the three complex resonance frequencies to be determined by a fit procedure of experimental data acquired. The algorithm used for fitting is called Levenberg-Marquardt method.

Figure 2.4 displays the real and imaginary parts of the TM11 triplet recorded with our ellipsoidal cavity in air at 293 K, while the values of the

three peak frequencies and half-widhts with their uncertainties are reported in Table 2.1.

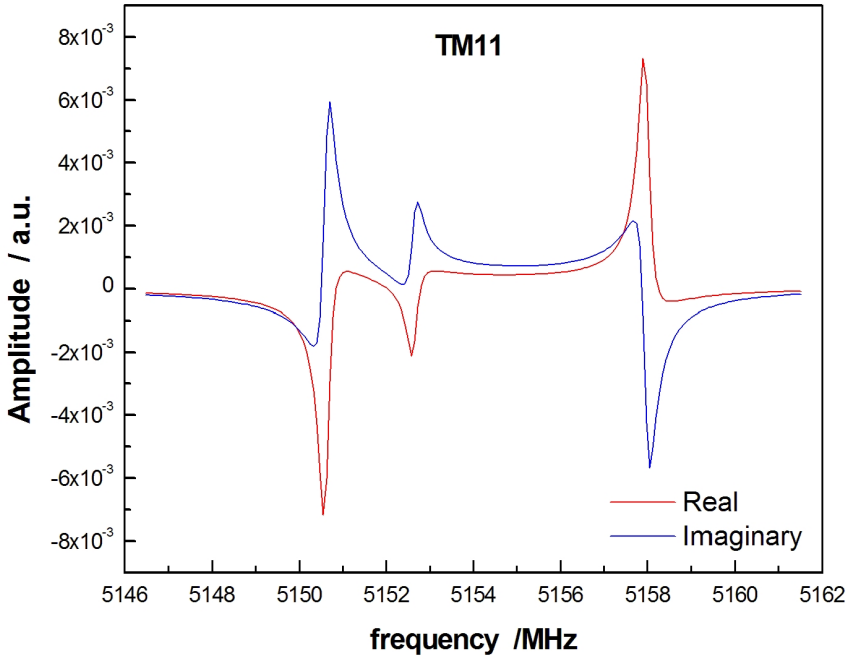

Figure 2.4: TM11 mode. The red line represents the real part of the resonance, while the blue one the imaginary part.

TM11 mode	value MHz	uncertainty MHz
f_x	5152.627	$9.883 \cdot 10^{-5}$
Δg_x	0.150	$9.883 \cdot 10^{-5}$
f_y	5150.607	$3.474 \cdot 10^{-5}$
Δg_y	0.151	$3.474 \cdot 10^{-5}$
f_z	5157.962	$3.461 \cdot 10^{-5}$
Δg_z	0.155	$3.461 \cdot 10^{-5}$

Table 2.1: Fit values of the three peak frequencies and half-widths Δg of the TM11 mode with uncertainties.

Separation among the three components of a TM1n or TE1n resonance frequency depends on the design values ϵ_1 and ϵ_2. In this case, where ϵ_2

is three times larger than ϵ_1, the experimental difference between the first and the third peak should be effectively about three times the difference between the first and the second peak. This kind of observation results useful in particular when the resonator is assembled. The best alignment of the hemispheres is obtained when the fractional frequency difference between the resolved components is minimized. Moreover, from the mode component splittings measured, it is possible to determine ϵ_1 and ϵ_2 values using Eq. (1.31) and compare the obtained experimental values with the theoretical ones.

Consider the TE11 resonance frequency modulo measured in vacuum at 290 K and shown in Figure 2.5.

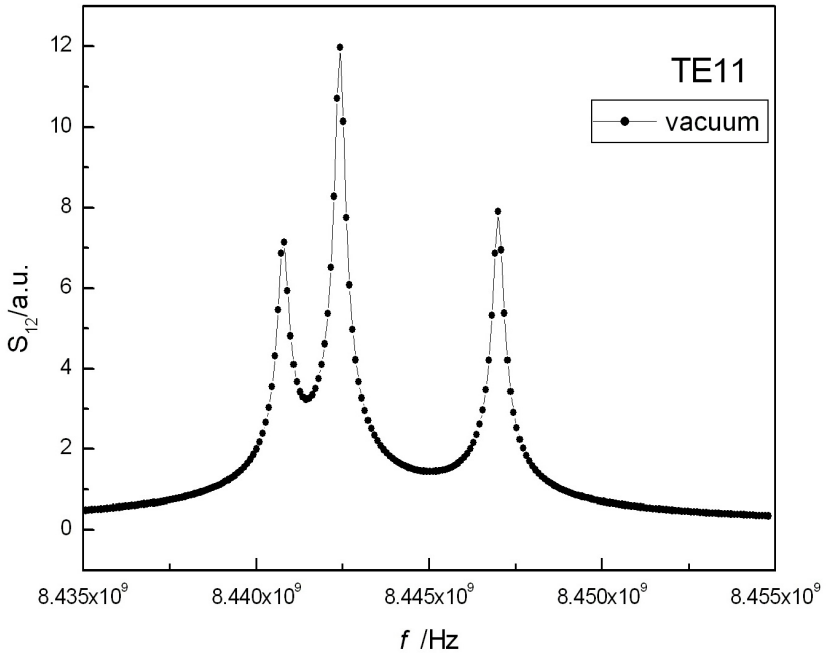

Figure 2.5: TE11 mode of the ellipsoidal cavity: triply degenerate microwave resonance splitted.

By defining the lowest f_1, intermediate f_2 and highest f_3 frequency components of the triplets, the fractional frequency splitting $\Delta f_{13}/\langle f\rangle = (f_3 - f_1)/\langle f\rangle$ results $7.37\cdot10^{-4}$, while $\Delta f_{12}/\langle f\rangle = (f_2 - f_1)/\langle f\rangle$ is $1.94\cdot10^{-4}$. Thus the difference between the first and the third peak is three times and half the difference between the first and the second peak. The measured splittings for the three measured modes are listed in Table 2.2, togheter with the values of ϵ_1 and ϵ_2 calculated from the measured splittings by inverting Eq. (1.31).

	TM11	TE11	TM12
$10^4 \cdot f_{13}/\langle f \rangle$	14.39	7.37	7.86
$10^4 \cdot f_{12}/\langle f \rangle$	3.96	1.94	2.26
$10^3 \cdot \epsilon_2$	3.45	3.69	3.36
$10^3 \cdot \epsilon_1$	0.95	0.97	0.97

Table 2.2: Measured fractional frequency splittings for the triplets TM11, TE11 and TM12 and corresponding values of ϵ_1 and ϵ_2 calculated using Eq. (1.31). These measurements were made in vacuum at 290 K.

The average values of ϵ_1 and ϵ_2 calculated from the peak splitting are $\epsilon_1 = (0.96 \pm 0.01) \cdot 10^{-3}$ and $\epsilon_2 = (3.50 \pm 0.12) \cdot 10^{-3}$. Thus the ϵ_1 and ϵ_2 values determined from microwave data are consistent with the design values. Moreover, analysing Eq. (1.31), it is apparent that, if for TE modes the separation among peaks is constant because it depends only on ϵ_1 and ϵ_2, for TM modes it changes from mode to mode due to its further dependence on mode eigenvalue ξ_{1n}.

An other aspect to consider is the half-width of the resonance frequencies. It is a good rule comparing the measured halfwidths $g_{\rm exp}$ with the same quantities $g_{\rm calc}$ calculated using literature values to understand if, apart from the skin effect, there are other energy loss mechanisms. In our case, if we consider literature values of the electrical resistivity of gold $\rho_{\rm Au} = [2.051 + 0.008T/(^\circ{\rm C})] \cdot 10^{-8}$ Ω·m [36], a satisfactory agreement is found between $g_{\rm exp}$ and $g_{\rm calc}$. In fact the relative excess halfwidths $\Delta g/\langle f \rangle = (\langle g_{\rm exp} \rangle - g_{\rm calc})/\langle f_{\rm exp} \rangle$ is found to be less than 2 ppm. This slight discrepancy is possibly due to a difference between the bulk resistivity $\rho_{\rm Au}$ and that of the electroplated cavity surface. For the three modes measured in vacuum at 290 K, in Table 2.3 the fractional excess half-widths are listed and plotted in Figure 2.6.

Mode	Fractional excess half-widths $10^6 \cdot (\langle g_{\rm exp} \rangle - g_{\rm calc})/\langle f_{\rm exp} \rangle$
TM11	1.98
TE11	1.93
TM12	0.95

Table 2.3: Fractional excess half-widths for the TM11, TE11 and TM12 triplets in vacuum at 290 K.

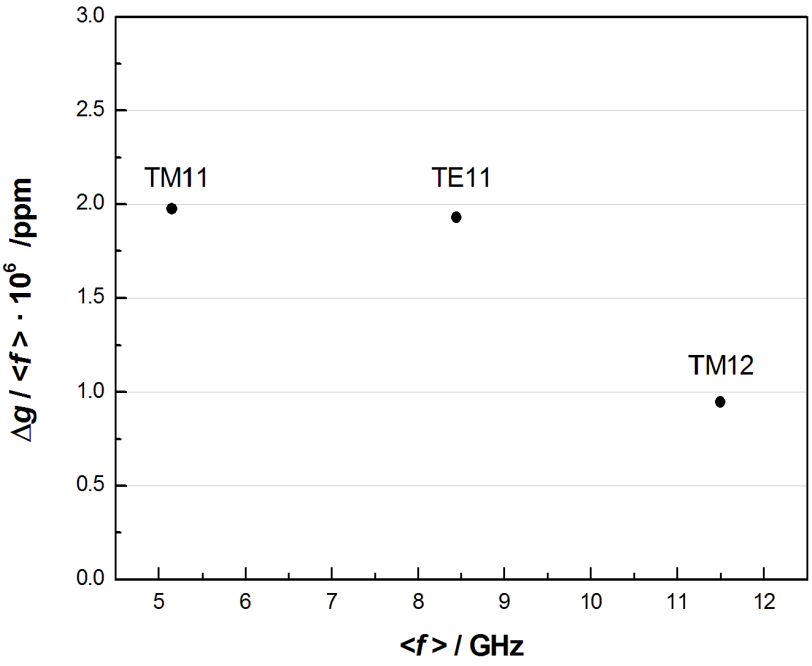

Figure 2.6: Fractional excess half-widths in ppm of the TM11, TE11 and TM12 triplets.

2.3 Preliminary measurements

The value of the cavity radius a is relative only to the specific conditions of temperature and pressure in which it was measured. Because experiments in humid mixtures would be realised over wide ranges of temperature and pressure, it was fundamental to characterise the cavity as a function of T and p.

The radius variation dependence on temperature is described by the thermal expansion coefficient of the material comprising the resonator, while the pressure dependence is given by the isothermal compressibility coefficient.

2.3.1 Thermal expansion coefficient

To estimate the thermal expansion coefficient α_{th} of the maraging steel shell, frequencies of three degenerate modes, TM11, TE11 and TM12, were measured in vacuum in the temperature range between 320 K and 460 K, approximately the range in which experiments in humid mixtures would be done.

With these measurements, an experimental determination of the cavity radius, to compare with the nominal one, was obtained. Moreover, a mode agreement evaluation about the cavity radius value was possible and the cavity thermal expansion coefficient was determined.

Modes were measured at seven temperatures and the radius values were obtained for each mode by inversion of Eq. (1.33), using the eigenvalues for the ellipsoid. Figure 2.7 shows obtained radius values.

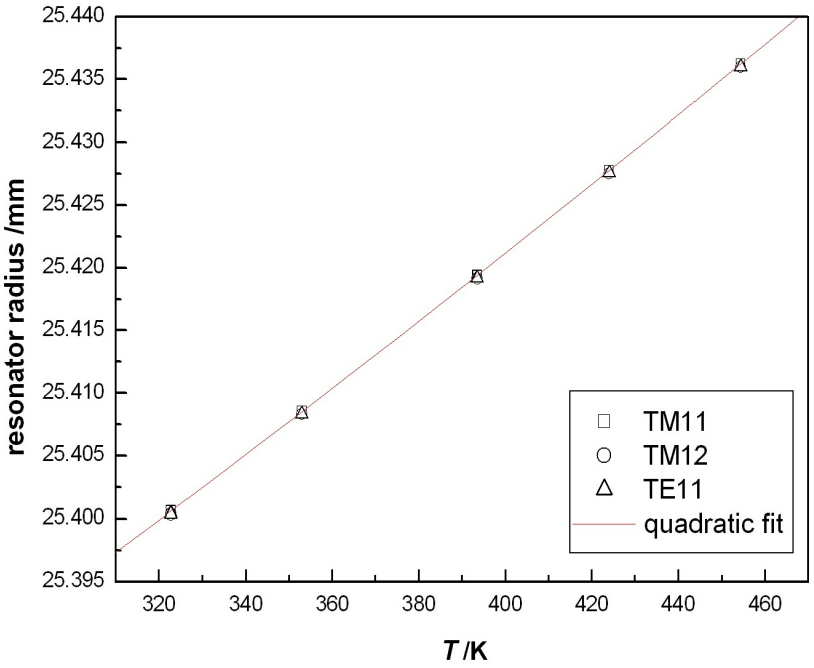

Figure 2.7: Dependence of the resonator radius on the temperature.

At each temperature the measured modes agree in the radius value and, fitting data with a quadratic curve ($y = A + Bx + Cx^2$), the cavity dimension dependence on the temperature is obtained. The dependence on temperature of the geometric dimensions of the cavity is given by Eq. (2.2):

$$V(T) = V(T_0)[1 + \beta\Delta T + \gamma(\Delta T)^2 + ...] \tag{2.2}$$

where $\Delta T = T - T_0$, V is the volume of the resonator at the temperature T and $V(T_0)$ is the volume at the temperature T_0, so, for the cavity radius, we can write :

$$a(T) = a(T_0)[1 + \alpha_{\text{th}}\Delta T + \lambda(\Delta T)^2 + ...]. \tag{2.3}$$

Combining Eq. (2.3) with the A and B parameter values obtained from the fitting procedure, the thermal expansion coefficient of the resonator is determined. The obtained value is $\alpha_{\text{th}} = (1.062 \pm 0.006) \cdot 10^{-5}$ K^{-1}, which is comparable with the tabulated value reported in the technical data sheet of the VascoMax C-300 maraging steel.

2.3.2 Isothermal compressibility coefficient

The isothermal compressibility coefficient k_T of the shell was estimated from measurements of the microwave frequencies in helium at 482 K in the pressure range between 0.1 MPa and 1.9 MPa and the literature theoretical values of $\varepsilon_{\text{He}}(p, T)$ [14].

Maintained the temperature constant at 482 K, modes were measured at nine different pressures. From Eq. (1.33), the radius values were obtained for each mode, exploiting the relations: $c_{\text{He}} = c_0/n_{\text{He}}$ and $n_{\text{He}} = \sqrt{\varepsilon_{\text{He}}}$, where c_{He} is the speed of light in helium, c_0 is the speed of light in vacuum, n_{He} is the refractive index of helium and ε_{He} is the helium dielectric relative permittivity obtained from accurate *ab initio* calculations [37,38].

The dependence of the cavity radius from the pressure p is shown in Figure 2.8.

Radius values determined with the TM11 mode results slightly larger ($\Delta a = 9$ ppm) than those ones obtained with the other two modes. The red points in the graph represent the radius values obtained as average of the three modes results, while the red line is their fitting curve ($y = A + B \cdot x$).

Considering that the relation, which links the radius a of a spherical shell to the pressure, is:

$$\frac{\Delta a}{a_0} = \frac{k_T \Delta p}{3} \tag{2.4}$$

and that it can be re-written as:

$$a = a_0\Big[1 + \frac{k_T(p - p_0)}{3}\Big] \tag{2.5}$$

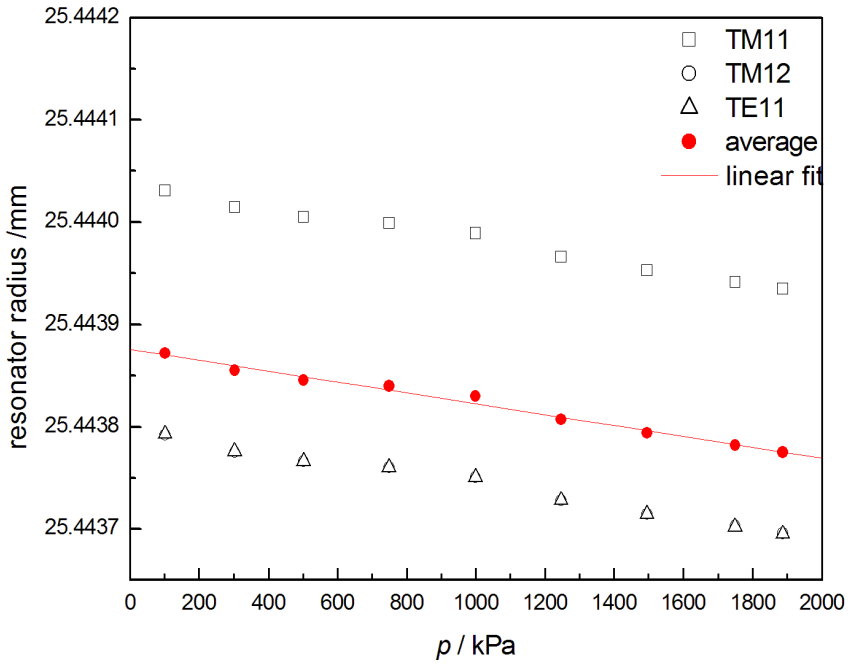

Figure 2.8: Variation of the resonator's effective radius as a function of pressure at 482 K, inferred from measurements of the microwave triplets and the literature value of $\varepsilon_{\mathrm{He}}(p,T)$ for helium.

where a_0 is the value of radius at pressure p_0, the isothermal compressibility coefficient is determined comparing the linear fit equation with Eq. (2.5). Making equal their slopes, the relation $B = a_0 \cdot k_T/3$ was found, from which $k_T = (6.27 \pm 0.26) \cdot 10^{-12}$ Pa^{-1} was obtained.

These empirical estimates of $\alpha_{\rm th}$ and k_T, consistent with tabulated properties of maraging steel, were used in this study to take in account the necessary corrections at the resonator dimensions when frequency measurements, made at different pressure and temperatures, were relating.

2.3.3 Microwave measurements in He between 0.1 and 1.9 MPa

Measurements in helium, realised to obtain k_T, were also used to evaluate the resonator performance. Because for a lot of helium properties *ab initio* calculations are available, we decided to use this gas as a standard for the calibration of the experimental apparatus.

Once filled the cavity with helium, microwave triplets TM11, TM12 and TE11 were measured maitaining constant the cavity temperature at 482 K and varying the pressure between 0.1 MPa and 1.9 MPa. From microwave measurements, experimental helium refractive index values were determined. In Figure 2.9 difference between refractive index determined experimentally and that one calculated *ab initio* is shown. Troughout this comparison, the quality of the resonator performance can be understood.

Ab initio values are calculated using Eq. (2.6):

$$\left(\frac{\varepsilon_{\rm r} - 1}{\varepsilon_{\rm r} + 2}\right) = A_\varepsilon \rho (1 + b\rho + c\rho^2 + ...) \tag{2.6}$$

where b and c are dielectric virial coefficients and A_ε is the molar polarizability in the limit of zero pressure. For helium, the quantity A_ε has been calculated *ab initio* with an uncertainty of less than 1 ppm [38]. Such accurate calculations can not be performed for any other gas. Observing Figure 2.9, it is possible to remark that the results for $n^2_{\rm exp}$ are independent of the triplet used at levels from $1.4 \cdot 10^{-8}$ to $8 \cdot 10^{-8}$ and that they are in agreement with *ab initio* values within 0.9 ppm.

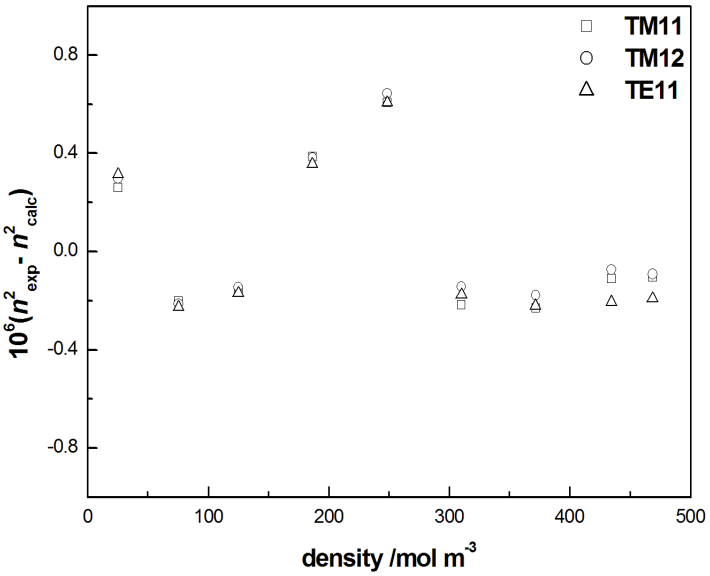

Figure 2.9: Deviation of $n(p,T)^2$ values for helium determined with the resonator from *ab initio* values. The resonator values are calculated using Eq. (2.6).

Chapter 3

Determination of the polarizability of pure water vapour

The molar polarizability $\wp_{\mathrm{w}}$ of water vapour is given by the Debye equation:

$$\wp_{\mathrm{w}} = \frac{1}{\rho}\left(\frac{\varepsilon_{\mathrm{r}} - 1}{\varepsilon_{\mathrm{r}} + 2}\right) = A_{\mathrm{w}} + \frac{B_{\mathrm{w}}}{T} \tag{3.1}$$

where ε_{r} is the dielectric constant of water vapour, ρ is the molar density and A_{w} and B_{w} are the Debye constants.

Among the experiments realised for the determination of these constants, the most recent goes back to about sixty years ago [39]. A critical compilation of the previous determinations of A_{w} and B_{w} was assembled by Hasegawa and Stokesberry [21] in 1975 as reported in Table 3.1 and plotted in Figure 3.1 and 3.2.

From examination of this data set, it is apparent that the determinations by Essen and Froome in two successive experiments, in spite of their high claimed accuracy, are not consistent with each other.

In a previous critical revision [40] of these results, which were obtained by measurements of the dielectric constant at a single temperature and used to deduce the dielectric moment making a comparison with extrapolated refractive data, Birnbaum and Chatterjee considered that only the experiments taken over a sufficient range of temperatures and pressures could allow an accurate determination of A_{w} and B_{w}.

The weighted means of these values for A_{w} and B_{w}:

$$A_{\mathrm{w}} = (3.96 \pm 0.32) \quad \mathrm{cm}^3\ \mathrm{mol}^{-1} \tag{3.2}$$

$$B_{\mathrm{w}} = (2.077 \pm 0.016) \cdot 10^4 \quad \mathrm{cm}^3\ \mathrm{mol}^{-1}\ \mathrm{K} \tag{3.3}$$

were used as reference values in the application of microwave resonators to hygrometry described in the following sections.

Author	Reference date	A_{w} $\mathrm{cm}^3\ \mathrm{mol}^{-1}$	$10^{-4} \cdot B_{\mathrm{w}}$ $\mathrm{cm}^3\ \mathrm{mol}^{-1}\ \mathrm{K}$
Groves and Sugden	1935	4.3 ± 1.2	2.074 ± 0.054
Stranathan	1935	4.03 ± 0.39	2.071 ± 0.014
Hurdes and Smyth	1942	3.4 ± 1.2	2.087 ± 0.053
Essen and Froome	1951	3.585 ± 0.011	2.061 ± 0.002
Birnbaum and Chatterjee	1952	3.84 ± 0.72	2.092 ± 0.024
Essen	1953	4.157 ± 0.012	2.041 ± 0.002
Boudouris	1958	3.99 ± 0.60	2.081 ± 0.020

Table 3.1: Compilation of available values for A_{w} and B_{w} prepared by Hasegawa and Stokesberry [21] in 1975.

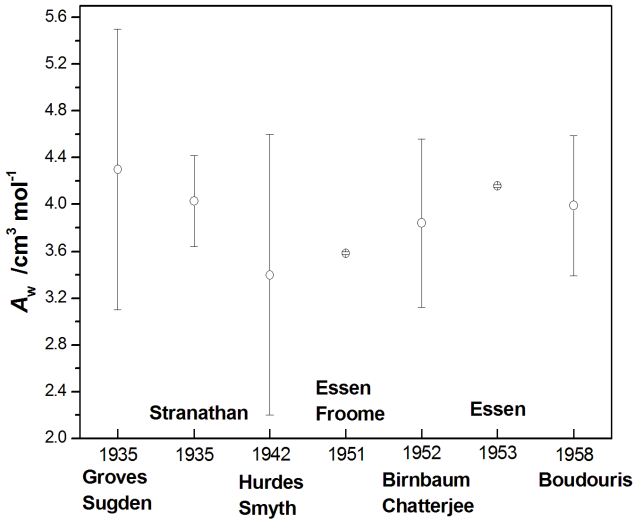

Figure 3.1: Representation of the A_{w} values with their uncertainties reported in the Hasegawa and Stokesberry's table.

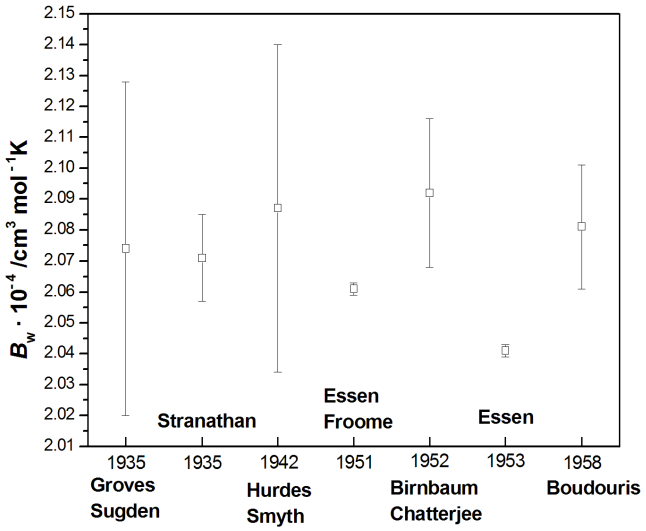

Figure 3.2: Representation of the B_w values with their uncertainties reported in the Hasegawa and Stokesberry's table.

While developing these applications, we noticed that the uncertainties $u(A_w)$ and $u(B_w)$ might represent a major source of uncertainty in the determination of the mole fraction of water vapour in a humid mixture with a microwave resonator, which will be described in Chapter 4. Motivated by this observation, we decided to repeat Birnbaum's experiment and measure the dielectric constant of water vapour over a rather wide range of pressure and temperature aiming at a more precise and accurate determination of the Debye constants.

Prior to presenting the results of this experiment, we briefly contrast the basic features of our experiment with that of Birnbaum. Birnbaum used a cylindrical resonator operated at 9.3 GHz. In contrast we have used a quasi-spherical resonator which enjoys a much higher precision in the determination of the microwave resonance frequencies and half-widths. This resonator, as described in paragraph 2.3, has been satisfactory characterised in its dimensional variations in response to temperature and pressure, allowing us to explore a wider $p-T$ region. Also we have taken advantage of the improvements in the metrology of temperature and pressure made over five decades. Finally, since 1995 a dedicated equation of state for water (IAPWS Formulation 1995 [32]) is available.

Our experiment was performed over the temperature range between 350

K and 505 K at pressures between 5 kPa and 2 MPa. Over these ranges of T and p, emphasised by the orange colour in Figure 3.3, only a few experimental $p\rho T$ data can be observed, particularly those of Kell et al [41]. However the IAPWS formulation estimates the relative uncertainty of the density of water vapour in this region as being only 0.03%.

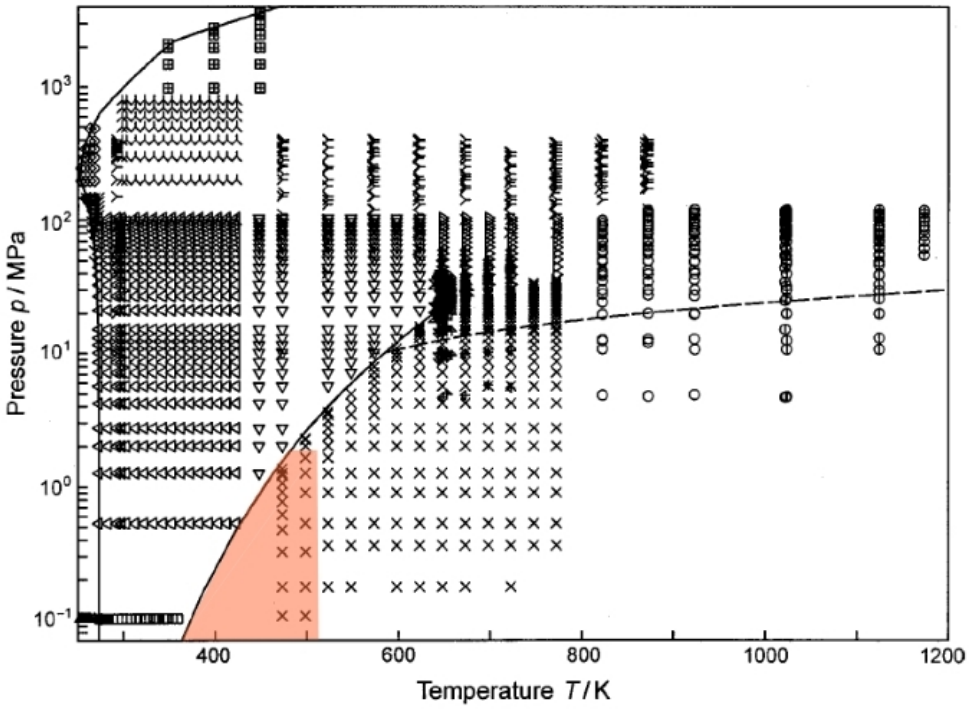

Figure 3.3: Distribution of the selected $p\rho T$ data used to develop the residual part of IAPWS-95 in a $p-T$ diagram. The orange area shows the T and p range in which the experiment was performed.

3.1 Experiment

The experimental apparatus used for this experiment is schematised in Figure 3.4.

The microwave resonator, previously described in Chapter 2, was inserted in a pressure-tight stainless steel vessel inside a temperature controlled oven. The vessel was connected to the external manifold through two pipe lines, one linked to the water sample reservoir and the evacuating system, the

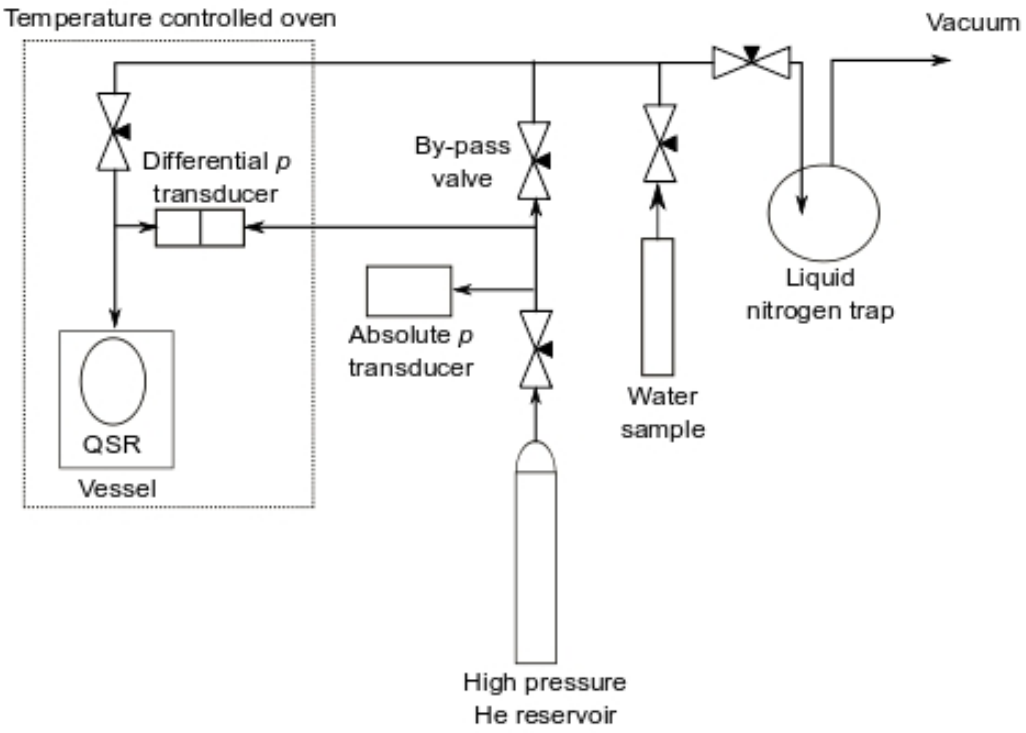

Figure 3.4: Diagram of the gas-handling system realised for the measurement of the water vapour polarizability.

other to the high pressure helium reservoir through a differential and an absolute pressure transducer. With a suitable system of needle valves, the first pipe line could be alternatively used both to fill with pure water vapour the manifold or to evacuate the cavity.

Degassed liquid water samples were necessary for the experiment. The water sample was initially prepared using a commercial purification system and successively undergone to repeated freeze-pump-thaw cycles to eliminate dissolved gases.

The pressure of the vapour in the sampling bottle was increased by heating and from the sampling bottle, with a valve, the water vapour was expanded into the manifold. To avoid water condensation in the part of the manifold at the front of the oven, all pipes were maintained heated. Moreover, a liquid nitrogen trap was inserted before the vacuum pump to capture water vapour and avoid damages to the pump during the evacuation procedure.

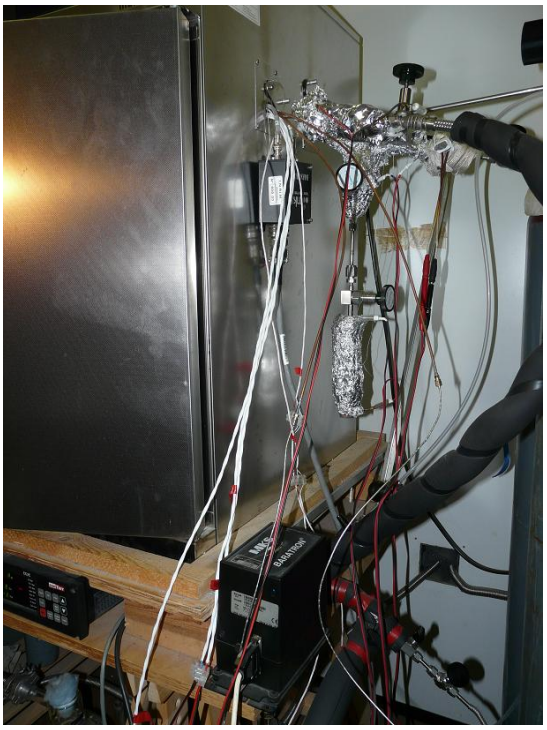

Figure 3.5: Image of the manifold outside the oven realised in INRiM laboratory for the determination of the polarizability of pure water vapour. The absolute pressure transducer, the water reservoir bottle and heated pipes are visible.

Figure 3.6: Image of the experimental set up inside the oven. The stainless steel vessel and the differential pressure transducer can be observed.

The temperature of the gas within the resonant cavity was estimated from the average of the readings of two capsule platinum resistance thermometers (PRTs) placed on the upper and lower parts of the cavity exterior; the PRTs were calibrated by the manufacturer and we conservatively estimated an uncertainty in the gas temperature of 0.05 K. Three heaters for a maximum of 80 W were also attached around the vessel to control the resonator temperature gradient.

The gas pressure was determined using two transducers: a differential one, placed inside the oven, and an absolute one put outside the oven since suitable to work only at ambient temperature and with dry gas. This pressure measurement configuration was adopted since we needed an instrument capable to stay in the oven and work at high temperature and, in the same time, to maintain separate the wet gas from the absolute pressure transducer. As a consequence of this configuration, the pressure of the water vapour in the resonator was obtained indirectly, measuring the pressure of dry helium needed to equal the pressure exerted by the water vapour on the other side of the differential transducer membrane and maintain the last one in a condition of equilibrium around zero.

Thus the pressure of the gas in the resonator was given by:

$$p_{\mathrm{res}} = p_{\mathrm{abs}} + p_{\mathrm{diff}} \tag{3.4}$$

where p_{res} is the pressure of the gas in the resonator, p_{abs} is the helium pressure measured by the absolute manometer, p_{diff} is the unbalanced between the pressures of the two membrane sides measured by the differential manometer.

Before starting the experiment, the zero of the differential transducer was calibrated. This operation was fundamental to guarantee a correct evaluation of p_{res}. The calibration was realized opening the by-pass valve and putting in communication, and so at the same pressure, the circuit sides maintained separate by the differential membrane. In this condition, the pressure difference Δp should be null. During calibration, the deviation of the membrane from the equilibrium state, which means both sides were at the same pressure, as a function of the temperature, from 313 to 473 K, and the pressure, from vacuum to 2 MPa, was recorded. Knowing this deviation, corrections to the measurement of p_{res} were applied. In Figure 3.7 are reported Δp values measured as a function of p_{abs} for five isotherms.

Observing Figure 3.7, it is apparent that the differential manometer zero values depended linearly on the pressure, with a slope which was about the same for all isotherms. The slope value is $m = -5.1 \cdot 10^{-3}$ with $u(m) = 3.15 \cdot 10^{-5}$. It was determined as average of the slopes obtained fitting each

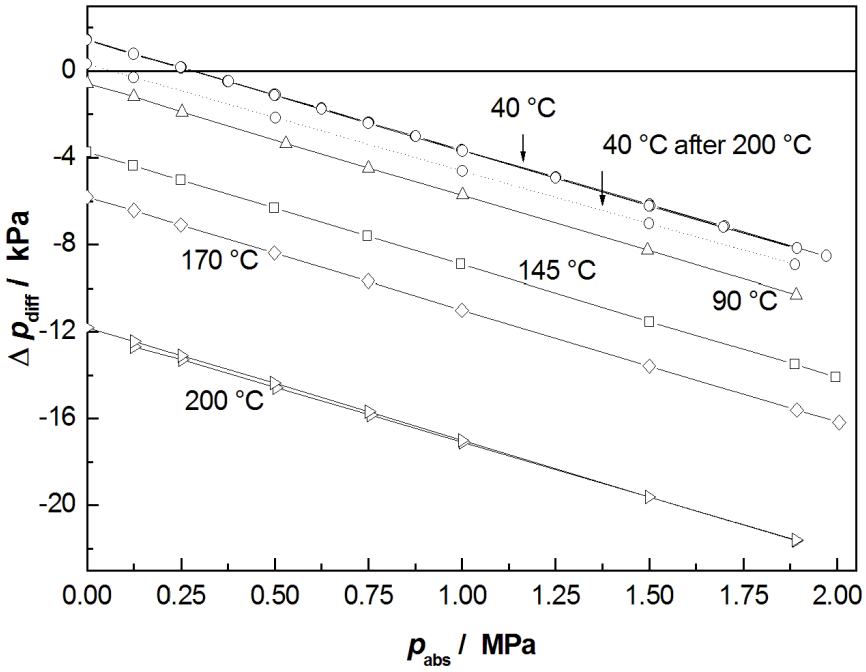

Figure 3.7: Differential transducer calibration: the deviation of the membrane from the equilibrium state as a function of the temperature and the pressure.

isotherm linearly. Moreover, different values of temperature cause a variable offset. For example, in vacuum, zero value changes between 2 kPa and -12 kPa, respectively for temperature between 313.15 K and 473.15 K.

Once known from calibration corrections to apply to the differential manometer measurements, p_{diff} values were determined using Eq. (3.5):

$$p_{\mathrm{diff}} = p_{\mathrm{read}}^{\mathrm{DIFF}} - p_{\mathrm{offset}}^{\mathrm{DIFF}} - m \cdot p_{\mathrm{abs}} \tag{3.5}$$

where $p_{\mathrm{read}}^{\mathrm{DIFF}}$ is the value measured by the instrument and $p_{\mathrm{offset}}^{\mathrm{DIFF}}$ is the Δp value obtained in vacuum at the temperature for which the water vapour pressure is desired. Applying Eq. (3.4), it was now possible to determine p_{res}.

Concerning the absolute pressure transducer, for $p = (0.13 \div 2.00)$ MPa a MKS absolute barometer was used, calibrated in the range between 54 kPa and 2 MPa against the national standard pressure balance maintained by the INRiM Mechanics Division, while for $p < 130$ kPa an atmospheric absolute pressure transducer (Druck DPI142) was used.

3.2 Results and discussion

Experimental data were recorded for nine isotherms with the temperature ranging from 355.5 K and 506 K, approximately one every 20 K. For each isotherm, pressure was varied between vacuum and an arbitrary maximum value chosen sufficiently below the saturation pressure to avoid water condensation in the cavity. As an example, for the isotherm at 355.5 K, the higher value of pressure reached was $p_{\mathrm{max}} = 42$ kPa, while for the isotherm at 506 K it was $p_{\mathrm{max}} = 2$ MPa.

For each value of T and p, two microwave resonance frequencies were measured: the TM11 and the TE11 modes. Measured frequencies were corrected for the skin effect and for the cavity radius variations caused by temperature and pressure. To apply the skin effect correction, modes were corrected using calculated halfwidth values g instead of the experimental ones. This choice was determined by the observed progressive enlargement of the experimental halfwidths with the increase of the pressure noticed for each isotherm and not justifiable by the skin effect. This phenomenon was interpreted as the effect of a further energy loss process such as water absorption.

The dielectric constant ε_{r} was obtained as mean value of $\varepsilon_{\mathrm{r}}^{\mathrm{TM11}}$ and $\varepsilon_{\mathrm{r}}^{\mathrm{TE11}}$ determined as:

$$\varepsilon_{\mathrm{r}}^{\mathrm{TM11}} = \left(\frac{f_0^{\mathrm{TM11}}(T_{\mathrm{s}})}{f^{\mathrm{TM11}}(T_{\mathrm{s}})} \right)^2 \tag{3.6}$$

$$\varepsilon_{\mathrm{r}}^{\mathrm{TE11}} = \left(\frac{f_0^{\mathrm{TE11}}(T_{\mathrm{s}})}{f^{\mathrm{TE11}}(T_{\mathrm{s}})} \right)^2 \tag{3.7}$$

where f_0 is the frequency in vacuum and T_{s} is the set point temperature, that is the exact T value of the isotherm at which water vapour ε_{r} is wanted.

Following the calculation of the gas density in the cavity using the water equation of state, a water polarizability value was obtained from each isotherm, fitting the quantity $(\varepsilon_{\mathrm{r}}-1)/(\varepsilon_{\mathrm{r}}+2)$ as a function of the gas density ρ. The slope of each fitting curve represents a $\wp_{\mathrm{w}}$ value. This is apparent from Eq. (3.8):

$$\frac{\varepsilon_{\mathrm{r}}-1}{\varepsilon_{\mathrm{r}}+2} = \left(A_{\mathrm{w}} + \frac{B_{\mathrm{w}}}{T} \right) \cdot \rho = \wp_{\mathrm{w}} \cdot \rho \tag{3.8}$$

For the sake of clarity, only part of the data are shown in Figure 3.8 and no uncertainties were drawn.

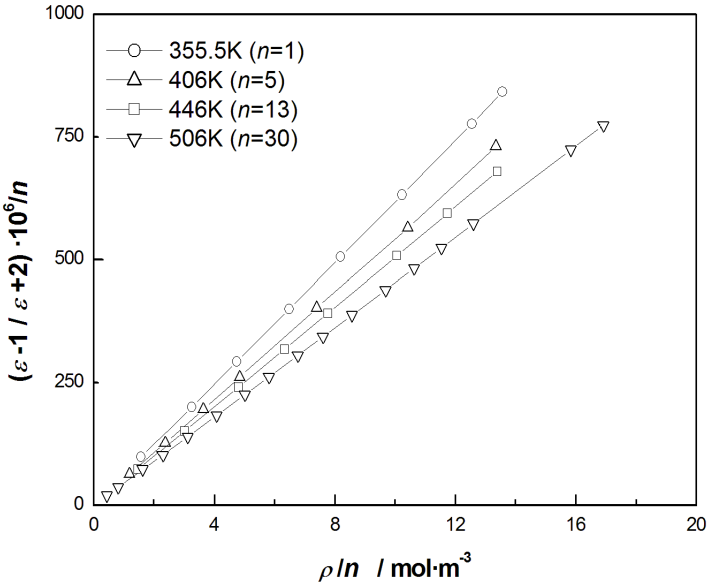

Figure 3.8: Quantity $(\varepsilon_{\mathrm{r}}-1)/(\varepsilon_{\mathrm{r}}+2)$ plotted as a function of the gas density ρ for four of the nine isotherms measured. Dielectric values are represented scaled for an arbitrary factor n.

Straight line resulted to be the best curve with which fitting isotherms at

temperature below 430 K, but it wasn't the same for isotherms at higher T. When interpolated with a linear equation, fit residuals showed a systematic distribution as a function of ρ, effect that disappeared when fitted with a quadratic curve such as:

$$\frac{\varepsilon_\mathrm{r}-1}{\varepsilon_\mathrm{r}+2} = \left(A_\mathrm{w} + \frac{B_\mathrm{w}}{T}\right) \cdot \rho + b(T) \cdot \rho^2. \tag{3.9}$$

Figure 3.9 shows residuals shape for isotherm at the higher temperature ($T = 506$ K) when fitted with both a straight line and a quadratic curve.

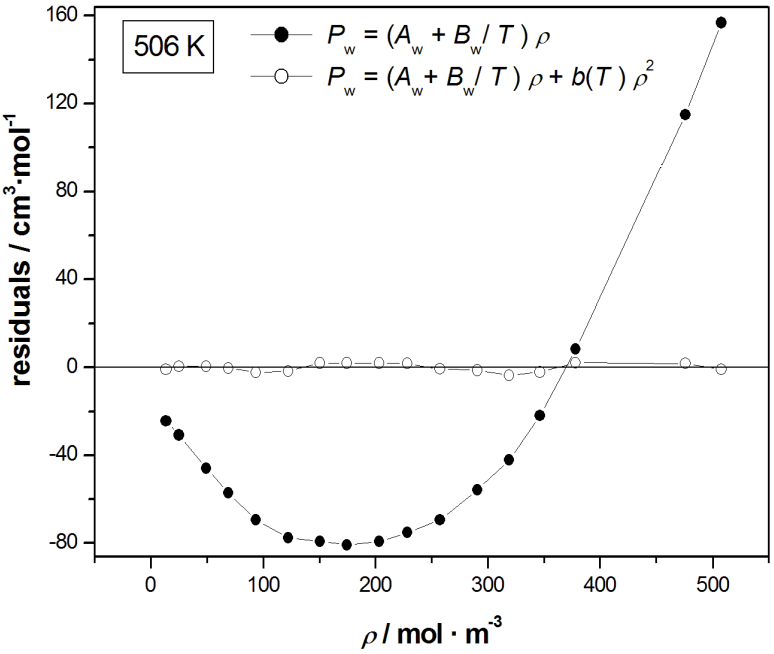

Figure 3.9: Residuals of the isotherm at $T = 506$ K when fitted with a straight line and a quadratic curve.

Comparing Eq. (3.9) with Eq. (1.44), it is apparent that ρ coefficient corresponds to $\wp_\mathrm{w}$, the molar polarizability of water in the limit of zero pressure, while the ρ^2 coefficient is the second dielectric virial coefficient $b_\varepsilon(T)$.

In Table 3.2 $\wp_\mathrm{w}$ values obtained from the fitting procedure of each isotherm with their combined uncertainties are listed.

The uncertainty values of $\wp_\mathrm{w}$ are obtained as combination of more contributions which come from the measurement of frequency, pressure, tempera-

T K	$\wp_w$ $cm^3 \cdot mol^{-1}$	$u_C(\wp_w)$ $cm^3 \cdot mol^{-1}$
356	61.330	0.342
376	58.519	0.155
406	53.574	0.095
426	51.668	0.142
446	49.835	0.087
456	48.821	0.054
466	47.951	0.034
486	46.086	0.027
506	44.490	0.047

Table 3.2: Values of $\wp_w$ and their combined uncertainties obtained from the fitting procedure of each isotherm.

ture, density. Recalling Eq. (3.1), it is apparent that the density ρ and the dielectric constant of water ε_r determine the value and uncertainty of $\wp_w$.

The uncertainty on the dielectric constant is determined by the uncertainty of measurements of frequencies in vacuum and in water vapour, since ε_r is obtained as mean value of ε_r^{TM11} and ε_r^{TE11}, determined using Eqs. (3.6) and (3.7).

Concerning the density, its uncertainty results from combination of water equation of state uncertainty with those of temperature and pressure measurements. As previously mentioned, the IAPWS, used for the calculus of the density, has, in the range $p - T$ of our interest, a relative uncertainty $u_r(\text{IAPWS}) = 3 \cdot 10^{-4}$.

Temperature measurement is affected by PRTs calibration uncertainty and temperature gradient ΔT, which quantifies the T nonuniformity in the cavity. Gas pressure measurement is given by the combination of Eq. (3.4) and Eq. (3.5), so its uncertainty is composed of a contribution which come from the absolute transducer and one from the differential manometer. This last one is given by the differential transducer zero dependence on p, previously quantified in m with a relative uncertainty $u_r(m) = 6.8 \cdot 10^{-3}$, the repeatability of zero with temperature and the uncertainty of the absolute transducer.

For the sake of clarity, in Table 3.3 the different sources of uncertainty on the measurement of $\wp_w$ for the isotherm at 506 K are reported.

Water polarizability values summarized in Table 3.2 are plotted in Figure 3.10 as a function of the inverse of temperature.

Source of uncertainty	$u_r(\wp_w)$
Frequency	$1.36 \cdot 10^{-3}$
Temperature, PRT calibration	$5.9 \cdot 10^{-5}$
Temperature, gradient	$0.4 \cdot 10^{-3}$
Absolute pressure	$2.7 \cdot 10^{-3}$
Differential pressure	$2.1 \cdot 10^{-2}$

Table 3.3: Sources and their contributions to the relative uncertainty of water polarizability.

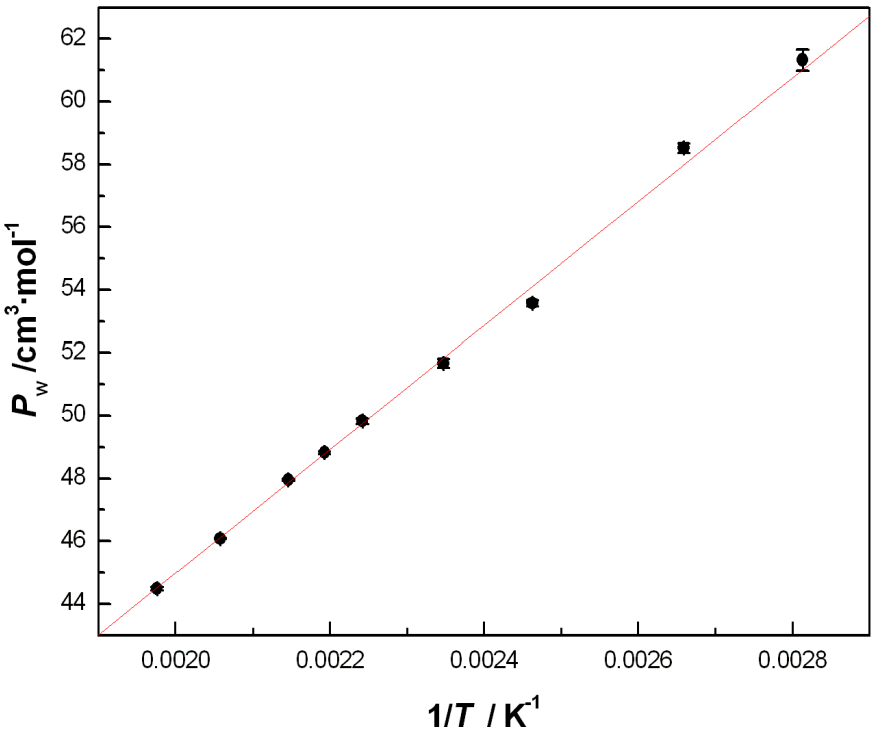

Figure 3.10: Water polarizability values as a function of the inverse of temperature fitted with a straight line. Coefficients obtained from the fitting procedure determine the Debye constant values.

Fitting this data with a weigthed linear curve ($y = a + b \cdot x$) and recalling Eq. (3.1), Debye constant values were found:

$$A_{\mathrm{w}} = (3.906 \pm 0.140)\ \mathrm{cm}^3\ \mathrm{mol}^{-1} \tag{3.10}$$

$$B_{\mathrm{w}} = (2.0607 \pm 0.0068) \cdot 10^4\ \mathrm{cm}^3\ \mathrm{mol}^{-1}\ \mathrm{K} \tag{3.11}$$

Knowing B_{w} and using Eq. (1.45), the dipole moment μ of water was also determined:

$$\mu = (1.839 \pm 0.003)\ \mathrm{D} \tag{3.12}$$

Fitting all isotherms with a quadratic curve as Eq. (3.9), values for the second dielectric virial coefficient $b_\varepsilon(T)$ of water were determined and experimental values obtained are shown in Figure 3.11.

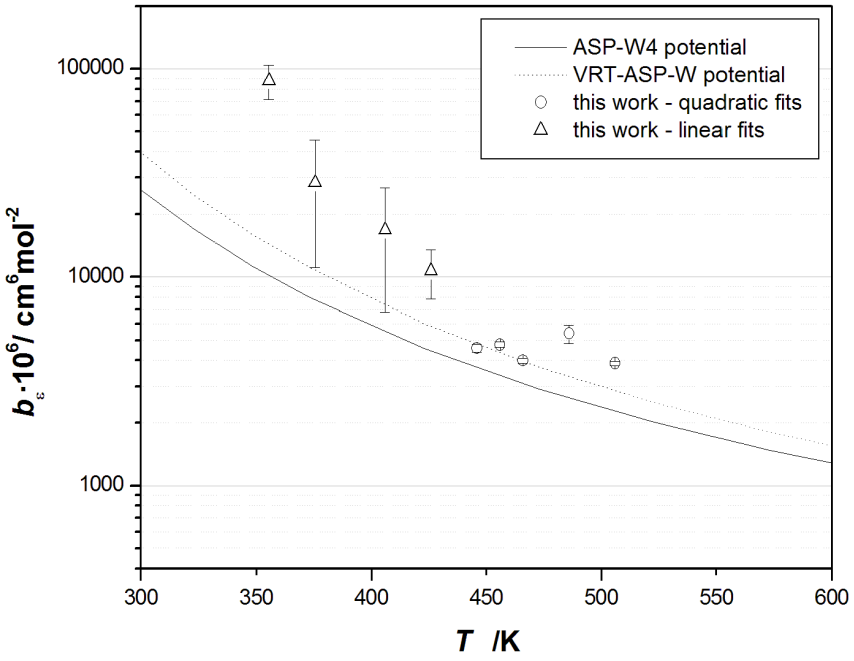

Figure 3.11: Comparison between experimental second dielectric virial coefficient $b_\varepsilon(T)$ values of water with theoretical models.

To our knowledge, this is the first experimental determination of such quantities. At the moment only theoretical models and computational methods of intermolecular potentials exist. The two curves plotted in Figure

3.11 represent the dielectric virial coefficient $b_\varepsilon(T)$ calculated using the ASP-W4 potential [42] and using the VRT-ASP-W potential (dot line), revised by Fellers [43]. Experimental values obtained in this work partially follow theoretical trends. A better investigation is necessary.

Chapter 4

Determination of water vapour mole fractions in humid gas mixtures

In this Chapter, the capability of the quasi-spherical microwave resonator in detecting the amount of water in a humid gas mixture is investigated.

The experiment carried out consists on flowing a humid mixture, produced by the INRiM humidity generator, through the cavity and comparing the mixture water vapour mole fraction x_w measured using the microwave technique with the value given by the generator.

The experiment was realised twice, using two different humid mixtures, H_2O/N_2 and H_2O/air, and two different INRiM humidity generators. One is the INRiM standard humidity generator for frost-point temperatures T_{fp} and it was used to produce mixtures with T_{fp} between 241 K and 270 K. The other one is a commercial two-pressure humidity generator and it was used to generate mixtures with a dew point temperature T_{dp} between 272 K and 291 K. The functioning of the microwave technique was tested over a range of x_w between $0.3 \cdot 10^{-3}$ and $21 \cdot 10^{-3}$. All the experiment was run at ambient pressure.

4.1 Determination of the water vapour mole fraction in a H_2O/N_2 mixture

4.1.1 Experiment

A first test of the performance of the microwave resonator as an hygrometer was carried out using the INRiM standard frost-point humidity generator [44]. The generator was used to flow H_2O/N_2 mixtures of variable composition.

The diagram of the manifold realised for this experiment is shown in Figure 4.1.

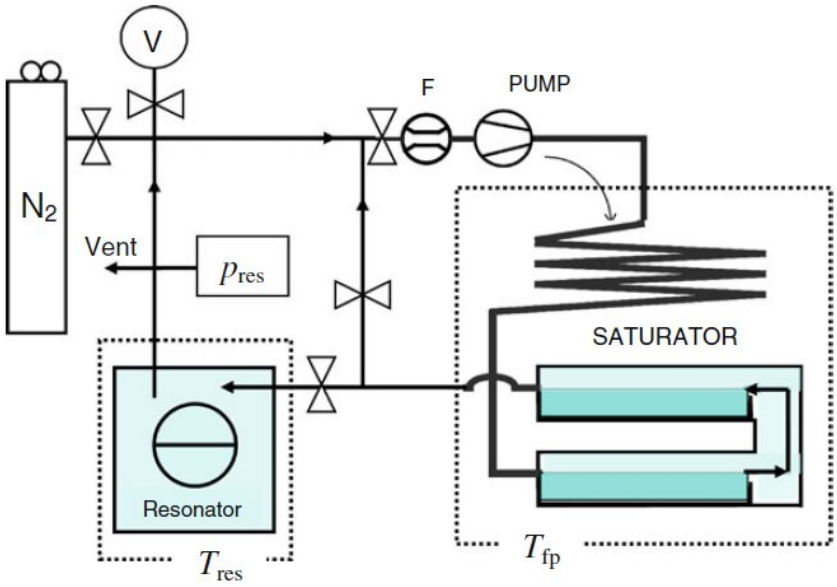

Figure 4.1: Diagram of the manifold realised for the microwave determination of the water mole fractions of H_2O/N_2 mixtures.

The generator was operated in re-circulation mode and frost-point temperatures between 241 K and 270 K were set on it. The gas of variable composition flowed through the manifold and the microwave resonator, contained in a vacuum- and pressure-tight stainless-steel vessel. The vessel was immersed in a liquid stirred bath which maintained the temperature stable within $\pm$ 0.1 K at a set point of 275.5 K. The temperature of the manifold

and of the resonator was always maintained higher than T_{fp} to avoid the condensation of the water vapour contained in the mixture.

The temperature of the gas within the resonant cavity was estimated from the average of the readings of two capsule platinum resistance thermometers (PRTs), embedded into copper blocks, clamped to bosses on the upper and lower parts of the cavity exterior.

The uncertainty of the determination of the gas temperature is estimated to be $u_C(T) = 0.05$ K. This value of $u_C(T)$ results from the combined influence of the thermal gradients measured across the resonator, typically less than 0.02 K, and the accuracy of the employed sensors, which is 0.035 K in reason based on their tolerance class (1/10 DIN) and the working temperature range (275 K to 293 K) of interest in this study.

The pressure of the gas within the vessel and the resonator was measured using a piezoresistive barometer (Druck Model DPI142) connected to the manifold by a short section of PTFE tubing.

Finally the system was connected to a dry scroll primary pump to evacuate the resonator when necessary.

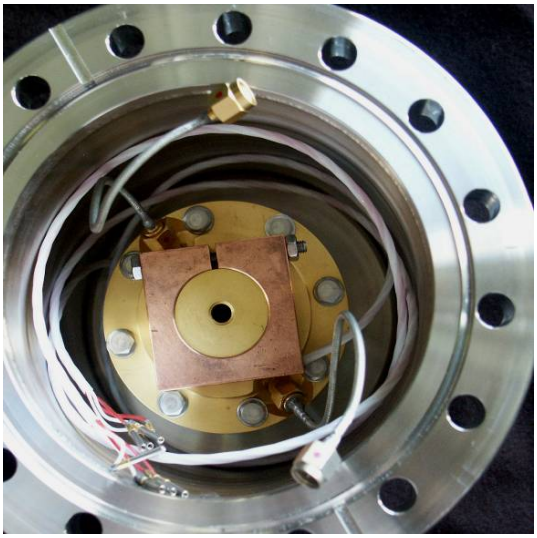

Figure 4.2: Resonator and microwave cables inside the stainless-steel vessel.

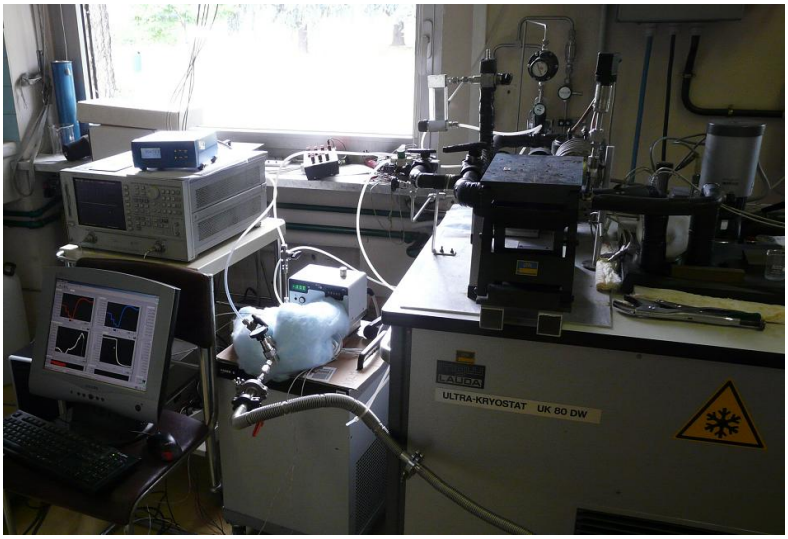

Figure 4.3: Images of the manifold realised in INRiM laboratory for the microwave determination of the water mole fraction of H_2O/N_2 mixtures of variable compostion. On the left: the network analyser (Agilent Technologies E5071C 300 kHz - 20 GHz, the barometer (Druck DPI142) and the liquid stirred bath; on the right: the INRiM standard frost point humidity generator.

Prior to flowing humid gas mixtures through the experiment, the generator outlet was isolated, the vessel and the resonator were evacuated by means of the dry pump and the mean corrected eigenfrequencies $\langle f_0 + g_0 \rangle$ of the modes TM11 and TE11 were measured at $T_0 = (275.48 \pm 0.05)$ K. Subsequently, the resonator was filled with dry nitrogen at a pressure $p_1 = (104.290 \pm 0.015)$ kPa and $\langle f_{p1}^{N_2} \rangle$ and $\langle g_{p1}^{N_2} \rangle$ were measured at $T_1 = (275.59 \pm 0.05)$ K.

From these data, upon applying frequency corrections for the compression of the resonator under pressure (see Eq. (2.5)) and the thermal expansion (see Eq. (2.3)) due to the slight difference $\Delta T = T_1 - T_0$, the permittivity of nitrogen at p_1, T_1 was calculated using Eq. (1.53) that, in this case, became:

$$\varepsilon_{N_2}^{exp}(p_1, T_1) = \left(\frac{\langle f_0 + g_0 \rangle}{\langle f_{p1}^{N_2} + g_{p1}^{N_2} \rangle} \right)^2. \tag{4.1}$$

The experimental value obtained was $\varepsilon_{N_2}^{exp} = (1.0005965 \pm 0.0000004)$. It differed from the expected value $\varepsilon_{N_2}^{calc} = (1.0005993 \pm 0.0000001)$ reported in literature [23,28] by 2.6 ppm. We identified in the undetermined contaminants present in the nitrogen sample, or in the underestimate of the

gas density, resulting from our imperfect determination of the pressure and temperature of the N_2 sample, the cause of such a discrepancy.

4.1.2 Results and discussion

After the calibration with dry nitrogen, the resonator temperature was maintained costant at 275.5 K, while the frost-point temperature T_{fp} of the generator was varied between 241.86 K and 270.01 K in seven steps. These variations of T_{fp} corresponded to changes in the water vapour mole fraction $x_{\mathrm{w}}^{\mathrm{gen}}$ between $0.312 \cdot 10^3$ and $4.401 \cdot 10^3$, as reported in Table 4.1, second column.

Values of $x_{\mathrm{w}}^{\mathrm{gen}}$ were calculated according to the formulation by Davis [45] and Giacomo [46], which make reference to the paper of Hyland and Wexler [47]. The mole fraction of water vapour x_{w} in the moist gas, in fact, can't be measured directly, but it can be derived either from a measurement of the relative humidity RH or from the measurement of the dew-point T_{dp}/frost-point T_{fp} temperature. In both cases, the saturation vapour pressure of water at the prevailing temperature and pressure is necessary. Expression for the water vapour pressure at saturation (p_{sv}) is given by:

$$p_{\mathrm{sv}} = e^{A \cdot T^2 + B \cdot T + C + D \cdot T^{-1}} \tag{4.2}$$

with $A = 1.2378847 \cdot 10^{-5}\ \mathrm{K}^{-2}$, $B = -1.9121316 \cdot 10^{-2}\ \mathrm{K}^{-1}$, $C = 33.93711047$ and $D = -6.3431645 \cdot 10^3$ K for vapour above liquid water, while $A = -1.3198825 \cdot 10^{-5}\ \mathrm{K}^{-2}$, $B = 1.0613868 \cdot 10^{-2}\ \mathrm{K}^{-1}$, $C = 29.32707$ and $D = -6.0245282 \cdot 10^3$ K for vapour above ice.

Once calculated p_{sv}, x_{w} was obtained using the following relations:

$$RH = \frac{x_{\mathrm{w}}}{x_{\mathrm{sv}}} \tag{4.3}$$

where RH is the relative humidity and x_{sv} is the water vapour mole fraction in saturated moist gas, expressed as:

$$x_{\mathrm{sv}} = \frac{p_{\mathrm{sv}}}{p} \tag{4.4}$$

where p is the pressure of the moist gas.

In the flowing configuration, a pressure drop Δp results between the humidity generator and the pressure vessel. From the indications of a flow

meter ($8.3 \cdot 10^{-5}$ m^3 s^{-1}) and a previous pressure drop determination reported in [44], we estimated $\Delta p = 120$ Pa and accordingly we corrected the total pressure in the saturator, which enters in the calculation of $x_{\mathrm{w}}^{\mathrm{gen}}$.

When the humid mixture was admitted into the cavity, resonance frequencies decreased from the reference values in dry carrier gas, nitrogen in this case, proportionally to the water content of the mixture. The TM11 and TE11 frequencies and their half-widths were measured and the dielectric permittivity of the mixture was determined using Eq. (4.5):

$$\varepsilon_{\mathrm{mix}} = \varepsilon_{\mathrm{N_2}}^{\mathrm{exp}} \left(\frac{\langle f_p^{\mathrm{N_2}} + g_p^{\mathrm{N_2}} \rangle}{\langle f_{\mathrm{mix}} + g_{\mathrm{mix}} \rangle} \right)^2 \tag{4.5}$$

with corrections applied to account for slight temperature differences between the measurements in the mixture and those done in dry gas.

Once $\varepsilon_{\mathrm{mix}}$ value was obtained, the water mole fraction $x_{\mathrm{w}}^{\mathrm{res}}$ was determined applying Eqs. (1.46 - 1.52) and Eqs. (1.56 - 1.58), with $\wp_{\mathrm{N_2}} = (\rho_{\mathrm{N_2}})^{-1} \cdot \left[(\varepsilon_{\mathrm{N_2}}^{\mathrm{exp}} - 1)/(\varepsilon_{\mathrm{N_2}}^{\mathrm{exp}} + 2) \right]$. Results obtained from this first test with their uncertainties are reported in Table 4.1.

The table is divided in three parts: one refers to the generator, one to the values obtained experimentally with the microwave resonator and the third part shows the comparison between $x_{\mathrm{w}}^{\mathrm{res}}$ and $x_{\mathrm{w}}^{\mathrm{gen}}$. In particular, in the first column the frost point temperature T_{fp} values, at which measurements were done, are reported, while in the third and fourth column the pressure p_{res} and the relative permittivity $\varepsilon_{\mathrm{mix}}$ of the mixture within the resonator are listed respectively. Moreover, values on the first line refer to measurements in dry nitrogen.

4.1.3 Uncertainty analysis

The uncertainty of our estimate of $x_{\mathrm{w}}^{\mathrm{res}}$ is dominated by the contribution of the uncertainty of the polarizability of water vapour $\wp_{\mathrm{w}} = A_{\mathrm{w}} + B_{\mathrm{w}}/T$, whose relative uncertainty at 275 K is $u_{\mathrm{r}}(\wp_{\mathrm{w}}) = 0.8\%$ and contributes to the uncertainty of $x_{\mathrm{w}}^{\mathrm{res}}$ as $u_{\mathrm{r}}(x_{\mathrm{w}}^{\mathrm{res}}) = 1.2\%$, and by the uncertainty in our determination of the mixture density.

The uncertainty on the pressure determination, equal to $u(p) = 15$ Pa, corresponds to a relative contribution to $x_{\mathrm{w}}^{\mathrm{res}}$ uncertainty of $u_{\mathrm{r}}(x_{\mathrm{w}}^{\mathrm{res}}) = 0.2\%$ at $T_{\mathrm{fp}} = 270$ K, which increases up to $u_{\mathrm{r}}(x_{\mathrm{w}}^{\mathrm{res}}) = 2.5\%$ at $T_{\mathrm{fp}} = 241$ K. Instead, the temperature combined uncertainty $u_{\mathrm{C}}(T) = 0.05$ K corresponds to a relative contribution on $x_{\mathrm{w}}^{\mathrm{res}}$ of $u_{\mathrm{r}}(x_{\mathrm{w}}^{\mathrm{res}}) = 0.07\%$ at the highest temperature, increasing up to $u_{\mathrm{r}}(x_{\mathrm{w}}^{\mathrm{res}}) = 0.6\%$ for $T_{\mathrm{fp}} = 241$ K.

Generator		Resonator			Comparison
T_{fp}(K)	$10^3 \times [(x_{\mathrm{w}}^{\mathrm{gen}} \pm U(x_{\mathrm{w}}^{\mathrm{gen}})]$	p_{res}(kPa)	$\varepsilon_{\mathrm{mix}}$	$10^3 \times [(x_{\mathrm{w}}^{\mathrm{res}} \pm U(x_{\mathrm{w}}^{\mathrm{res}})]$	$\frac{\lvert x_{\mathrm{w}}^{\mathrm{gen}} - x_{\mathrm{w}}^{\mathrm{gen}} \rvert}{\sqrt{U(x_{\mathrm{w}}^{\mathrm{gen}})^2 + U(x_{\mathrm{w}}^{\mathrm{res}})^2}}$
				Dry nitrogen	
241.86	0.312 ± 0.004	104.29	1.0005965	0.320 ± 0.018	0.43
251.40	0.814 ± 0.008	106.96	1.0006153	0.823 ± 0.026	0.33
260.02	1.835 ± 0.016	107.54	1.0006241	1.807 ± 0.046	0.58
261.49	2.094 ± 0.018	107.23	1.0006326	2.070 ± 0.052	0.44
264.70	2.784 ± 0.024	107.35	1.0006361	2.743 ± 0.068	0.57
267.35	3.504 ± 0.032	107.39	1.0006435	3.450 ± 0.084	0.60
269.19	4.102 ± 0.034	107.37	1.0006507	4.039 ± 0.098	0.61
270.01	4.401 ± 0.036	107.29	1.0006565	4.330 ± 0.106	0.63
		107.21	1.0006591		

Table 4.1: Water vapour mole fractions x_{w} and expanded uncertainties $U(x_{\mathrm{w}})$ (coverage factor $k = 2$) of H_2O/N_2 mixtures generated using INRiM humidity frost-point standard generator and measured using a microwave resonator.

4.1 Determination of the water vapour mole fraction in a H_2O/N_2 mixture

In Table 4.2 the uncertainty sources and their contributions to the relative uncertainty of the water mole fraction x_w^{res} are summarised.

Source of uncertainty	Unit	Relative uncertainty $u_r(x_w^{res})$
Water polarizability, $\wp_w$	$cm^3\ mol^{-1}$	1.2%
Pressure, p	kPa	2.5%
Temperature, T	K	0.63%
Resonance frequency, f	Hz	0.31%
Halfwidth, g	Hz	0.31%
Total uncertainty budget		2.88%

Table 4.2: Contributions to the relative uncertainty of the water mole fraction x_w^{res}.

Concerning the uncertainty of x_w^{gen}, it is given by the combined expanded uncertainty (coverage factor $k = 2$) of the INRiM humidity generator on the measurement of the frost-point temperature, which is $U(T_{fp}) = 0.05$ °C for -60 °C$< T_{fp} < 0$ °C [44]. The combined expanded uncertainty of T_{fp} corresponds to a relative contribution on the uncertainty of x_w^{gen} equals to $U_r(x_w^{gen}) = 0.53\%$ for $T_{fp} = 241$ K, decreasing to $U_r(x_w^{gen}) = 0.42\%$ at the highest temperature.

The quality of the agreement between the generator and the microwave hygrometer, may be conveniently expressed by the indicator $|x_w^{gen} - x_w^{res}|/\sqrt{U(x_w^{gen})^2 + U(x_w^{res})^2}$, where $U(x_w)$ is the expanded uncertainty with a coverage factor $k = 2$.

In Figure 4.4 the experimental values of x_w^{res} and the theoretical ones of x_w^{gen} with their uncertainties are graphically compared. On the y axis the relative difference between x_w^{gen} and x_w^{res} is represented ($\Delta x_w/x_w = (x_w^{gen} - x_w^{res})/x_w^{gen}$), while on the x axis the T_{fp} temperatures, at which measurements were done, are indicated. The blue lines refers to the generator, while the red points to the experimental values found using the microwave resonator.

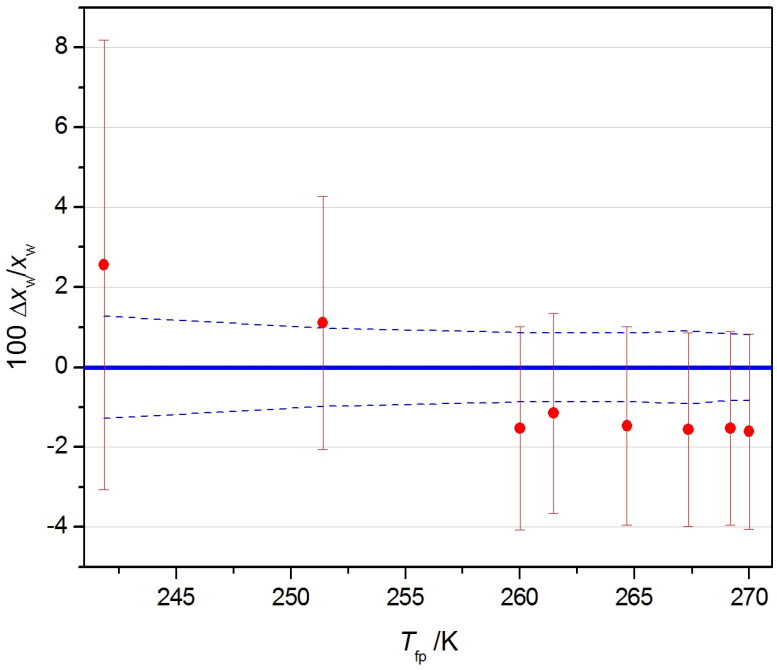

Figure 4.4: Relative difference between x_w^{gen} (blue lines) and x_w^{res} (red points).

4.2 Microwave hygrometry with H_2O/air mixtures prepared with a commercial two-pressure generator

4.2.1 Experiment

In the second experiment, with the aim of testing the performance of the microwave hygrometer as a bench instrument, the resonator was simply inserted in the test chamber of a commercial two-pressure humidity generator (Thunder Scientific Corporation mod 2500).

The operating conditions are different from those of the previous test with the frost-point generator. In fact this time the carrier gas was air taken from the laboratory ambient and the water mole fractions in the mixture were higher than that measured previously.

The samples of air, whose composition was not precisely known or determined, were drawn from the laboratory ambient and compressed in the saturation chamber of the generator at four different pressures, comprised in the range of 108.7 kPa $< p_{\mathrm{sat}} <$ 394.6 kPa, corresponding to a relative humidity RH_{gen} generated in the expansion test chamber of approximately 25%, 50%, 75% and 90%.

The temperature of the chamber was maintained constant at (293.15 $\pm$ 0.05) K, while the relative humidity was first increased from the lowest to the highest set point and successively decreased, in order to check for the measurement repeatability.

In Figure 4.5 a schematic diagram of the experimental set-up is illustrated, while Figure 4.6 shows the commercial two-pressure generator used for this experiment and the microwave resonator put inside the test chamber.

Each change in the humidity set point of the generator was tracked by a corresponding change of the microwave frequencies of the resonator with a responding time constant on the order of 40 min. This delay is mostly due to the time that the replacement of the gas sample within the volume of the test chamber (0.1 m^3) takes. The time spent is determined by the inlet flow set on the generator ($8.3 \cdot 10^{-5}$ m^3 s^{-1}). Secondarily, additional time is needed for the mass diffusion of the replacing sample from the test chamber to the resonator interior, with a time constant determined by the diffusivity of water vapour into air at ambient temperature ($2.6 \cdot 10^{-5}$ m^2 s^{-1}) [48] and the limited sectional area of the holes machined through the resonator shell ($8.3 \cdot 10^{-6}$ m^2).

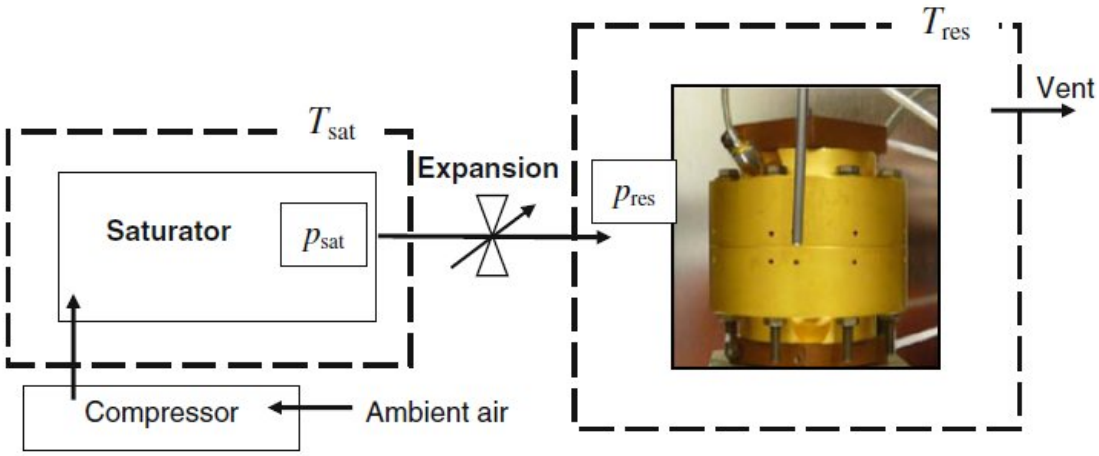

Figure 4.5: Schematic diagram of the experimental apparatus used in the second test. The microwave resonator is illustrated as inserted in the climatic chamber of the commercial two-pressure humidity generator.

Figure 4.6: The commercial two-pressure humidity generator (Thunder Scientific Corporation mod 2500) used in the experiment with the microwave resonator in the test chamber.

If needed by a particular application, the response time might be substantially reduced by directly flowing humid samples through the resonator or by enlarging the dimensions of the inlet-outlet holes. The latter alteration of the resonator design would have a predictable effect on the microwave resonances [20] and thus a negligible impact on its performance in terms of achievable accuracy.

The nominal values of the water mole fractions x_w^{gen} were estimated on the basis of the temperature and pressure readings of the instrumentation embedded in the generator, with an overall uncertainty $u_C(x_w^{gen}) = 1.2 \cdot 10^{-4}$, corresponding to $u_C(RH) = 5 \cdot 10^{-3}$, as declared by the manufacturer.

Since air from the laboratory ambient was used for this experiment, it was not possible to measure the permittivity of dry air as we did with nitrogen in the previous experiment. Thus, to calculate x_w^{res}, the permittivity of the H_2O/air mixtures was determined from the squared ratios of the resonance frequencies previously measured in vacuum and those measured when the humid mixture fills the resonator:

$$\varepsilon_{H_2O/air} = \left(\frac{\langle f_0 + g_0 \rangle}{\langle f_{H_2O/air} + g_{H_2O/air} \rangle} \right)^2 \tag{4.6}$$

after that dimensional corrections to account for pressure and temperature differences between different sets of measurements are applied.

Figure 4.7 shows the shape of the triplet degenerate mode TM11. The black line is the resonance measured when the cavity is evacuated, while the blue and red lines are obtained when a mixture of humid air with respectively $RH = 50\%$ and $RH = 90\%$ flows through the cavity. As it is possible to observe, the frequency values decrease while the humidity and so the water vapor in the mixture increases.

Solving Eqs. (1.46 - 1.52) and Eqs. (1.56 - 1.58), x_w^{res} values were determined. Air was treated as a single dry component of a binary humid mixture and its standard composition [29] was assumed, neglecting the presence of CO_2 in the sample. This simplifying assumption has an irrelevant impact on the determination of x_w^{res}. If we consider the presence of about 400 ppm of CO_2 in the air sample, the second density virial B_{air} changes by 0.03 cm^3 mol^{-1}, with a corresponding relative increase of the mixture permittivity by 0.16 ppm.

4.2.2 Discussion

Results and uncertainties obtained in this second experiment are reported in Table 4.3.

Generator		Resonator		Comparison
T_{dp}(K)	$10^3 \times [(x_{\mathrm{w}}^{\mathrm{gen}} \pm U(x_{\mathrm{w}}^{\mathrm{gen}}))]$	$\varepsilon_{\mathrm{mix}}$	$10^3 \times [(x_{\mathrm{w}}^{\mathrm{res}} \pm U(x_{\mathrm{w}}^{\mathrm{res}}))]$	$\frac{\lvert x_{\mathrm{w}}^{\mathrm{gen}} - x_{\mathrm{w}}^{\mathrm{gen}} \rvert}{\sqrt{U(x_{\mathrm{w}}^{\mathrm{gen}})^2 + U(x_{\mathrm{w}}^{\mathrm{res}})^2}}$
272.59	6.00 ± 0.24	1.0005703	5.98 ± 0.24	0.06
272.55	5.98 ± 0.24	1.0005728	5.94 ± 0.24	0.12
282.50	12.02 ± 0.24	1.0006201	11.83 ± 0.34	0.46
282.50	12.00 ± 0.24	1.0006209	11.85 ± 0.34	0.36
288.66	18.01 ± 0.24	1.0006701	17.65 ± 0.46	0.69
288.66	18.01 ± 0.24	1.0006706	17.70 ± 0.46	0.60
291.54	21.61 ± 0.24	1.0007005	21.17 ± 0.54	0.74

Table 4.3: Water vapour mole fractions x_{w} and expanded uncertainties $U(x_{\mathrm{w}})$ (coverage factor $k = 2$) of H_2O/air mixtures prepared with a commercial two-pressure humidity generator and determined with the microwave hygrometer set within the generator test chamber. The resonator is maintained at $T = (293.13 \pm 0.10)$ K and $p = (98.20 \pm 0.04)$ kPa.

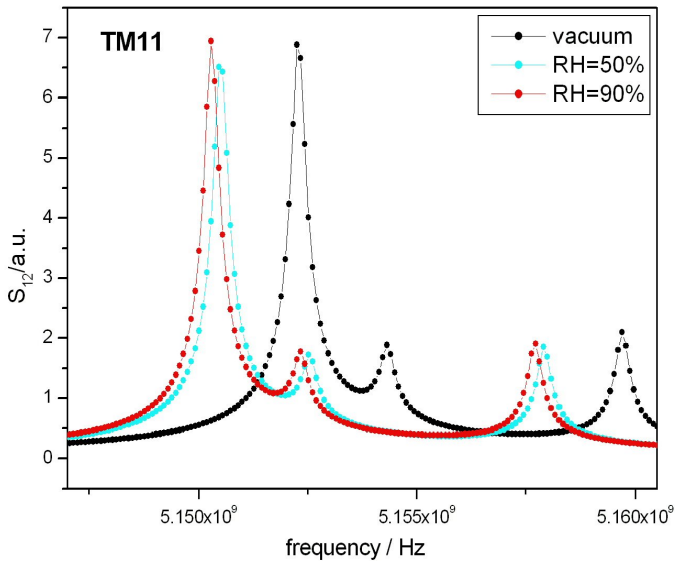

Figure 4.7: Triplet degenerate mode TM11 in vacuum (black), humid air with $RH = 50\%$ (blue line) and humid air with $RH = 90\%$ (red line).

Observing data in Table 4.3, it is clear that the agreement between the generator and the resonator was worse for samples with higher relative humidity. Currently, we have not a satisfactory explanation for this trend and further investigations are necessary. However, it is worth of remarking that not only the good repeatability has been demonstrated, but also that the microwave determination x_w^{res} of the generated water mole fractions and x_w^{gen} are in all case consistent with $|x_w^{gen} - x_w^{gen}|/\sqrt{U(x_w^{gen})^2 + U(x_w^{res})^2} \leq 0.8$.

The uncertainty of x_w^{res} values in Table 4.3 is dominated by the imperfect estimate of the polarizability of water with a constant relative contribution to $u_r(x_w^{res}) = 1.2\%$, while the imperfect estimate of $\rho(p,T)$ in the test chamber, due to the uncertainty of the temperature and pressure determination, contributes to $u_r(x_w^{res})$ between a maximum of 1.5% for $RH \sim 25\%$ to a minimum of 0.4% for $RH \sim 90\%$.

The uncertainty sources and their contribution to the relative uncertainty of the water mole fraction x_w^{res} are summarised in Table 4.4.

Concerning the uncertainty of x_w^{gen}, it depends on the relative humidity uncertainty of the two pressure generator $u(RH_{gen}) = 0.5\%$, as declared by the manufacturer, and that corresponds to a relative contribution $u_r(x_w^{gen}) = 0.5\%$.

In Figure 4.8 x_w^{res} and x_w^{gen} values with their uncertainties are graphically compared. On the y axis the relative difference between x_w^{gen} and x_w^{res} is

Source of uncertainty	Unit	Relative uncertainty $u_r(x_w^{res})$
Water polarizability, $\wp$	$cm^3\ mol^{-1}$	1.2%
Pressure, p	kPa	0.17%
Temperature, T	K	1.5%
Resonance frequency,f	Hz	0.17%
Halfwidth, g	Hz	0.17%
Total uncertainty budget		1.94%

Table 4.4: Contributions to the relative uncertainty of the water mole fraction x_w^{res}.

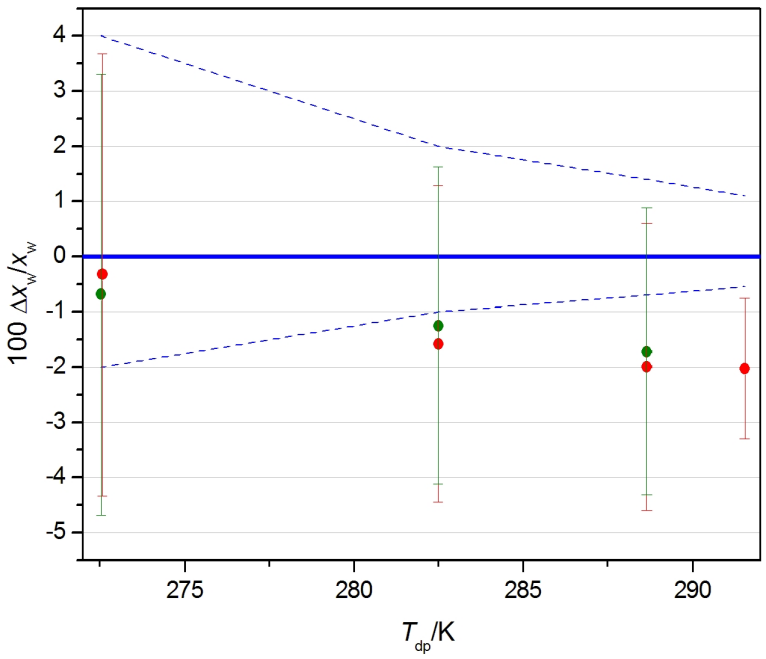

Figure 4.8: Relative difference between x_w^{gen} (blue lines) and x_w^{res} (red points).

represented ($\Delta x_w/x_w = (x_w^{gen} - x_w^{res})/x_w^{gen}$), while on the x axis the T_{dp} temperatures, at which measurements were done, are indicated. The blue lines refer to the generator values, while the red points refer to the experimental values determined with the microwave resonator.

Results obtained show that calculated and measured values agree within their combined expanded uncertainty. The quality of the agreement is indeed remarkable, considering that the water mole fraction in the mixtures spans the range between 3 parts in 10^4 and 2.1 parts in 10^2, with a corresponding relative permittivity which differs from unity by less than 700 parts in 10^6.

Chapter 5

The microwave QSR as a condensation hygrometer

As final step of this research project, we decided to use the quasi-spherical microwave resonator as a condensation hygrometer and to compare its performance with that of a calibrated chilled-mirror hygrometer.

In Chapter 4 of this work, the possibility to use a microwave cavity for the determination of the amount fraction of water vapour in different humid mixtures was shown, but this is not enough to demonstrate the potential of the resonator as hygrometer. The QSR in fact, to be used as condensation hygrometer, has also to be able to identify the temperature value at which a humid mixture starts to condensate, that means to identify the dew-point temperature T_{dp}.

To understand the behaviour and the dynamics of the device in these particular conditions, the cavity was subjected to five tests, in which the humidity and flow rate of the air supply and the temperature of the resonator were varied.

Finally, the ability of the device to reproducibly follow step-changes in humidity was tested and the agreement with a calibrated hygrometer was verified.

The experiments and the results described below were realised and obtained during my secondement at the National Physical Laboratory (NPL), in Teddington (UK). During this period a suitable experimental test bench was built and the experiments were carried out.

5.1 Experimental apparatus

The microwave cavity and the method used for data acquisition and analysis were the same previously described in Chapter 2.

The resonator temperature was measured using two 100 Ω capsule platinum resistance thermometers (PRTs), embedded in copper slabs attached to the top and bottom of the resonator. These thermometers had previously been calibrated at INRiM, with an estimated uncertainty of 0.01 °C.

The temperature of both PRTs was continuously measured with a resistance bridge (ASL F700) and the average of both readings provided an estimate of the temperature of the resonator, T_{res}, and thus, assuming the thermal uniformity of the experiment, of the gas contained within its interior. The PRT readings were used to implement proportional-integral (PI) control of the temperature of water flowing through two copper blocks attached to the resonator. This temperature control system allowed an automated modulation of up to 0.3 °C in T_{res}. In addition, to improve the thermal stability and uniformity of the cavity, it was wrapped in nitrile rubber foam.

Concerning the additional ports in the resonator wall, they were used to connect the QSR to the gas manifold in Figure 5.1. Humid air was generated using a commercial two-pressure humidity generator (Thunder Scientific Corporation model 2500) at a flow rate of 10 standard litres per minute (slm) and a pressure of approximately 200 kPa, chosen to give optimum stability in the generated dew-point temperature T_{dp}. Most of the gas flow was vented to the laboratory by a relief valve; of the remaining flow, regulated using a mass-flow controller (Teledyne-Hastings HFC-302), 500 standard cubic centimetres per minute (sccm) were directed through a chilled-mirror hygrometer (MBW DP3-D) and from 50 sccm to 400 sccm through the resonator interior.

To enhance thermal insulation, and to provide mechanical support, the resonator was placed inside a 20-litre stainless steel vessel.

A second chilled-mirror hygrometer (MBW 373 LX) was used to measure the dew point at the outlet of the vessel.

Both hygrometers were calibrated at NPL and their measurement uncertainty was $u(T_{\mathrm{dp}}) = 0.02$ °C (with a coverage factor $k = 1$) for the range of dew-point temperatures used in this work (9 °C $< T_{\mathrm{dp}} <$ 18 °C).

With the exception of the transitory phases, when water accumulates within the resonator by condensation, the difference in the dew-point temperatures indicated by the two hygrometers was always less than their combined uncertainty. The hygrometers were vented into the laboratory, where the ambient pressure was measured by a barometer (Druck DPI142). For the range of applied flow-rates, the flow impedance from the resonator interior and the measurement chambers of the chilled-mirror hygrometers to atmo-

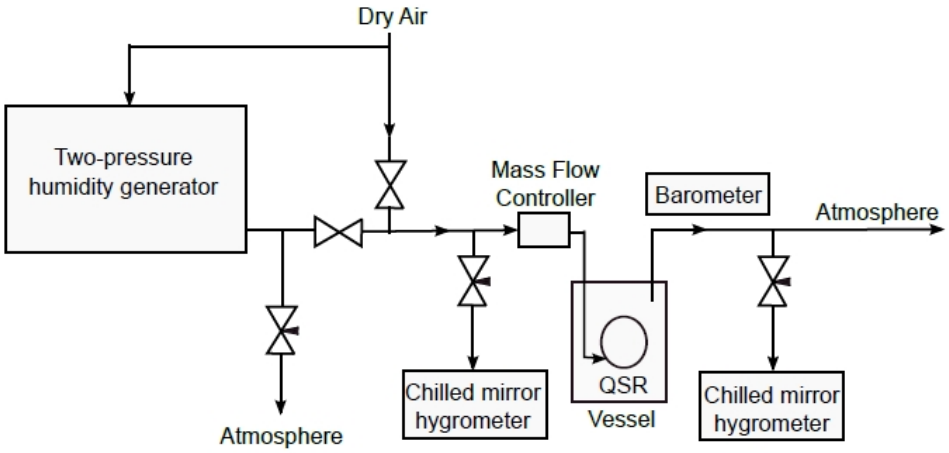

Figure 5.1: Diagram of the gas-handling system realised for condensation tests at NPL.

sphere were low enough that the interior pressure could be assumed to be equal to the barometer reading.

Figure 5.2: Experimental apparatus realised at the Acoustic Thermometry laboratory of NPL for condensation tests.

5.2 Detecting condensation using microwave resonances

From Eq. (1.59) it is appearent that in both pure gases and mixtures, the ratio of two normal modes of a resonator, for example a TM1n and a TE1n mode, remains invariant and is simply equal to the ratio of the corresponding eigenvalues, despite possible changes of the cavity temperature and pressure and the corresponding dielectric permittivity variations. This statement is valid until a drop of water condenses on the resonator surface. When this happens, the effect on the resonant frequency is made dependent and the ratio of two normal modes of the cavity is no longer constant.

For these reasons, we identified in the ratio $\frac{\langle f_{1n}^{\mathrm{TM}} \rangle}{\langle f_{1n}^{\mathrm{TE}} \rangle}$ in Eq. (1.59) a suitable test-quantity to detect condensation and determine the dew-point temperature T_{dp} of the mixture.

5.2.1 Preliminary tests in dry air

In preparation for the subsequent investigation of the microwave hygrometer performance with a humid air sample, we conducted an initial test to verify to what extent the mode frequency ratios remained constant in absence of water. The invariance of the ratios TM11/TE11 and TM12/TE11 (where TM1n/TE11 $= \langle f_{1n}^{\mathrm{TM}} \rangle / \langle f_{11}^{\mathrm{TE}} \rangle$) sets a lower sensitivity limit to the possible observation of the perturbation $\langle \Delta f_{\mathrm{d}} \rangle$ (Eq. (1.58)) when condensation takes place.

To accomplish this test, dry air ($T_{\mathrm{dp}} < -55$ °C) was flown through the resonator at a rate of 100 sccm, while varying the temperature of the resonator between a maximum of 13.60 °C and a minimum of 13.30 °C in steps of 0.05 °C, as it is shown in Figure 5.3.

Since the dew-point temperature of the flowing air sample is much lower than the resonator temperature ($T_{\mathrm{dp}} \ll T_{\mathrm{res}}$), we can assume the resonator internal surface to be essentially *dry* during the test, that means with no more than few monolayers of adsorbed water.

For each temperature change, the frequency of each resonance would show an anticorrelated variation, as a consequence of the thermal expansion of the cavity. To a lesser extent, the frequency variation should be positively correlated to the temperature change, due to the variation in the air density.

These expectations were confirmed by the experimental observation of the resonance frequencies. Figure 5.4 shows the variation of the mean frequency $\langle f_{11}^{\mathrm{TM}} \rangle$ (chosen for the purpose of illustration) in response to the variation of T_{res}.

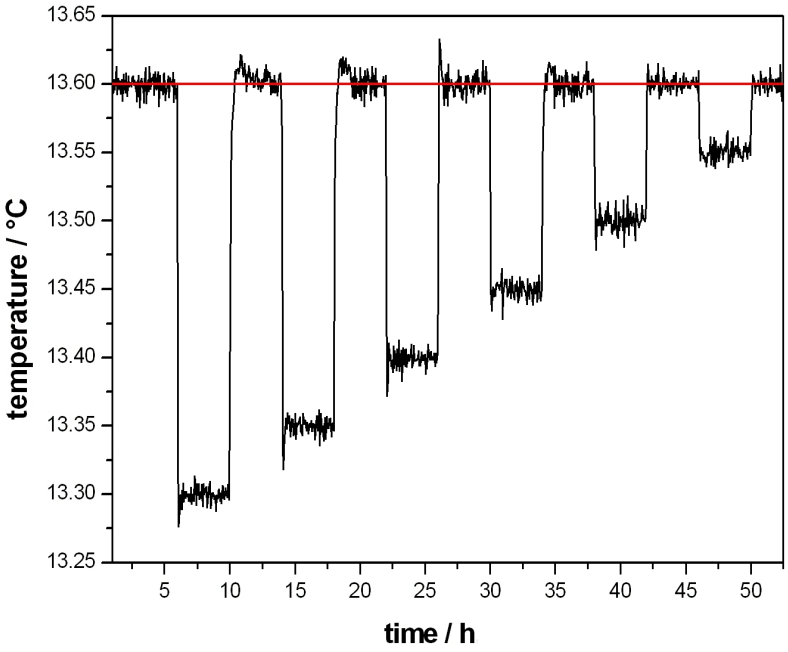

Figure 5.3: Record of the induced variations of the resonator temperature T_{res}.

The mean frequency $\langle f_{11}^{\mathrm{TM}} \rangle$ undergoes a relative increase of 3.0 parts in 10^6 (ppm) in response to a temperature decrease of 0.30 °C. Such relative change is in good quantitative agreement with the combined effects of the decrease in the cavity radius, which increases the mode frequency of 3.2 ppm, and the estimated increase of the refractive index of air (in response to the increase of density), which decreases the mode frequency by 0.6 ppm. In addition, the slow non-monotonic variation of $\langle f_{11}^{\mathrm{TM}} \rangle$ was found to be correlated to the variations in the laboratory pressure.

In the course of the same test, the ratios $\langle f_{11}^{\mathrm{TM}} \rangle / \langle f_{11}^{\mathrm{TE}} \rangle$ and $\langle f_{12}^{\mathrm{TM}} \rangle / \langle f_{11}^{\mathrm{TE}} \rangle$ remained constant within ± 0.1 ppm, shown in Figure 5.5 and 5.6. The value of this ratios thus provides an empirical estimate of the ratio $\xi_{1n}^{\mathrm{TM}} / \xi_{11}^{\mathrm{TE}}$ when no condensate is present within the resonator.

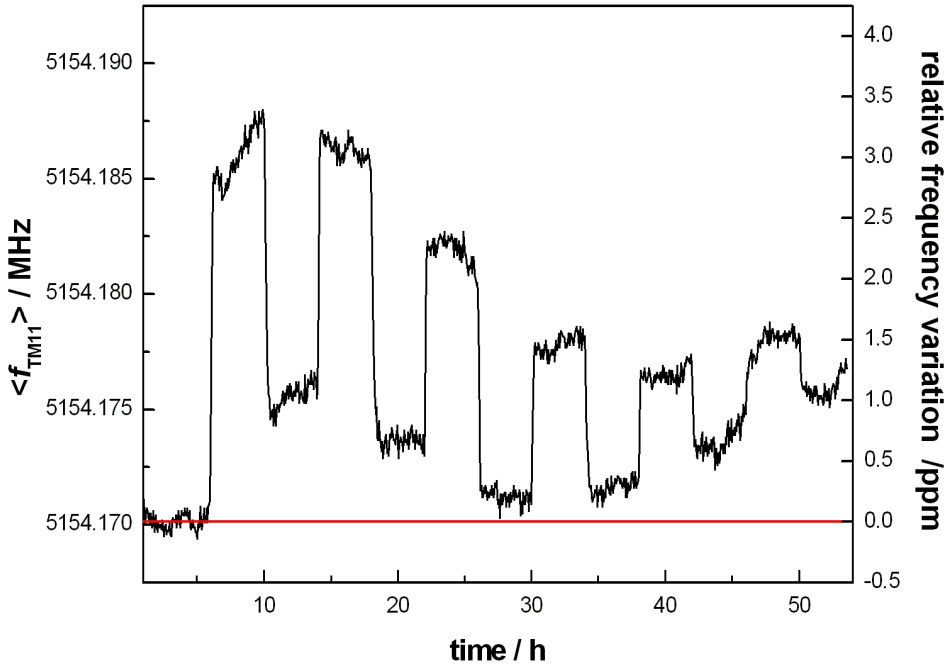

Figure 5.4: Absolute and relative variations of the mean resonance frequency of mode TM11 $\langle f_{11}^{\mathrm{TM}} \rangle$ in responce to variations in the resonator temperature.

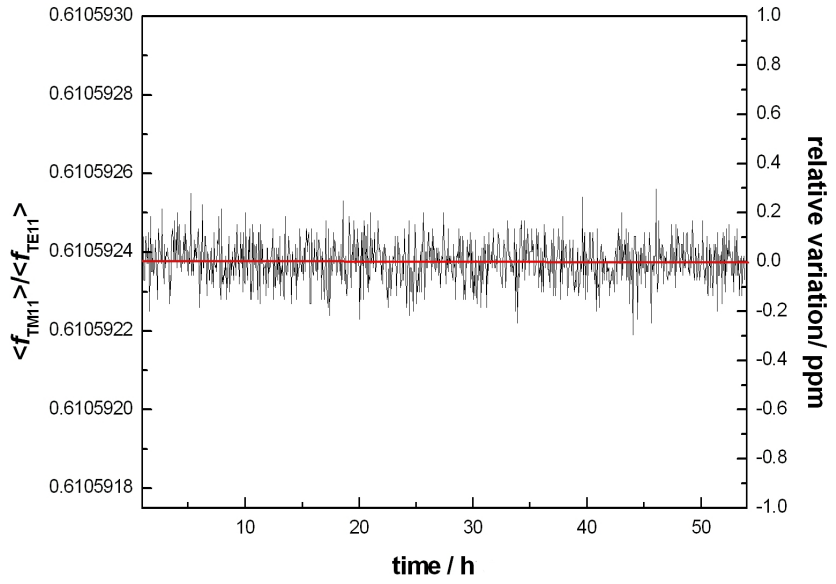

Figure 5.5: Absolute and relative variation of the ratio $\langle f_{11}^{\mathrm{TM}} \rangle / \langle f_{11}^{\mathrm{TE}} \rangle$ in response to the resonator temperature profile.

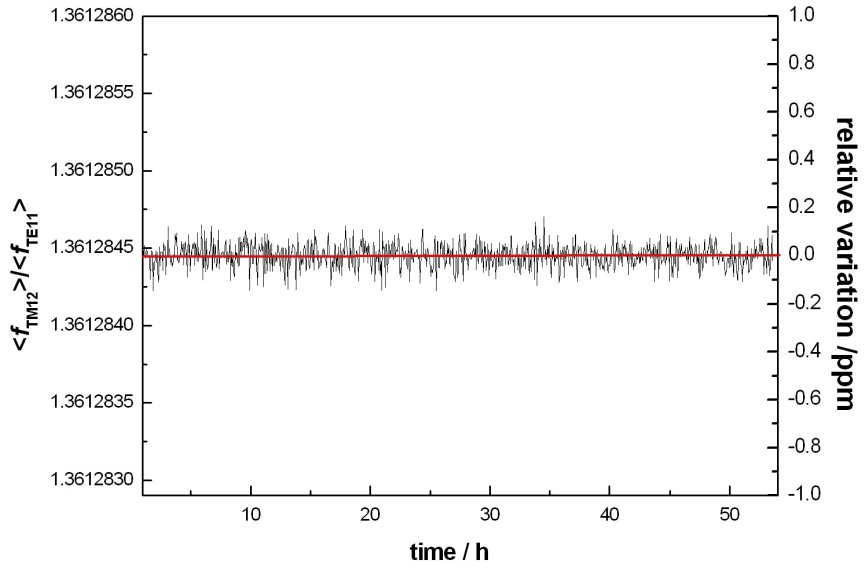

Figure 5.6: Absolute and relative variation of the ratio $\langle f_{12}^{\mathrm{TM}} \rangle / \langle f_{11}^{\mathrm{TE}} \rangle$ in response to the resonator temperature profile.

5.2.2 Condensation tests in humid air

The temperature variation test described above was repeated by flowing humid air through the resonator, with a nominal dew-point temperature of $T_{\mathrm{dp}} = 13.42$ °C at a rate of 100 sccm.

During the test, the resonator temperature T_{res} was alternatively varied below and above the T_{dp}. The lowest temperature of the resonator was thus 0.15 °C below T_{dp}, and the highest temperature was 0.15 °C above T_{dp}.

Differently from the observations in dry air, as a consequence of condensation the frequency ratios did not remain constant during the test. The relative difference of $\langle f_{11}^{\mathrm{TM}} \rangle / \langle f_{11}^{\mathrm{TE}} \rangle$ and $\langle f_{12}^{\mathrm{TM}} \rangle / \langle f_{11}^{\mathrm{TE}} \rangle$ from their reference values previously measured in dry air are illustrated in Figure 5.7 and 5.8.

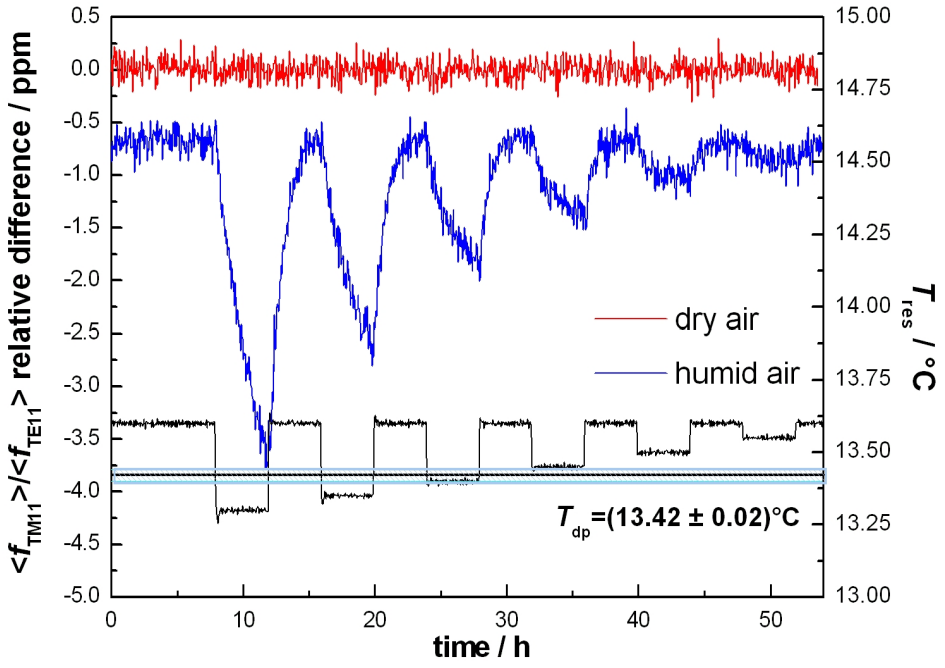

Figure 5.7: Relative difference between the frequency ratio $\langle f_{11}^{\mathrm{TM}} \rangle / \langle f_{11}^{\mathrm{TE}} \rangle$ measured in humid air (blue line) and in dry air (red line). The resonator temperature profile (black line) is also represented.

From the observation of the data in Figure 5.7, it is apparent that when

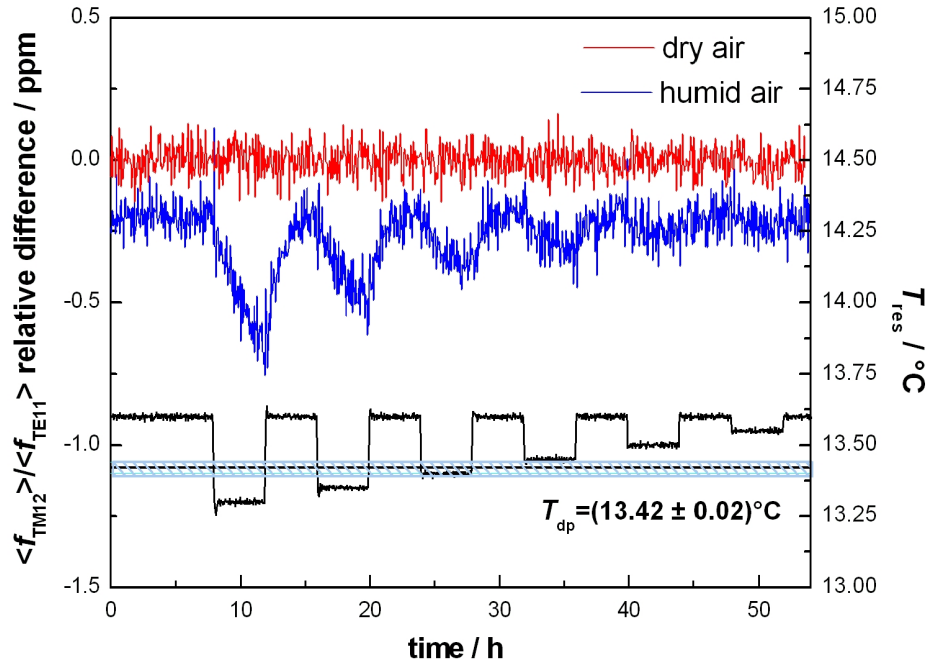

Figure 5.8: Relative difference between the frequency ratio $\langle f_{12}^{\mathrm{TM}} \rangle / \langle f_{11}^{\mathrm{TE}} \rangle$ measured in humid air (blue line) and in dry air (red line). The resonator temperature profile (black line) is also represented.

$T_{\mathrm{res}} = 13.60$ °C, a temperature which is higher than the dew-point of the incoming humid sample, the value of the ratios remain constant, though lower by 0.7 ppm than the dry air values. Seemingly, this slight reduction indicates that condensate layer is present on the cavity surface. We think that it might be due to an increase in surface adsorbed water. Also, this difference might be a consequence of a frequency dependence in the permittivity of water vapour, which would affect the two modes differently.

Independently from the cause of this discrepancy, we remark that, as in the previous tests with dry air, these ratios remain invariant as for as T_{res} is maintained above T_{dp}. As soon as $T_{\mathrm{res}} < T_{\mathrm{dp}}$, the ratios steadily decrease, indicating that water is being condensed on the resonator surface. Each time that T_{res} is raised back to 13.60 °C, the mode ratios return to their initial values, implying that the condensed water is evaporated from the surface. Moreover, when $T_{\mathrm{dp}} < T_{\mathrm{res}} < 13.60$ °C, the ratios initially decrease but then appear to settle towards new steady values (*plateaus*). It seems that only when $T_{\mathrm{res}} < T_{\mathrm{dp}}$, continuous accumulation of water occurs, as we expected.

Assuming that the average values of TM11/TE11 and TM12/TE11 previously measured in dry air correspond to the condition of perfectly dry cavity, in this case the volume of condensed water in the resonator equals to zero ($V_{\mathrm{w}} = 0$), from the value of the mode ratios and using Eq. (1.65), we can estimate the equivalent volume of water formed on the resonator internal surface.

In Figure 5.9 the estimated volume of the water accumulated during the experiment is shown with the correspondent average layer thickness. For the resonator used in this work, which has a radius of $a = 25.4$ mm, 1 mm^3 of condensed water is equivalent to a layer with a thickness of 123 nm, supposing that the water is distributed uniformly.

It is interesting to observe that, for $T_{\mathrm{res}} = 13.60$ °C, the value of the frequency ratios correspond to a water volume of 0.5 mm^3 inside the resonator, which means an average condensate layer thickness of 62 nm on the cavity surface. Though the thickness of the layer is more than we would expect from typical surface adsorption phenomena, however, the agreement between the results obtained from the two frequency ratios, which stands out from Figure 5.9, is remarkable, particularly if we consider the simplifying assumptions of the electromagnetic model and the large difference (a factor 6.4) in sensitivity to the water condensation of the two mode ratios examined. Finally, those results seem to suggest that the rate of water accumulation depends on the difference between the resonator temperature and the dew-point of the mixture which flows through the cavity.

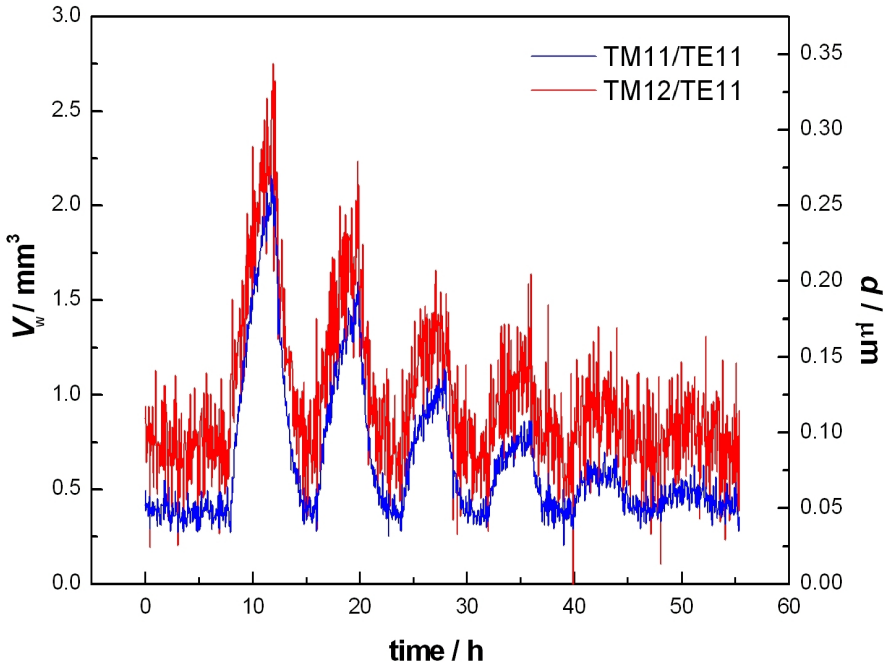

Figure 5.9: Volume of water accumulated during the experiment and correspondent average layer thickness. The volume is calculated from the mode ratios TM11/TE11 (blue line) and TM12/TE11 (red line).

5.3 Modelling the resonator as an ideal condenser

To improve our understanding of the previous observations and to develop a model capable of quantitative predictions of water accumulated in the resonator, we assume that the resonator acts as an ideal condenser to do some simple calculations and considerations.

Under this assumption, when $T_{\mathrm{res}} < T_{\mathrm{dp}}$, water contained in the incoming gas condenses on the surface of the resonator until the vapour pressure of water in the gas is equal to the saturation vapour pressure $p_{\mathrm{w}}(T)$ at T_{res}. In these conditions, from a flowing gas supply at a dew point above the resonator temperature, water continuously accumulates and the gas leaving the resonator should have a dew point temperature equal to T_{res}. On the contrary, when $T_{\mathrm{res}} > T_{\mathrm{dp}}$, water contained in the incoming gas evaporates until no condensate is present inside the cavity.

On the basis of this simple model, the amount of water accumulated within the resonator in a given period of time can be calculated as a function of four parameters: the mass-flow rate $\mathrm{d}n/\mathrm{d}t$, measured by the mass-flow controller and expressed in standard cubic centimetres per minute (sccm); the pressure of the gas in the resonator p; the dew-point temperature of the incoming gas sample T_{dp}; the temperature of the resonator T_{res}.

The measured flow rate can be converted from sccm to mole per second using the ideal gas equation:

$$\frac{\mathrm{d}n}{\mathrm{d}t} = \frac{p_{\mathrm{stp}}}{RT_{\mathrm{stp}}}\frac{\mathrm{d}V}{\mathrm{d}t} = 7.436 \cdot 10^{-7} \cdot Q \quad \mathrm{mol\ s^{-1}} \tag{5.1}$$

where $R = 8.314$ J mol^{-1} K^{-1} is the molar gas constant, $T_{\mathrm{stp}} = 273.15$ K and $p_{\mathrm{stp}} = 101325$ Pa are the standard temperature and pressure (STP) and $\mathrm{d}V/\mathrm{d}t = Q(10^{-6}/60)$ m^3 s^{-1} is the volumetric flow rate at STP. Thus, for example, a flow of 100 sccm corresponds to $\frac{\mathrm{d}n}{\mathrm{d}t} = 7.436 \cdot 10^{-7} \cdot 100$ mol s^{-1} in SI units.

The amount of water that accumulates in the resonator in a given period of time is given by the difference between the water amount coming in and the amount going out. Because $T_{\mathrm{dp}} > T_{\mathrm{res}}$, the rate at which water accumulates is given by:

$$\frac{\mathrm{d}n_{\mathrm{w}}}{\mathrm{d}t} = \frac{\mathrm{d}n}{\mathrm{d}t}(x_{\mathrm{in}} - x_{\mathrm{out}}) = 7.436 \cdot 10^{-7} \cdot Q(x_{\mathrm{in}} - x_{\mathrm{out}}) \quad \mathrm{mol\ s^{-1}} \tag{5.2}$$

where x_{in} and x_{out} are the mole fractions of water in air at dew point temperatures T_{dp} and T_{res} and respectively:

$$x_{\mathrm{in}} = \frac{p_{\mathrm{w}}(T_{\mathrm{dp}})}{p}, \tag{5.3}$$

$$x_{\mathrm{out}} = \frac{p_{\mathrm{w}}(T_{\mathrm{res}})}{p}, \tag{5.4}$$

where p is the pressure in the resonator, which is closely approximated by the barometric pressure in the laboratory, and $p_{\mathrm{w}}(T)$ is the saturation vapour pressure of water. Suitable functions for calculating $p_{\mathrm{w}}(T)$ were taken from [32].

Since the microwave measurements provide an estimate of the volume of water accumulated on the resonator surface, it is convenient to convert the molar accumulation rate to a volumetric accumulation rate. Considering that the molar mass of water is 18 g·mol^{-1} and the density is 10^3 kg·m^{-3}, we obtain:

$$\frac{\mathrm{d}V_{\mathrm{w}}}{\mathrm{d}t} = 48.19 \cdot Q(x_{\mathrm{in}} - x_{\mathrm{out}}) \ \ \mathrm{mm}^3\ \mathrm{h}^{-1}. \tag{5.5}$$

As a verification of the validity of the model of the resonator as an ideal condenser, we compared its predictions of the values of $\mathrm{d}V_{\mathrm{w}}/\mathrm{d}t$ with the water volumetric accumulation results obtained experimentally. This test was repeated for different values of flow rate.

The experiment consisted in maintaining the resonator at a constant temperature $T_{\mathrm{res}} = 13.1$ °C, while a flow of humid air with $T_{\mathrm{dp}} = 13.5$ °C passes through it at a fixed flow rate. After several hours of measurement, the condensed water is removed from the cavity by a flow of dry air. This test was repeated using different flow rates between 50 sccm and 400 sccm in steps of 50 sccm.

The results in Figure 5.10 show that, the rate with which water accumulates on the surface of the cavity is flow dependent.

For all flow rates, the accumulated volume is a nearly-linear function of time and the values obtained from the two mode ratios are in agreement, until a critical point is reached and a sudden change takes place. Beyond this point, the two mode ratios disagree and the shape of the curves radically changes. The sudden nature of this event seggests that, when the volume

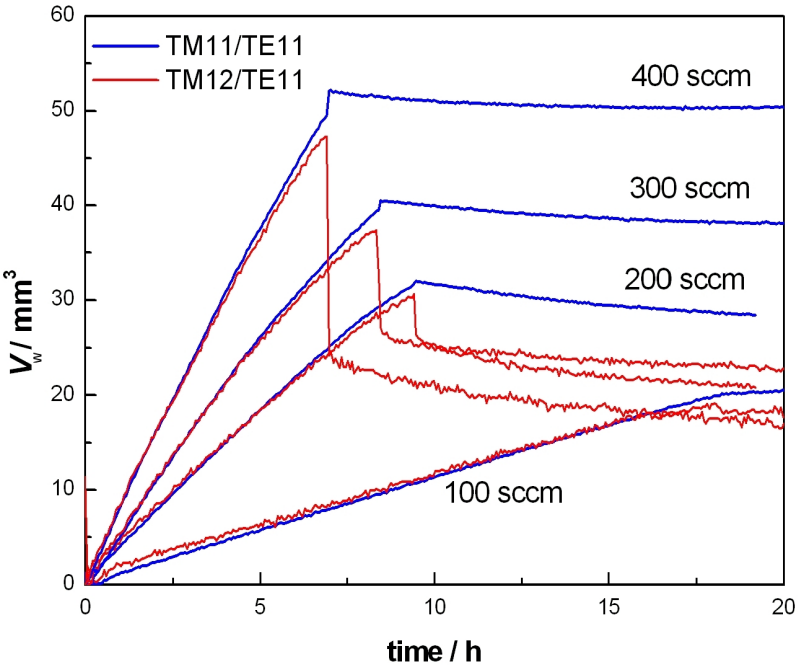

Figure 5.10: Volume of water accumulated at selected flow rates. The volume is calculated from the mode ratios TM11/TE11 (blue line) and TM12/TE11 (red line).

of water accumulated on the resonator surface reaches a critical amount, aggregation of the condensed water into a large droplet might take place, such as can be observed on a chilled-mirror hygrometer if unstable control allows it to undershoot in temperature. We also observed a sudden increase in width of the resonances, presumably due to dielectric losses in the large droplet.

For each flow rate, the accumulation rate $\mathrm{d}V_\mathrm{w}/\mathrm{d}t$ can be calculated from a linear fit to the subset of data before the critical point is reached. The experimental $\mathrm{d}V_\mathrm{w}/\mathrm{d}t$ values obtained are plotted in Figure 5.11 as a function of the flow rate and compared with the theorical values predicted by the ideal-condenser model.

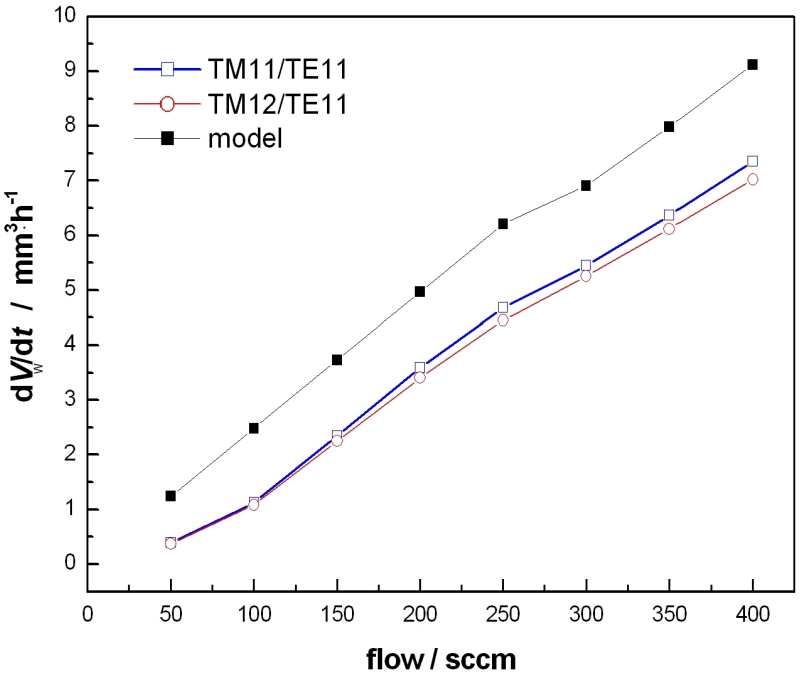

Figure 5.11: Water accumulation rate as a function of the flow, calculated from the mode ratios TM11/TE11 (blue line) and TM12/TE11 (red line) and considering the model of an ideal condenser.

The slight "kink", that can be observed in the graph between 250 sccm and 300 sccm, is due to a decrease in T_dp of 0.06 °C following a re-filling of the humidity generator. The agreement between the two mode ratios is remarkable and, considering there are no experimentally determined parameters in these calculations, the agreement between the electromagnetic and ideal-condenser models appears satisfactory.

The water accumulation rate was also studied at a constant flow of 300 sccm of humid air with $T_{dp} = 13.5$ °C as a function of resonator temperature, which is varied to be above and below the dew point temperature. T_{res} was varied between 13.7 °C (starting value) and 13.0 °C (minimum). Every four hours of measurement, T_{res} was reduced in steps included between 0.05 °C and 0.15 °C. Mid-way through the sequence, the resonator was purged with dry air to prevent the achieving of the critical volume point, observed in Figure 5.10.

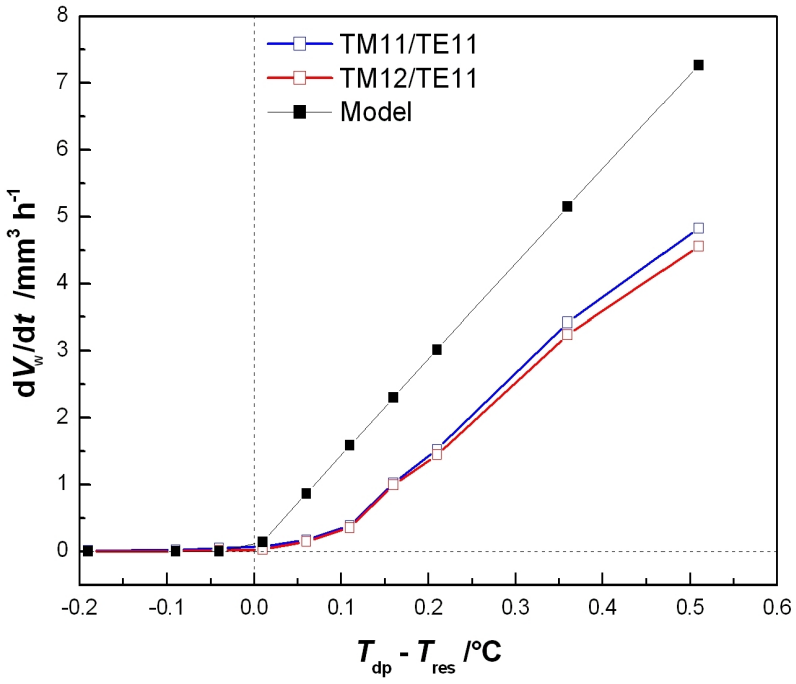

Figure 5.12: Water accumulation rate as a function of the temperature difference between the dew-point temperature and the resonator temperature, calculated from the mode ratios TM11/TE11 (blue line) and TM12/TE11 (red line) and considering the model of an ideal condenser.

In Figure 5.12 the experimental accumulation rates are plotted versus the temperature difference $(T_{res} - T_{dp})$. It is apparent from these data that no water condensation takes place when $T_{res} > T_{dp}$, while, when $T_{res} < T_{dp}$, water accumulates at a rate that is roughly proportional to $|T_{res} - T_{dp}|$. It is interesting to note that when $T_{res} < T_{dp}$, the slope of the experimental and modelled curves would nearly coincide if a shift of 0.1 °C was applied.

5.4 Practical test of the microwave resonator as a dew-point hygrometer

In a final test the resonator was used as a dew-point hygrometer and its performance was evaluated.

In a conventional chilled-mirror dew-point hygrometer, condensation in the form of dew or frost is induced on a small mirror embedded within the instrument. The mirror is cooled until drops of water start to condensate on its surface and, at this point, its temperature is controlled so that a layer of condensate of constant optical thickness is maintained on its surface. Changes in layer thickness are detected measuring the intensity of a beam of light reflected from the mirror.

In our experiment, the mirror surface is represented by the cavity inner surface and the beam of light by the steady microwave field and the temperature control is actuated on the entire resonator. This is realized using a proportional-integral algorithm such that the water volume, consequently the thickness, is held constant on the resonator.

For this test, we chose to maitain constant the value of the water volume in the cavity at 3.3 mm^3, which is easily detectable and responds to an average layer thickness of 400 nm.

In this experiment the flow rate was set to 300 sccm and T_{dp} was first decreased from 13.5 °C to 9.5 °C in steps of 1 °C and then increased back up to 13.5 °C. Since the temperature control system only allowed for 0.3 °C of automated modulation, the temperature of the cooling water was manually changed in 1 °C steps with T_{dp}. After each change in the dew-point, the resonator typically took about three hours to reach a stable temperature; once that stability was reached, measurements were recorded for at least four hours. The responding performance of the resonator in comparison with the dew-point hygrometer is shown in Figure 5.13.

The mean values of T_{dp} and T_{res} are compared in Figure 5.14.

For the range of dew-point temperature investigated, the difference between T_{dp} and T_{res} is fairly constant, with an average value of $(T_{dp} - T_{res}) = 0.08$ °C and a standard deviation of 0.02 °C. This difference, larger than the combined uncertainty of $u(T_{dp}) = 0.02$ °C and $u(T_{res}) = 0.02$ °C, could be explained by the non-uniformity of the resonator temperature, which would imply a difference between the actual temperature of the cavity and its measured estimate. Improvements in the thermal uniformity could significantly reduce this difference. The variability in $(T_{dp} - T_{res}) = 0.08$ °C at the repeated dew-points, it is at most 0.03 °C. This repeatable performance is comparable with that typical of a chilled mirror hygrometer.

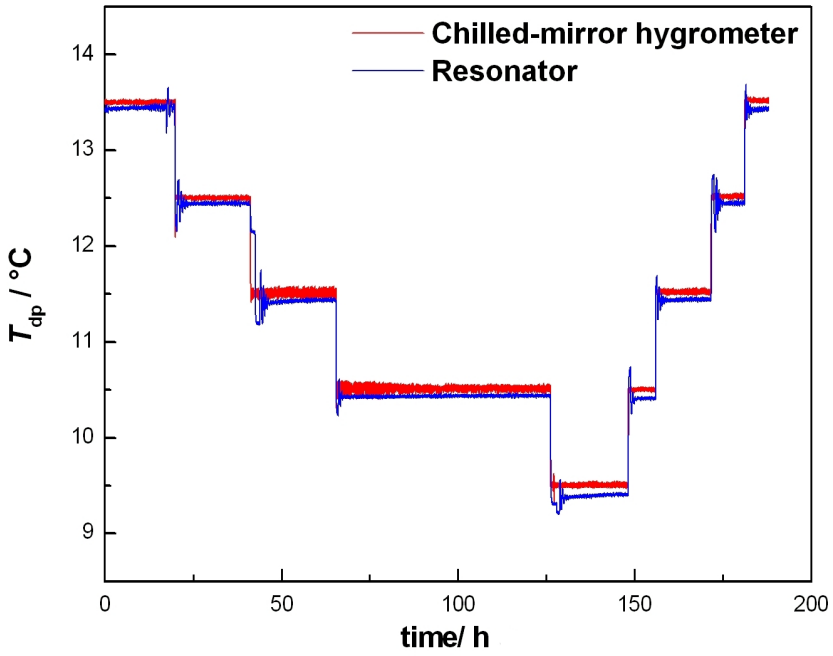

Figure 5.13: Chilled-mirror hygrometer (red line) and resonant hygrometer (blue line) performances.

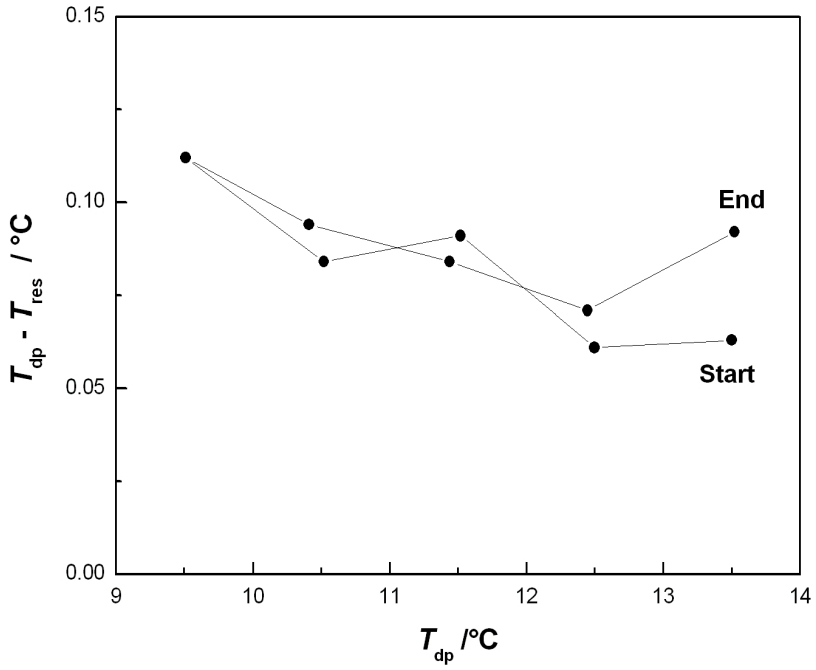

Figure 5.14: Comparison between dew-point values measured by the chilled-mirror hygrometer and the resonator.

Chapter 6

Conclusions

Laboratory and field measurements of humidity in air near atmospheric pressure are well established. However, there is a current need to measure dew point (and other humidity parameters) in diverse industrial gases, at a wide range of pressures and temperatures. Measurement needs include natural gas (pressures to at least 7 MPa), nuclear reactor heat exchange gases (H_2, He and CO_2 to several MPa), and various others. The options for robust sensors tolerant to contamination and drift-free operation in these varied conditions are currently limited. Such applications would potentially benefit from a novel versatile technique for measurements of dew point, if it could tolerate these extreme industrial conditions.

The research work described and discussed in this thesis was inserted in this context of needs, exploring the potential of a microwave resonator in addressing these issues. Because of their simple, rugged design and the remarkably high accuracy in the measurement of resonance frequencies, microwave resonators could possibly offer a solution to these challenging metrological requirements. Particularly, a triaxial ellipsoidal microwave resonator was subjected to different kinds of experiments to demonstrate its validity for hygrometry.

Initially, with the aim of reducing the uncertainty currently associated to the literature values of the constants in the Debye equation, the dielectric constant of pure water vapour was measured in the temperature range from 320 K to 470 K at pressures up to 1.7 MPa. The results obtained from these measurements were only partly satisfactory, as the aimed reduction of the uncertainty was modest. However, from these same results, the second dielectric virial coefficient of water vapour and its temperature dependence could be determined. To the author's knowledge, this is the first experimental determination of such quantities ever reported, and its relevance is stressed

by the possible capability of these results to test the theoretical models and the computational methods of intermolecular potentials. Additionally, the same experiments demonstrated the capability of the microwave technique to maintain its performance over the extended temperature and pressure range required by several industrial hygrometric applications.

Successively, the microwave technique was tried with measurements in humid binary mixtures at ambient pressure, comparing the relative humidity of H_2O/air and H_2O/N_2 mixtures alternatively produced by a standard humidity available at INRiM and measured using the microwave resonator. Summarizing the results of these tests, the reference and measured water mole fractions x_w were found to agree within their combined expanded uncertainty. The quality of the agreement is remarkable, considering that x_w in these mixtures spans the range between 3 parts in 10^4 and 2.1 parts in 10^2, corresponding to relative permittivities which differ from unity by less than 700 ppm.

Finally, the microwave QSR was subjected to tests of its capability to perform direct measurements of the dew-point temperature T_{dp}. Again this capability was satisfactorily demonstrated, although in this case a difference of (0.08 ± 0.02) °C in the dew-point temperature measured by the resonator and the reference chilled mirror hygrometer was observed. This difference, which was larger than the combined uncertainty of T_{dp} measured by the hygrometer and the resonator, is likely to be due to the imperfect thermal uniformity of the resonator, caused by the limited performance achieved in thermostatting the apparatus.

Considering the experimental tests and the results summarized above as a whole, the microwave device presented here might offer some interesting advantages with respect to traditional hygrometers. Firstly, the same instrumentation may be used in two ways: to measure the water fraction in a gaseous mixture well away from saturation conditions, or alternatively, for a direct measurement of the dew point. Measurement of water fraction requires the independent knowledge of the permittivity and the equation of state of the mixture components. However, the saturation curve or condensation temperature can be found even when this information is unavailable. The versatility implied by this two-fold capability is unique among hygrometric instrumentation.

When used as a condensation hygrometer, the method described in this work allows a quantitative estimate of the thickness and volume of the condensate layer. As the device capabilities will be further developed, a combined microwave and optical dew-point detector would allow the microwave signature of optically significant condensed layers to be studied. The mi-

crowave technique also offers the possibility to assess the spatial uniformity of the condensate layer by examining the relative perturbations of the individual modes within a triplet.

A few weak points in the performance of the microwave technique became evident from the results of the reported experiments. However, these difficulties could be overcome by designing a purpose-built device. As implemented in this work, and in contrast to traditional instrumentation (i.e. chilled mirror hygrometers), the microwave device showed an exceptionally slow response. However, simply using copper as the fabricating material and eliminating the unnecessary excess mass would reduce the response time significantly. In this work a network analyzer was used for precise tracking of the resonator resonance frequencies. While this type of instrument is both costly and bulky, simpler oscillators and/or dedicated electronics would significantly reduce these drawbacks. Additionally, other microwave functionality could be implemented, such as a high-power heating mode which could rapidly remove condensed layers.

Speculating about possible developments of this research, the potential of the microwave method might be tested over a wider temperature and pressure range and for a variety of humid gases different from nitrogen and air. Finally we note that the use of a quasi-spherical resonator is a complication which we believe is not strictly necessary. By appropriate choice of modes, a cylindrical resonator could be used and this would offer several advantages, most notably reduced cost of manufacture.

Appendix A

Glossary of hygrometric quantities

For a better understanding of this work, some definitions of measured quantities in hygrometry and of interest for us are reported. These definitions are taken from " A Guide to the Measurement of Humidity", published by the Institute of Measurement & Control in 1996, ISBN 0-904457-24-9, and prepared by the National Physical Laboratory and the Institute of Measurement & Control.

Absolute humidity - The mass of water vapour present in unit volume of moist air of a given temperature and pressure.

Dew point (or dew-point temperature) - The temperature at which dew, or condensation, forms, on cooling a gas. This is the temperature at which air becomes saturated in equilibrium with water. Negative dew points, with respect to supercooled water below 0 °C, are always shown with a minus (-) sign. The term "dew point" is often used generally to include "frost point". However in the range just below 0 °C, where either frost or dew (supercooled water) can form, the values of dew point and frost point differ.

Frost point (or frost point temperature) - The temperature at which frost point forms on cooling a gas. This is the temperature at which air is saturated in equilibrium with ice.

Mole fraction - The mole fraction of a component is the ratio of the amount (number of moles) of that component to the total amount of substance present. It is expressed as a dimensionless ratio.

Relative humidity - The ratio of the actual vapour pressure to the saturation vapour pressure over a plane liquid water surface at the same temperature, expressed as a percentage If e is the actual vapour pressure and e_s is the saturation vapour pressure:

$$\text{relative humidity (in \%)} = \frac{e}{e_s} \times 100$$

Saturation vapour pressure (of water) - The maximum pressure of water that can exist at a given temperature.

Vapour pressure - That part of total pressure contributed by the water vapour.

List of Tables

List of Figures

LIST OF FIGURES

Bibliography

[1] S. Bell, R. Benyon, N. Bose, M. Heinonen. Int.J.Thermophys (2008) 29: 1537-1543.

[2] Sito internet. *http://www.euromet.org/projects.*

[3] K.D. Froome, L. Essen. *The Velocity of Light and Radio Waves.* New York: Academic Press, 1969.

[4] P.J. Mohr, B.N. Taylor, D.B. Newell. J. Phys. Chem. Ref. Data 37, 3 (2008).

[5] Institute of Measurement and Control. *A Guide to the Measurement of Humidity.* ISBN 0-904457-24-9, 1996.

[6] M.R. Moldover, M. Waxman, M. Greenspan. High Temp.−High Pressures 11, 75 (1979).

[7] M.R. Moldover, J.P.M. Trusler, T.J. Edwards, J.B. Mehl, R.S. Davis. J.Res.Natl.Bur.Stand. 93, 2 (1988).

[8] J.B. Mehl, M.R. Moldover. Physical Review A 34, 4 (1986).

[9] R.J. Underwood, D. Flack, P. Morantz, G. Sutton, P. Shore, M. de Podesta. Metrologia 48 (2011): 1-15.

[10] J.B. Mehl. Metrologia 46 (2009): 554-559.

[11] J.B. Mehl, M.R. Moldover, L. Pitre. Metrologia 41 (2004): 295-304.

[12] L. Pitre, M.R. Moldover, W.L. Tew. Metrologia 43 (2006): 142-162.

[13] E.F. May, L. Pitre, J.B. Mehl, M.R. Moldover, J.W. Schmidt. Rev. Sci. Instrum. 75, 10 (2004).

[14] J.W. Schmidt, R.M. Gavioso, E.F. May, M.R. Moldover. Phys. Rev. Lett. 98, 254504 (2007).

[15] E.F. May, M.R. Moldover, J.W. Schmidt. . Phys. Rev. A 78, 032522 (2008).

[16] E.F. May, M.R. Moldover, J.W. Schmidt. Mol. Phys. 107, 15785 (2008).

[17] P.H. Huang, D.C. Ripple, M.R. Moldover, G.E. Scace. *A reference standard for measuring humidity of air using a re-entrant radio frequency resonator.* Presented at the 5^{th} international symposium on humidity and moisture (Rio de Janeiro, Brazil, 2006).

[18] E.U. Condon. Rev. Modern Phys. 14 (1942): 341-389.

[19] A.B. Bronwell, R.E. Beam *Theory and Application of Microwaves.* Radio Communication Series, Ed. McGraw-Hill Book Company,Inc, pp. 380 (1947).

[20] R.J. Underwood, J.B. Mehl, L. Pitre, G. Edwards, G. Sutton, M. de Podesta. Meas. Sci. Technol. 21, 075103 (2010).

[21] S. Hasegawa, D.P. Stokesberry. Rev. Sci. Instrum. 46, 7 (1975).

[22] R. Djaozandry, J.M. St-Arnaud, K.T. Bose, M.F. Frechette. Rev. Sci. Instrum. 69, 3 (1998).

[23] J.W. Schmidt, M.R. Moldover. Int. J. Thermophys. 24, 2 (2003).

[24] E.B. Ewing, D.D. Royal. J. Chem. Thermodynam. 34 (2002): 1985-1999.

[25] P.W. Atkins *Physical Chemistry.* Ed. Oxford University Press, Cap.22.

[26] *Experimental Thermodynamics.* Vol.VI. Ed. by A.R.H. Goodwin, K.N. Marsh, W.A. Wakeham. (2003): 434-435.

[27] A.D. Buckingham, R.E. Raab. Trans. Faraday. Soc. 54 (1958): 623-628.

[28] A.H. Harvey, E.W. Lemmon. Int. J. Thermophys. 26, 1 (2005).

[29] E.W. Lemmon, R.T. Jacobsen, S.G. Penoncello, D.G. Friend. J. Phys. Chem. Ref. Data 29, 3 (2000).

[30] P. H. Huang. *Thermodynamic properties of moist air containing 1000 to 5000 ppm_V of water vapor.* Presented at the Workshop on moisture measurement and control for microelectronics (Gaithersburg, MD, 1993).

[31] R. Span, E.W. Lemmon, R.T. Jacobsen, W. Wagner, A. Yokozeki. J. Phys. Chem. Ref. Data 29, 6 (2000).

[32] W. Wagner, A. Pruss. J. Phys. Chem. Ref. Data 31, 2 (2002).

[33] A.H. Harvey, P.H. Huang. Int. J. Thermophys. 28, 2 (2007).

[34] R.F. Harrington. *Time-harmonic electromagnetic fields.* New York: McGraw-Hill, pp. 321-325 (1961).

[35] R. Underwood, D. Flack, P. Morantz, G. Sutton, P. Shore, M. de Podesta.Metrologia 48 (2011): 1-15.

[36] R.A. Matula. J. Phys. Chem. Ref. Data 8, 4 (1979).

[37] J.B. Mehl. C. R. Phys. 10 (2009): 859-865.

[38] G. Lach, B. Jeziorski, K. Szalewicz. Phys. Rev. Lett. 92, 23 (2004).

[39] G. Boudouris. J. Res. Natl. Bur. Stand. (U.S.) D 67, 631 (1963).

[40] G. Birnbaum, S.K. Chatterjee. J. Appl. Phys. 23, 2 (1952).

[41] G.S. Kell, G.E. McLaurin, E. Whalley. Proc. R. Soc. London A 425 (1989): 49-71.

[42] C. Millot, J-C. Soetens, M.T.C. Martins Costa, M.P. Hodges, A.J. Stone. J. Phys. Chem. A 102 (1998): 754-770.

[43] R.S. Fellers, C. Leforestier, L.B. Braly, M.G. Brown, R.J. Saykally. Science 284 (1999): 945-948.

[44] A. Actis, V. Fernicola, M. Banfo. *Proceedings of TEMPMEKO '99, 7th International Symposium on Temperature and Thermal Measurements in Industry and Science*, ed. by J. F. Dubbeldam, M.J. de Groot (Edauw Johannissen bv, Delft, 1999), pp. 185-190.

[45] R.S. Davis. Metrologia 35 (1998): 49-55.

[46] P. Giacomo. Metrologia 18 (1982): 33-40.

[47] R.W. Hyland, A. Wexler. ASHRAE Trans. 89, 500 (1983).

[48] R.B. Montgomery. J. Atmos. Sci. (Prev. J. Meteorol.) 4, 193 (1947).

Acknowledgements

Each chapter of this thesis is strictly connected to what my life has been in these last three years.

It is the story of a scientific educational path and professional growth with the idea to become one day a researcher, even if the hope to see it realised is becoming fainter and fainter because of Italian economic, political and cultural situation. But that's not all. This thesis also represents my personal and interior growth which has taken place in these three years.

I always considered the Ph.D qualification as a target to reach, a challenge to face and win, a challenge with myself and to evaluate myself and now here I am, while I summarise in few pages all the job done and omit all faced difficulties, near to the end of this work and life experience.

I don't know if I would have been able to arrive where now I am without the support, encouragement, patience and aid of some persons, but I am sure that their contribution was fundamental and for this reason I would like to thank them.

A special Thank you is for Dario and my parents, who are the most important persons of my life.

Thank you to my dear friend Marialaura, who always trusted in me. Without her I would never started.

Thank you to Zazà, Paola and Renata, my friend from a lot of time and I hope forever.

Thank you to Elena, more a friend than a doctor, who let me to start a long travel of knowledge of myself.

Thank you to Chiara and Alba who were able to make me smile even in difficult situations.

Thank you to my new English friends: Robin and Anna, Michael, Jenny, Gavin, Stephanie, Mark, Jessica. Thank you not only for your competence and expertise,but also for your kindness and cordiality. You welcomed me in your group as one of the family, making really pleasant the time I spent in Teddington. In the future I hope to continue to collaborate and keep in touch with you.

Thank you to Simona, Alberto, Mario, Paolo, Chiara I and Chiara II for your company, suggestions and advices, for chats and laughs, for delicious dinners, extreme adventures (these ones are in particular due to Simona!) and also for discussions and heated opinion and idea debates.

Finally thank you to Roberto, Daniele and Giuliana because they gave me the possibility to work and make experience with them in INRiM, because they guided me during my doctorate, let me to write this thesis and improved my knowledge.

Hoping I didn't forget anyone...

Rugiada

Ringraziamenti

Ogni capitolo di questa tesi è strettamente legato a quella che è stata la mia vita in questi ultimi tre anni.

Si tratta della storia di un percorso di formazione scientifica e di crescita in ambito lavorativo nella speranza, sebbene sempre più fievole a causa del panorama economico, politico e culturale italiano, di poter un giorno diventare ricercatore. Ma non solo. Questa tesi rappresenta anche un mio percorso di crescita interiore e personale avvenuto nell'arco di questi tre anni.

Ho sempre guardato al titolo di "dottore in ricerca" come ad un traguardo da raggiungere, una sfida da affrontare e vincere, una sfida con me stessa e per valutare me stessa e dopo tutto eccomi qui a riassumere in poche pagine il lavoro svolto, tacendo tutte le difficoltà affrontate, e sempre più vicina alla conclusione di questa mia esperienza di lavoro e di vita.

Non so se sarei riuscita ad arrivare dove ora mi trovo in assenza del sostegno, dell'incoraggiamento, della pazienza e dell'aiuto di alcune persone, ma so per certo che il loro contributo è stato fondamentale e per questo vorrei ringraziarle.

Un Grazie speciale va a Dario ed ai miei genitori, che sono le persone più importanti della mia vita.

Dico Grazie alla mia cara amica Marialaura, che ha sempre avuto fiducia in me e senza la quale non avrei neanche iniziato.

Grazie a Zazà, Paola e Renata, amiche ormai da tanto tempo e speriamo per sempre.

Grazie ad Elena, ormai più un'amica che un medico, che mi ha permesso di iniziare un lungo viaggio di conoscenza di me stessa. Grazie a Chiara e ad Alba, che hanno saputo strapparmi un sorriso anche nei momenti difficili.

Grazie ai miei nuovi amici inglesi: Robin ed Anna, Michael, Jenny, Gavin, Stephanie, Mark, Jessica. Vi ringrazio per la vostra gentilezza e cordialità oltre che per la vostra competenza e professionalità. Mi avete accolto nel vostro gruppo come se fossi una di famiglia, rendendo il periodo da me trascorso a Teddington estremamente piacevole. In futuro mi auguro di continuare a restare in contatto e a collaborare con voi.

Grazie a Simona, Alberto, Mario, Paolo, Chiara I and Chiara II per la compagnia, i suggerimenti e i consigli, le chiacchiere e le risate, le cene da buon gustai, le avventure estreme (questo è merito soprattutto di Simona!) e anche per le discussioni e gli accesi confronti di opinioni ed idee.

Infine grazie a Roberto, Daniele e Giuliana per avermi dato l'opportunità di lavorare e fare esperienza con loro presso l'INRiM, per avermi guidato durante il dottorato, permesso di scrivere questa tesi e per aver accresciuto il mio bagaglio culturale.

Nella speranza di non aver dimenticato nessuno...

Rugiada